AN INVESTIGATION OF SELF-GENERATED MAGNETIC FIELDS AND ELECTRON EMISSION IN LASER PRODUCED PLASMAS

Roger Salisbury Case

NAVAL POSTGRADUATE SCHOOL
Monterey, California

THESIS

An Investigation of Self-Generated Magnetic Fields and Electron Emission in Laser Produced Plasmas

by

Roger Salisbury Case, Junior

Thesis Advisors: Fred. R. Schwirzke
Arthur H. Guenther

March 1974

An Investigation of Self-Generated Magnetic Fields and Electron Emission in Laser-Produced Plasmas

by

Roger Salisbury Case, Junior
Captain, United States Air Force
B.A., Colgate University, 1964
M.S., United States Air Force Institute of Technology, 1966

Submitted in partial fulfillment of the
requirements for the degree of

DOCTOR OF PHILOSOPHY

from the
NAVAL POSTGRADUATE SCHOOL
March 1974

ABSTRACT

An experimental study of magnetic signals from laser-produced plasmas has been performed. From 2 to 30 joules of laser energy impinged upon metallic and hydrocarbon targets in pulse lengths of from 4 to 80 nanoseconds, and at incident angles of 0° and 45°. Two magnetic signals were detected using inductive probes; one whose peak intensity is temporally coincident with, and whose rise time is a function of the incident laser pulse length; the second longer-lasting and time-delayed from the arrival of the laser pulse on target. The first signal results from electrons emitted anisotropically from the laser-produced plasma. This emission current is limited by space charge effects, and is strongly dependent upon the ambient gas pressure over the range of 10^{-6} to 10^{+1} Torr. The second magnetic signal arises from misaligned temperature and density gradients within the laser plasma. The dependencies of these signals on residual gas pressure, laser pulse length and shape, and spatial location have been evaluated.

TABLE OF CONTENTS

LIST OF TABLES

LIST OF FIGURES

LIST OF SYMBOLS

Symbol	Meaning
A	Atomic Weight
A_p	Area of Magnetic Probe
a,a'	Numerical Constant
b	Numerical Constant
B	Magnetic Field Intensity
c	Speed of Light
C	Capacitance
d	Radius of Helmholtz Coils
dl(dA)	Elemental Length (area)
e	Electronic Charge
E	Electric Field Intensity
f	Frequency
H(f)	Frequency Transfer Function
i	Current
i_e, i_s	Emission Electron Current
I	Laser Intensity
j	Current Density
k	Boltzman's Constant
K	Electrostatic Wave Number
k_o	Laser Beam Wave Number
K_{coil}	Calibration Coil Parameter
L,L_c	Inductance, Coil Inductance
L	Plasma Characteristic Length

L_n	Plasma Density Gradient Length
L_T	Plasma Temperature Gradient Length
L_r	Numerical Filtering Parameter
m_e	Mass of The Electron
m_i	Mass of i^{th} Ion
n, n_e	Number Density
N	Number of Wire Turns on Helmholtz Calibration Coils
N_f	Number of Fourier Terms in Filter Function
P_L	Laser Power
P, P_e	Pressure, Electron Pressure
r	Radial Coordinate
R	Spatial Coordinate $(r^2+z^2)^{1/2}$
$\bar{R}$	Average Plasma Radius
$r_{f.s.}$	Radius of The Laser Beam Focal Spot
R_m	Magnetic Reynold's Number
T, T_e	Temperature, Electron Temperature
t	Time
t_o	Magnetic Diffusion Time; Matching Time For SGMF Computer Self-Similarity Solution
U_s	Space Charge Potential
V	Voltage
v, v_e	Velocity, Electron Velocity
v_o	Plasma Instability Parameter
W	Plasma Work Function
X(f)	Input Signal
Y(f)	Output Signal

z	Axial Coordinate
Z	Atomic Number
$\overline{Z}$	Average Charge State of Plasma
α	Numerical Constant
β	Pressure Dependence Exponent
ρ	Density
μ_o	Permeability of Free Space
λ_D	Debye Length
σ	Conductivity
ω	Angular Frequency
γ_E	Spitzer Parameter
τ_L	Laser Pulse Length
Λ	Couloumb Logarithim
∇	Vector Gradient
∇_z	Vector Gradient in z Direction

ACKNOWLEDGEMENTS

I wish to acknowledge several people without whom this effort would never have come to the successful conclusion that it has. Special thanks go to Dr. Fred Schwirzke and Dr. Arthur Guenther, my thesis advisors, for their encouragement and able assistance.

Also, thanks are in order to Dr. Daniel N. Payton, III, Dr. Winston K. Pendleton, Mr. Larry Seftor, and Mr. Joseph F. Janni for their competent technical expertise and assistance in performing both the theoretical and experimental portions of this experiment.

Certainly, however, my most special thanks go to my wife, Polly, for her understanding, patience, and overall confidence, without which this work would have never been completed.

I. INTRODUCTION

Since the term "plasma" was first applied to ionized gases by Langmuir in 1928, the study of such collections of ions and electrons has continued to increase in scope and importance because of the wide range of physical situations in which plasmas are found. In most plasma physics studies, such as AC and DC arcs, gas discharge tubes, exploding wire experiments, and other plasma generation schemes, electromagnetic fields are used to produce the plasma. Since its development in the late 1950's, the laser has proven very useful in the generation of hot dense plasmas which are effectively free of such externally applied electromagnetic fields. With the advent of the Q-switch, much higher power densities became available for such plasma studies.

The discovery of the phenomena, which were investigated with magnetic probes in this thesis, arose from the study of laser-produced plasmas. These phenomena are the emission and propagation of energetic electrons from a laser-produced plasma into a pre-ionized background plasma, and the generation, propagation, and decay of self-generated magnetic fields (SGMF).

Interest in electron emission currents from laser-produced plasmas has increased recently because of the possibility that plasma instabilities may play an important role in such electron emission. SGMFs arise when temperature and density gradients are nonparallel to one another. Such magnetic fields

may contribute to the development and growth of various plasma instabilities, influence the dynamics of the laser plasma expansion if their magnitudes become sufficiently large, and affect the cross field transport coefficients.

Another source of interest in these two phenomena is their application as a plasma diagnostic technique, as in using these magnetic signals to evaluate the degree of uniformity of implosion in proposed laser initiated fusion experiments. The aim of such experiments is to heat a pellet to fusion temperatures and densities by tailoring the laser pulse length, pulse shape and energy so that such pellets when irradiated from many directions will be symmetrically imploded by the shock waves which are formed in the material.

In an ideal spherical implosion, temperature and density gradients remain everywhere parallel, and no SGMFs are generated. The work reported herein, and the results of prior investigations of SGMFs (Refs. 1-6) all used either planar or thin fiber target geometries, and nonspherical expansions resulted. Because of the directed plasma expansion, and the fact that finite width laser beams were incident upon semi-infinite planar targets, nonparallel temperature and density gradients were generated. Magnetic fields were, therefore, generated in an azimuthal direction with a symmetry axis which was the target normal (see Figure 1). Such data can be compared with that which will be obtained from the pellet implosion experiments to evaluate the uniformity of the implosion. The observation of electron emission currents flowing in the

ambient background gas is also of importance for laser fusion studies, as their number density and energy may indicate the degree to which instability or anamolous heating occurs in the imploding fusionable material.

The work reported in this thesis is directed toward more fully understanding these phenomena. The thesis problem follows from the investigations of SGMFs referred to earlier and of electron emission currents (Refs. 7-12):

(1) What are the source and accelerating mechanisms, spatial characteristics, time history, and pressure dependence of the electron current flow which occurs when high intensity lasers are incident upon hydrocarbon and metallic foil targets.

(2) How does the time history and magnitude of SGMFs change as the incident laser parameters of pulse shape, pulse length, wavelength, and background gas pressure are varied.

In answer, in this thesis, are reported the two component magnetic signals which have been obtained when ruby, Nd glass, and CO_2 laser pulses of from 2 to 30 joules in 4 to 80 nanoseconds full width at half maximum intensity (FWHM) were incident upon planar hydrocarbon and metallic foil targets. The laser beam was incident at angles of 0° and 45° relative to the target normal; background gas pressures ranged from 10^{-6} to 10^{+1} Torr of air. The effects of target material, pulse length and shape, laser wavelength, ambient gas pressure, and total laser energy have been investigated in this study. Additionally, the results of modeling the SGMF phenomenon on a computer (Refs. 13-14) are compared with the experimental results obtained here. As a new result, an early time signal (ETS) due to electrons which are emitted by the laser-produced

plasma into the photoionized background plasma has been detected. Secondly, the time history of the SGMF signal indicates that a different regime has been investigated when compared to that in which magnetic signals were previously detected from laser-produced plasmas.

II. THEORY

A. SELF-GENERATED MAGNETIC FIELDS

A description of the generation, propagation, and dissipation of the late time SGMFs is included in the two fluid MHD equations. When the momentum transfer equations for the ion and electron species are linearized in the manner of Spitzer (Ref. 15) and the gravitational potential term neglected, the equation of motion for the plasma as a whole is obtained.

$$\rho \frac{\vec{dv}}{dt} = \frac{\vec{j}}{c} \times \vec{B} - \nabla \vec{P} \qquad (1)$$

as is the generalized Ohm's Law (current equation)

$$\frac{m_e}{ne^2} \frac{\vec{dj}}{dt} = \vec{E} + \frac{\vec{V}}{c} \times \vec{B} + \frac{1}{ne} \nabla \vec{P}_e - \frac{\vec{j}}{nec} \times \vec{B} - \frac{\vec{j}}{\sigma} \qquad (2)$$

where $\vec{V}$ refers here to the plasma flow velocity. These equations, when combined with Maxwell's equations for the electromagnetic fields, an equation of state for the plasma, and the mass continuity equation, form a complete set which describes the behavior of the plasma. To obtain the equation which describes the generation propagation, and decay of the magnetic field, one returns to the electron component equation of motion. The electron plasma frequency is much larger than any experimental frequencies of interest, which allows the neglect of the electron inertia term. Solving for the electric field yields

$$\vec{E} = \frac{\vec{j}}{\sigma} - \frac{1}{ne} \nabla \vec{P}_e - \frac{\vec{V}_e}{c} \times \vec{B} \qquad (3)$$

where $\vec{V}_e$ refers to the electron velocity, not the plasma flow velocity $\vec{V}$. This value of the electric field is inserted into Maxwell's equation relating electric field intensity to the time derivative of the magnetic field yielding:

$$\frac{\partial \vec{B}}{\partial t} = \nabla \times \vec{V}_e \times \vec{B} - \frac{c}{\sigma} \nabla \times \vec{j} + \nabla \times \frac{c}{ne} \nabla P_e \qquad (4)$$

Assuming an equation of state for the plasma of the form $P_e = nkT_e$, and simplifying the resulting expression produces an equation which describes the generation, propagation, and decay of the SGMFs (Ref. 4).

$$\frac{\partial \vec{B}}{\partial t} = \nabla \times \vec{V}_e \times \vec{B} + \frac{c^2}{4\pi\sigma} \nabla^2 B + \frac{k}{ne} \vec{\nabla} T_e \times \vec{\nabla} n \qquad (5)$$

The first term on the right-hand side of (5) describes the convective transport of the magnetic field, a situation in which the magnetic Reynold's number (Ref. 16) is much greater than 1. In such situations, the field moves with the local plasma velocity, typically on the order of 10^7 cm/sec for laser-produced plasmas (Refs. 5, 7).

Term two describes a situation in which the magnetic field diffusion time is small compared with the time required for

the transport of the field a characteristic distance L at the convective transport velocity. The diffusion time is the e-folding period in which Ohmic losses dissipate the magnetic field energy, $B^2/8\pi$. It is approximated by replacing the second term in (5) by $c^2B/4\pi\sigma L^2$, where L is a length characteristic of the plasma under investigation. The solution of the resulting equation is

$$B = B_o \, e^{-t/t_o} \tag{6}$$

where the diffusion time t_o is defined as

$$t_o \equiv \frac{4\pi\sigma L^2}{c} \tag{7}$$

Note that the magnetic Reynold's number, R_m, referred to earlier is the ratio of term 1 to term 2 on the right-hand side of (5).

$$R_m = \frac{4\pi\sigma L V_e}{c^2} \tag{8}$$

Magnetic diffusion is dominant where $R_m << 1$, a situation which occurs either due to laser plasma cooling or if the plasma temperature never reaches a high enough value to effectively "freeze" the magnetic field into the laser plasma.

The third term on the right-hand side of (5) is the one which describes the generation of the magnetic field. As is evident from its dependence upon temperature and density

gradients, it will reverse sign upon the inversion of either gradient, or their relative orientation one with the other. For situations as in those used herein, i.e., planar targets, at pressures of less than a few Torr, the SGMFs are cyclindrically symmetric about the target normal, independent of the laser incidence angle. A corresponding independence of the direction of ejection of plasma plume on the laser incidense angle has been observed in the laser plasmas produced by Q-switched ruby systems for pressures of less than a few Torr (Ref. 17). Note that this does not uniquely determine the sign and orientation of the gradients responsible for the fields, since their vector product is involved, and several combinations will yield the same polarity field. A further description of this source term can be found in References 2, 5, 7, and 14.

B. LASER PLASMA ELECTRON EMISSION -- THE EARLY TIME SIGNAL (ETS)

In this investigation, an "early time signal" (ETS) has been observed and attributed to electrons which have been emitted from the laser plasma while the laser is still incident upon the target, and which then flow through the partially photoionized background gas plasma. A number of investigators have detected the presence of electrons which are emitted from laser plasmas (Refs. 7-12), though little theoretical effort has been reported on emission from such a "plasma cathode." Herein, source mechanisms for this electron emission are discussed. Thermionic electron emission, certain plasma instabilities, and laser beam self-focusing phenomena are discussed

since all may contribute to the emission observed in this experiment.

1. Thermionic Emission From a Plasma

The concept of thermionic emission must be modified for use in describing the electron emission responsible for the ETS. Additionally, the influence of space charge and the geometry of the emitting surface of the laser plasma must be considered.

In the derivation of the Richardson-Dushman equation (Ref. 18) which describes thermionic emission, a Fermi-Dirac electron distribution function is used as the emitting surface is a metallic solid. In a plasma, the distribution function is much more closely a Maxwellian. When the Richardson-Dushman equation is modified using a Maxwellian distribution function, a planar emitting surface of plasma of area $\pi\bar{R}^2$ at a temperature T(°K) is introduced, the emission current from the planar "plasma cathode" is given by

$$i_e = \pi\bar{R}^2 ne \ (kT/2\pi m_e)^{1/2} \ e^{-\frac{W}{kT}} \qquad (9)$$

where W is the "work function" of the plasma, and space charge effects have been temporarily neglected. As discussed by Siller (Ref. 12), the work function W is of order kT, i.e., the average thermal energy of the plasma.

At times in the laser plasma formation when the laser is still incident upon the plasma, and the plasma plume has not expanded very far, the lateral extent of the plasma

is large compared to its depth, and one is correct in applying a formula derived assuming a planar rather than spherical surface. For instance, at a time 5 nanoseconds after the laser pulse arrives, the aspect ratio, i.e., lateral extent to depth from the target of the laser plasma, is about 3. As above stated, equation (9) neglects the effects of space charge, which can radically decrease the electron emission from a thermionic source and is closely tied to the ambient gas pressure in the "plasma cathode".

When electrons are removed over a significant distance (greater than a Debye length), a large potential is rapidly produced which prevents further emission and decelerates the electrons already emitted. This space charge effect is incorporated by introducing the space charge potential, U_S, into the exponent of the formula (9).

$$i_s = i_e \, e^{-\frac{eU_S}{kT}} \qquad (10a)$$

This implies that a local potential minimum is formed on the cathode surface which limits the emission. An estimation of the space charge potential which is established is obtained from an estimate of the temperatures and densities of the laser plasma and the photoionized background plasma. One uses equation (10a) for each of the two plasmas, and assumes a quasi-steady state. For the laser plasma, equation (10a) becomes

$$i_1 = \alpha n_{e_1} \sqrt{T_1}\, e^{-\frac{(W_1 + U_S)}{kT_1}} \tag{10b}$$

where the subscript 1 corresponds to the laser plasma, and 2 to the photoionized background plasma. The corresponding equation for the background plasma, which is taken to be at the reference potential, is

$$i_2 = \alpha n_e \sqrt{T_2}\, e^{-\frac{W_2}{kT_2}} \tag{10c}$$

where W_1 and W_2 are plasma work functions (Ref. 12).

To relate the space charge potential, U_S, to the plasma parameters of temperature and density, a quasi-steady state is assumed and the thermally emitted currents are equated, $i_1 = i_2$. Solving for U_S yields

$$U_S = \frac{kT_1}{2e} \mathrm{Ln}\left\{ \frac{n_1^2 T_1}{n_2^2 T_2} \right\} - W_1 + \frac{T_1}{T_2} W_2 \tag{11}$$

Where W_1 and W_2, the plasma work functions are of order kT. In detail, they are related to the ion masses as (Ref. 19).

$$W_i = \frac{kT_i}{2e} \mathrm{Ln}\left\{ \frac{T_e m_i}{T_i m_e} \right\} \tag{12}$$

Assuming the plasmas are in equilibrium, i.e., $T_i \tilde{\approx} T_e$, one solves equation (11) for U_S as

$$U_S = \frac{kT_1}{2e} \, \mathrm{Ln}\left[\frac{n_1^2 T_1 m_1}{n_2^2 T_2 m_2} \right] \qquad (13)$$

A question to be addressed here is why the electron emission is anisotropic, as implied by the experimental results later presented. At early times in the laser plasma formation and expansion processes, when these electrons are emitted, the plasma surface is nearly planar. The emission from such a planar source, then, is preferentially perpendicular to the target. It is not until the hydrodynamic expansion begins to dominate that a more nearly hemispherical shape becomes evident. Additionally, a hemispherical emission geometry will not give rise to a measurable magnetic field in the azimuthal direction, as is the ETS. Note also that the relatively small magnetic field produced by a continuing anisotropic emission will be indiscernable in the larger, more intense SGMF.

If the SGMF intensity is sufficiently strong, as has been predicted by theoretical computer modeling of the phenomenon (Refs. 13, 14), then the electron emission parallel to the target will be reduced because of the gyration of these electrons around the magnetic field lines. By symmetry, only along the target normal where the azimuthal field must go to zero, will these electrons not be influenced by the magnetic fields. This is a second explanation for the anisotropic emission of electrons from the plasmas.

2. Plasma Instabilities as an Electron Source

The presence of large thermal and density gradients, and possibly very strong magnetic fields at the focal spot (Refs. 14, 20, 21), may contribute to the formation of plasma instabilities, which in turn, may contribute to rapid local plasma heating or to electron emission directly.

One mechanism, which has been proposed to cause the acceleration in the space charge free interior and subsequent emission of electrons from a laser-produced plasma, is the result of a collisionless interaction of the laser radiation with the plasma due to the spatial change of the refractive index. This interaction has been invoked as the source mechanism for the high energy electrons of 100 KeV recently observed in laser-produced plasmas by Siller, and others (Ref. 12). They derive an expression for the minimum threshold laser intensity for which the instability occurs for temperatures of >100 e.V. as

$$I > 2.08 \times 10^{14}\ T^{0.25}\ (\text{watts/cm}^2 - \text{e.V.}) \qquad (14)$$

This restriction on the incident laser intensity seems to rule out the application of this phenomenon to this experiment, where the laser intensity was $5.0 - 9.0 \times 10^{12}$ watts/cm^2, and that of Siller, where it was 10^{10} watts/cm^2. This problem was resolved by postulating that localized laser beam self-focussing was occuring, and that filaments were created in which the local intensity of the laser beam was increased

sufficiently to meet the above criterion. The authors additionally derived an expression relating the maximum current density to the total area and number of these filaments, arriving finally at a relationship between the emission current and the laser power, P_L, as

$$j \propto b\, P_L^{\left(1 - \frac{a}{4}\right)} \qquad (15)$$

where it was assumed that the temperature of the laser-produced plasma was functionally dependent upon the laser power by a power law, i.e., $T \propto P_L^{\alpha}$. Generally, similar experimental conditions were used in this experiment as compared to that for which this theory was derived in Reference 12.

It is also possible that the emission of these fast electrons may be related to the magnetic fields which are self-generated within the laser plasma. For example, the ion-ion two stream instability is enhanced and present at significantly lower electron temperatures when magnetic fields are present (Ref. 22). As above, such an instability could cause the laser plasma which is flowing into the photoionized background gas to deposit a portion of its energy into a localized volume and cause a large local temperature increase, and in turn, an increase in thermal electron emission.

3. Pressure Dependence of Magnetic Signals From Laser Plasmas

The pressure dependence of the SGMF signal has been rather thoroughly investigated in two previous studies (Refs. 4 and 5), and will be discussed in Section III. The ETS pressure

dependence, however, has not been previously explained though a number of investigators have observed pressure-dependent electron emission current effects (Refs. 8, 9).

The background gas in this experiment is photoionized by UV photons produced by the laser plasma. To relate the emission current, i_s, to the plasma parameters, we consider the thermal emission currents crossing the background plasma laser plasma interface. Such currents are described by equations (10b) and (10c), in which space charge effects are included. From equation (10b), we have an expression for the emission from the laser plasma, and from equation (13), one for space charge potential U_s. However, equation (13) for U_s has been derived assuming that the interface between the laser-produced plasma and the background plasma, in which the probe is located, is stationary. In fact, it moves outward from the target surface with a velocity U, where U is of the order of 0.1-0.15 V_{th}, where V_{th} is the thermal velocity of a laser-produced plasma electron. As a result, the dynamic space charge potential U_s is effectively less negative by an amount $\beta \equiv (V_{th}/(V_{th}+U))^2$. The plasma motional velocity effectively increases the current out of the laser plasma. The result of this decrease in space charge potential modifies the relationship for U_s to

$$U_s = \frac{kT_1}{2e} \operatorname{Ln}\left(\frac{n_1^2 T_1 m_1}{n_2^2 T_2 m_2}\right)^{\beta} \qquad (16)$$

For the experimental situation, U is of the order of 1.0 - 2.0 x 10^7 cm/sec, while V_{th} is on the order of 10^8 cm/sec. Then if we define $\beta \equiv (V_{th}/(V_{th} + U))^2$, then $\beta \equiv 0.69 - 0.83$. To evaluate the effects of the background gas pressure upon the electron emission current, insert equation (16) into equation (10b) to obtain

$$i = g(n,T_1,T_2,m_1,m_2,\alpha)n_2^{\beta} \qquad (17)$$

where $g(n,T_1,T_2,m_{1_{\alpha_1}},m_1)$ is given by $(n_1{}^2T_1M_1)^{1-\beta}(T_2m_2)^{\beta/2}M_e{}^{-1/2}$

Note that $n_2 \to 0$, $U_S \to \infty$, i.e., the emission current ceases at low pressures. Recall that the magnetic field, B, is proportional to the emission current, i_S, and that the background density, n_2, is proportional to the background pressure, P_2. As the background pressure increases, a power law dependence, P^{β}, is expected. An additional phenomenon occurs when the pressure is increased to a value where the mean free path of the emission electrons becomes comparable to the experimental chamber dimensions. As this occurs, the electrons emitted by the laser plasma close their current paths closer and closer to the diagnostic probes, until at last the current loops close entirely between the target and the diagnostic probes. The effect is that the net enclosed current seen by the magnetic probes is zero, and no magnetic field is detected. For electrons emitted with the average thermal energy of the laser plasma, which will be calculated to be on the order of 12.5 e.V., this effect should occur at or near a pressure of 10^{-3} Torr.

To incorporate this phenomenon, recall that for energies below a KeV, the electron range in air has been observed to scale inversely with pressure (Ref. 23). The effect is to decrease the magnetic field signal with increasing pressure, i.e.,

$$B \propto i_s \propto aP^{\beta} \cdot P^{-1} = a\, P^{\beta-1} \tag{18}$$

where β has been shown to be of the order 0.69 - 0.83 for the experimental conditions in this experiment. Then, for pressures greater than about 10^{-3} Torr, the pressure scaling of the magnetic field is

$$B = a^1\, P^{-0.3} \tag{19}$$

III. PREVIOUS WORK -- RELATED EFFORTS

Four areas related to previous investigations of laser plasmas are discussed below: (A) work primarily directed toward the study of SGMFs; (B) experimental studies displaying magnetic field occurrence in laser-produced plasmas; (C) electron emission from laser plasmas; (D) background gas pressure dependence of SGMFs and electron emission from laser plasmas.

A. SELF-GENERATED MAGNETIC FIELDS (SGMF)

Stamper, et al (Ref. 2) were the first to investigate SGMFs from solid targets in an experiment studying the diamagnetism of a laser-produced plasma. They used a variable 30 to 45 ns FWHM laser pulse, produced by a Nd glass laser, a long (54 inch) focal length lens, and delivered up to 60 joules to their lucite fiber target; the ambient background gas in their vacuum chamber was nitrogen, typically at pressures of a few mTorr. A background gas pressure dependence of the field magnitude was observed, as was the effect of differing target materials. When a 250-micron (lucite) fiber was used as the target, definite asymmetrical effects ascribed to the target geometry were observed. However, no systematic parameter study was reported with respect to these effects. A theory attributing the SGMF to either or both thermoelectric effects or misaligned temperature and density gradients was presented and rather sketchily discussed. Stamper has

subsequently published related articles discussing other possible source mechanisms for such magnetic fields at very high incident laser fluxes (Ref. 27). These are not directly applicable to the work reported herein.

Another experimental study of these SGMFs was performed at the Naval Postgraduate School (NPS), Monterey, California. It was begun by Davis (Ref. 3) and has been continued by McKee and Bird (Refs. 4, 5). In their work, a 7.5-joule, 25-nanosecond FWHM laser pulse at a wavelength of 1.06μ was employed. Davis' early work used a mylar target, one magnetic probe, and one electrostatic probe in the attempt to observe magnetic fields in ambient gases of air and nitrogen at pressures of 1.0-1000 mTorr. Only a few data were taken, but the azimuthal nature of the fields was confirmed, and the first mention of the possible significance of electronic heat conduction occurred.

A more complete experimental investigation of SGMFs using magnetic probes was conducted by McKee and continued by Bird, using double electrostatic probes. The laser pulse was focussed onto a 5-mil mylar target at background pressures of 0.1-1000 mTorr. A detailed spatial mapping was obtained by passively integrating the dB/dt vs. time probe signals with an RC integrator, and then spatially resolving these data into contour plots, time being parametric. Again, as in Stamper's early work, the peak magnetic field propagated with the velocity of the laser plasma as it expanded into the background. A systematic variation of the nitrogen background pressure was performed, and an amplification of the field magnitude by

a factor of six was observed over the pressure range of 1.0 to 250. mTorr. The results were interpreted by assuming that nonparallel temperature and density gradients are responsible for these SGMFs. The fields were found to be symmetric about the target normal, even though the laser beam was incident at 30° to the target normal. Late (i.e., long after laser shut off) field reversal effects were presented, along with the explanation of these effects as being related to temperature and density gradient reversals. An important conclusion which they drew from their data was that the magnetic field was being continuously generated even after the laser had shut off.

Bird's work investigated the spatial and temporal relationships between the magnetic fields and density profiles, the effects due to various background gases and gas pressures, and differing target materials. Perhaps most interestingly, Bird observed a two-component magnetic field similar to that evident in the data presented herein: a near instantaneous magnetic pulse was observed with his magnetic probes. This "early" signal lacked the time delay behavior associated with a "frozen" SGMF pulse. Two other effects are of particular interest in his work: (1) the magnetic field was found to be spatially in front of the density profile and (2) a late time, field reversal occurred at the front of the expanding laser plasma near the axis of symmetry of the field (i.e., target normal). The second effect is important because it strengthens the contention that the nonparallel temperature and density gradients are responsible for SGMFs.

One other important study of SGMFs performed by Giovanelli and McCall (Ref. 6) used a 10-joule, 50-picosecond laser pulse. In it, their magnetic probe detected SGMFs when polyethylene targets 130 or 25 microns thick were irradiated at a background pressure of 0.5 mTorr. Magnetic fields of 1.0 to 3.0 gauss were detected which displayed a time delay corresponding to a propagation velocity of about 10^7 cm/sec, and were of a polarity which corresponded to a positive current flowing away from the target, i.e., the signal polarity was opposite to that reported by Stamper (Ref. 2), the Monterey investigators (Refs. 3-5), and that measured in this experiment. An explanation for this phenomenon has been given by Widner (Ref. 25).

Giovanelli and McCall also successfully performed Wright's "gedanken" experiment (Ref. 14) of reversing the roles of the temperature and density gradients (see (5)) and therefore, reversing the magnetic field polarity by using two laser pulses separated in time by eight nanoseconds. They also observed an intense electrostatic discharge when the laser was first incident upon their targets, but no signal corresponding to the ETS.

In summary, then, experimental efforts relating to SGMFs indicate the following: (1) the $(\nabla T_e \times \nabla n_e)$ term in equation (5) is responsible for the observed self-generated magnetic fields; (2) the late time behavior of the self-generated fields is closely coupled to the ambient background gas pressure and degree of photoionization; (3) experimental observations at the Naval Postgraduate School confirm the existence of the

early signal investigated herein; and (4) all prior data have been taken at a wavelength of 10600 Å and at laser pulse lengths of >20 nanoseconds FWHM.

Theoretical efforts to find and model the source mechanisms of these SGMFs have occurred at a number of laboratories over the last two years. These include the theoretical efforts of Stamper to more fully describe the generation of SGMFs (Ref. 24) and the computer simulation efforts of Wright and Widner at Sandia Laboratories (Refs. 13, 14), Zimmerman, Scharlman, and Wood at Lawrence Livermore Laboratory (LLL) (Ref. 20), and Clark and Book at the Naval Research Laboratory (Ref. 21). In these efforts, the objective was to either modify pre-existing one- or two-dimensional computer codes to include the (∇P_e) source term for the fields, or to write such a computer code to simulate these SGMFs. Generally, the regime worked in was that of the strong field limit, whereby the magnetic fields generated react back upon the expanding plasma and strongly influence its expansion characteristics. The results predict that for multi-hundred joules laser pulses delivered in tens of picoseconds, megagauss fields near the focal spot should be produced (Refs. 13, 20, 21, 26). Late time behavior, i.e., hydrodynamic expansion and subsequent laser plasma -- ambient plasma interactions have not been modeled in similar detail, though Widner (Ref. 13) has developed a self-similar scaling model for these fields.

In all such computer experiments, the fields generated are azimuthal and created primarily in toroidal rings at the

edge of the focal spot (see Figure 1) not in the center of the laser focal spot. A supporting experimental result, observed herein is that magnetic fields with magnitudes of up to one-half the original field were measured when the hole formed in a thin mylar target by a first laser pulse was fired into by a second laser pulse. In other words, there is experimental evidence which confirms the idea that the SGMFs are produced primarily at the edges of the focal volume where density and temperature gradients are nonparallel, rather than in the center of the focal spot as originally proposed by Stamper.

B. RELATED EFFORTS/SIMILAR PHENOMENA

A number of authors have reported studies on laser-gas breakdown in which phenomena occurred which elucidate the above discussed SGMFs. Korobkin and Serov (Ref. 1) measured a spontaneous magnetic dipole moment in a laser spark in 1967. Unfortunately, no further details are available than those sketchily reported in a short letter. The magnitude of their measured magnetic moment, 2-3 gauss x cm^3 may be interpreted as arising from the gas breakdown in which the initial particle densities a thousand to a million times less dense than those characteristic of solid target laser plasmas. Field reversal was observed by varying the portion of the focussing lens through which the beam passed before initiating gas breakdown. This was a puzzling effect which the authors attributed to turbulence in the plasma and ray optic effects. Their experiment is the first found in the literature in which magnetic

fields have been spontaneously generated by a laser incident on either a gas or solid target.

Askar'yon, and others (Ref. 27) used an inductive loop and two separate laser pulses to detect currents induced in the laser plasma by both laser pulses. They stated that a nonpotential field, $E_{n.p.}$, is generated by radiation pressure, which produced closed current loop within the laser plasma. They varied the signal polarity by changing the incidence angle of the beam relative to the target normal, an effect not observed in any of the experiments relating to SGMFs produced by laser irradiation of solid targets. By spacing two separate laser pulses 240 ns apart, they observed an order of magnitude increase in signal strength, which they attributed to an increased preionized volume through which the B field producing currents could flow. They also noted that by reversing their Q-switching prism rotation direction, they reversed the polarity of the second magnetic signal. This was attributed to an incidence angle effect, and not further discussed. The above experiments present data which indicate the presence of closed current loops within the laser plasma and in the background gas are necessary conditions for the production of self-generated magnetic fields.

C. LASER PLASMA ELECTRON EMISSION

The early time signal investigated in this work is attributed to electron emission from the laser plasma into the background plasma, produced by photoionization of the ambient background gas. In addition to measuring the presence of such

electrons, investigators have studied: (1) the effects of the background gas pressure on the total emission current (Refs. 8, 9, 11); (2) the anisotropic nature of this emission (Ref. 10); (3) the influence of laser power density (Ref. 9); (4) the degree to which space charge may be important in such emission (Ref. 11); (5) the role of absorbed gases in electron emission processes (Ref. 9); and (6) the importance of nonlinear and/or nonthermionic source and accelerating mechanisms in such emission (Ref. 12). Below, these experimental results will be briefly reviewed and the portions applicable to this experiment pointed out.

Arifov, and others (Ref. 8) studied laser induced current pulses from a gas target with microwave and magnetic probe diagnostics; electron currents were measured using the experimental chamber as the electron collector. Background gas pressures of from 3.0×10^{-6} to 0.5 Torr, and a laser pulse of 1.5 joules in 60 ns FWHM, were used. A 10-20 gauss magnetic field was externally applied parallel to the target normal. They measured an electron current pulse arriving very much earlier than the main plasma cloud, which they believed to be space charge neutralized by a "foreplasma" created by the initial U-V radiation pulse from the laser produced plasma. This effect was observed with both microwave and magnetic probe diagnostics. They observed an additional magnetic signal with a magnetic probe from the foreplasma at pressures above 0.1 mTorr which preceded the main diamagnetic signal from the plasma cloud. In the context of the experiment reported herein,

this result is interpreted as one of the first experimental observations of the ETS. As a function of pressure, the peak in their measured electron current pulses of 100 amperes occurred at 10.0 mTorr. Below 1.0 mTorr a power law dependence of the current on the pressure, of the form $i_e = kP^a$, where $0.5 < a < 0.7$ for their range of experimental investigation, was measured. They attributed the electrons to either thermionic emission from the plasma or emission from the solid target by interacting photons emitted by the plasma.

Isenor (Ref. 9) performed a series of experiments in which the background gas pressure of O_2, N_2, and H_2 was varied and the effects on electron emission from solid Zn and Ta targets studied. The laser energy was 50 millijoules delivered in 50 ns FWHM. Background gas pressures of 10^{-6} to 10^{-4} Torr were used. Two electron peaks were observed, one coincident with the laser pulse, the second time delayed by the approximate transit time of the plasma from the target to the collector. The prompt component of the emission was stopped by the application of a 10 V negative bias on the collector, from which the author inferred a maximum electron energy in the prompt component of 10 e.V. Results also indicated that absorbed gas pressure was found to be reasonably linear, i.e., $i_e = kP^a$, where $a = 1$, over the range of pressures used (see equation (17)); peak currents detected were of the order of 10 amperes.

Basov and others (Ref. 28) interpret their data to indicate an apparent charge separation caused by the emission of electrons

by the plasma produced by their laser on solid targets. Using electrostatic probes, they measured a null point between positively and negatively charged components of the plasma flare, evaluated its velocity as a function of the time from laser pulse arrival onto their target, and its velocity dependence on the laser power. A short statement was made that the decaying flare emits electrons that should give rise to a magnetic field whose magnitude is tens of oersteds (gauss). However, no further explanation or discussion was presented.

Andreev and others (Ref. 11) studied thermionic emission from a plasma produced by a Q-switched laser (3.5 joules in 50 nanoseconds FWHM) on solid Al and Pb targets at background pressures of from 10^{-1} to 10^{-4} mTorr of air. Most measurements, however, were obtained at pressures of between 10^{-2} to 10^{-3} mTorr. Their measurements led them to the conclusions that the electron emission is limited in their experiment by space charge effects, and that a minimum in the potential is formed in the target collector gap of several hundred volts. Maximum currents were on the order of one ampere with an accelerating potential of an unspecified magnitude placed on the anode (collector). Experimentally determined temperatures were on the order of 10 e.V., and no dependence of the plasma expansion velocity upon laser energy was observed.

Langer and others (Ref. 10) measured the anisotropy in electron and ion emission from a laser-produced plasma by using multiple electrostatic shielded detectors in various symmetry planes about the target normal. A background pressure

of 0.001 mTorr was used with two lasers that produced 30 Megawatt pulses at wavelengths of 6943Å and 10600Å respectively. When the laser beam was incident normal to the target, emission was found to be cylindrically symmetric about the target normal but to consist of multiple lobes. Laser beam polarization was shown to have no effect on the emission by a systematic variation of this parameter. Astigamatism, however, artifically introduced into the experimental arrangement by orienting the focussing lens at 30° to the laser beam axis, produced a significant skewing of the electron and ion angular emission characteristics. A reasonably isotropic emission was observed only for a carbon target, but no explanation was offered for this result.

Three papers presented at the Monterey APS Division of Plasma Physics meeting in November 1972 support the idea that electrons are emitted from laser plasmas in significant numbers and energies ranging from a few e.V. to many KeV.

Godwin, and others (Ref. 29) imply the presence of a very high energy stream of electrons from their X-ray polarization measurements. These data were obtained from an experiment at Los Alamos Scientific Laboratory (LASL) in which a polyethylene target was hit with a 10-joule, 50 picosecond, Nd glass laser pulse. The background gas pressure was 0.5 mTorr. The beam was incident at an angle of 13° relative to the target normal, and a hole was formed in the target during each shot. Shearer, and others (Ref. 30) similarly imply a high energy non-Maxwellian tail in the electron distribution function from their laser

plasma experiments in which anomalously high reflectivities were measured. As in the LASL data, no direct measurement of electron flux was made. Olsen, and others (Ref. 31) at Sandia Laboratories, correlate neutron production and high reflectivity, and imply a non-Maxwellian tail in the electron distribution function in their laser plasma experiments.

D. PRESSURE DEPENDENCE OF THE SGMF AND THE ETS

Previous investigators have experimentally measured, and theoretically modeled the observed dependence of the SGMF signals as a function of the gas pressure of the ambient background gas. Additionally, several investigators have observed the dependence of the intensity of the electron emission from laser plasmas as a function of the gas pressure, though no theory of the pressure effects has to date been postulated.

Bird (Ref. 5), who continued McKee's (Ref. 4) work, has proposed a model of the pressure dependence of the SGMF signals, which is related to the interaction of the expanding plasma by the background gas. In his model, the background gas acts to confine the expanding laser plasma, allowing the axial density gradient responsible for the SGMF signal to increase in magnitude in direct proportion to the cube root of the confining background density, i.e., $B(max) \propto p^{1/3}$. A good correlation between experimental and theoretical predictions was obtained for pressures up to 250 mTorr, where the peak magnetic field intensity began to decrease with pressure. This high pressure decrease which began at 250 mTorr was explained as being caused by the production of a reverse polarity magnetic field

near the front of the expanding laser plasma. Such a field is said to result from a strong momentum coupling to the background gas, i.e., the laser plasma "piles up" on the background gas, regenerates nonaligned gradients and in turn generates a magnetic field of opposite polarity to that originally produced. Such an effect has been theoretically predicted using a two-dimensional computer simulation of such fields by Widner (Ref. 25).

The pressure dependence of electron emission has been previously investigated, though no theoretical explanation for the observed pressure dependencies was offered, except for that developed in the theory section herein.

IV. EXPERIMENTAL ARRANGEMENT AND EQUIPMENT

The equipment used for this investigation consists of four different laser systems, a fast photo diode to monitor laser output energy and power, a vacuum system and the experimental chamber, gas back fill manifold, magnetic probes, and recording oscilloscopes. Figure 2 is a block diagram of the arrangement with the magnetic probes shown schematically.

A. VACUUM CHAMBER

The vacuum chamber was constructed of stainless steel with ports arranged as shown in Figure 3. The top was sealed by a 13" by 13" square piece of one-inch plexiglass constructed with magnetic probe vacuum feed throughs to enable systematic variation of the probes' locations from outside the evacuated experimental volume. When miniature probes were constructed, the feed throughs in the top port were eliminated. The side ports were plexiglass and used for vacuum electrical feed throughs for the probe signals. The front optical port was a 5" diameter uncoated quartz flat. The metal foils used as targets in this work were mounted on a rotating holder so that multiple shots could be obtained without breaking vacuum. A 28-cm meniscus lens was used for focussing because of damage sustained at the internal focus of the planoconvex lens used initially.

The vacuum system and pressure gauging system consisted of a 2" air-cooled diffusion pump, without cold trap, and

mechanical roughing pump. The ultimate vacuum obtainable with this arrangement was 5×10^{-6} Torr. A pressure of 0.5 mTorr was obtained with a five-minute pump-down time. An adjustable leak was used to accurately vary the fill gas pressure in the regime of $5 \times 10^{-6} - 10^{+1}$ Torr.

B. LASERS

Several laser systems were used as energy sources during the course of this experiment. Four pulse lengths: 4 ns, 6 ns, 16 ns, and 40-50 ns, were studied at a wavelength of 6943Å (ruby), a pulse length of 30 ns was used at a wavelength of 10600Å (Nd doped glass), and one pulse length of 80 ns was used at a wavelength of 10.6μ (CO_2). Data and interpretation of the information obtained using the CO_2 and Nd lasers are presented in Appendix D.

A Spacerays Time Varying Reflectivity (TVR) laser system was used in obtaining most of the data presented here. It was operated in 4, 6, and 16 ns pulse widths at a wavelength of 6943Å (see Appendix A for a discussion of TVR lasers).

The second laser system used in this experiment was a Korad K-1500 Q-switched ruby system. The characteristics of this system were a 40-50 ns FWHM pulse length and an energy output up to 5.0 joules. The data obtained with the K-1500 system illuminated the differences between the short pulse data obtained with the Spacerays TVR laser system and those which were obtained at the longer 40-50 ns pulse length.

The Korad K-1500 system was also converted to operate in the TVR mode at a pulse length of five nanoseconds FWHM. The

laser power available from this system was from 0.1 - 1.1 gigawatts.

All the data taken on the Spacerays TVR and K-1500 laser systems were at laser beam incidence angles of 45° to the target normal. The reason for this incidence angle was three-fold. First, the original objective of this experiment was to attempt to reproduce a series of laser-produced X-ray experiments, and to correlate magnetic field signals with X-ray data; these experiments had been performed at a 45° incidence angle. Secondly, a non-normal incidence angle allowed the collection of data along the target normal without interference with the incident laser beam. Thirdly, laser damage caused by laser energy reflected from the target which retraces its optical path through the laser rods is minimized by using non-normal incidence angles.

C. DELAY LINES

Co-axial lines were calibrated for time delay and signal attenuation and used to time-delay the incident laser pulse and the magnetic probe signals for simultaneous recording on one oscilloscope. The incident laser pulse, undelayed in time, was used to trigger the oscilloscopes on which these data were recorded. In this manner, a measure of the delay time between the laser pulse and the arrival of the magnetic probe signals is obtained whose accuracy is limited by the digitalization of the data which were recorded on Polaroid.

Table 1 is a summary of the delay lines used and their characteristics.

TABLE I

Delay Line Characteristics[+]

Delay Line Number	Measured Time Delay (ns)[++]	Transmission Factor (%)[+++]	Where Used
1	73.5	82	-----
2	102.5	78	-----
1 + 2	176.0	67	Probe signal
3	81.0	82	-----
4	67.0	81	Laser signal delay
5	75.5	82	-----
3 + 5	157.0	68	Probe signal delay
6	123.0	--	Laser signal delay

+ Delay lines constructed of coil RG58U cable.
++ Error ± 2 ns.
+++ ±3% measured at 5MHz.

The cables were not corrected for their frequency dependence attenuation effects since the effect is negligible in the range over which significant signal frequency components were observed in the data (1-20 MHz).

These signals were recorded on Tektronix 519 and Hewlett Packard 180 oscilloscopes having rise times of 0.3 ns and 2.0 ns, respectively.

D. SIGNAL DIAGNOSTICS

The diagnostic used to evaluate the presence, time history, magnitude and other characteristics of the SGMFs and the ETS was magnetic (inductive) probes. A fast photo diode was used to monitor the laser output pulse shape and energy for the ruby and Nd glass laser; a photon drag detector was used to monitor pulse shape and energy on the CO_2 laser.

Magnetic inductive loops have been used in the field of plasma physics to observe time varying magnetic signals under a large variety of experimental conditions, and their design and construction have varied quite widely. Initial design parameters, i.e., coil diameter, wire size and number of turns, electrostatic shielding, coil insulation, shaft length, and co-axial cable connection to the probe, were comparable to those constructed by McLaughlin (Ref. 32) and used by Davis, McKee, and Bird. A typical probe of this design is shown schematically in Figure 4. As the experiment progressed, the probes were redesigned in order to be able to insert them at desired angles and positions to check the cylindrical symmetry of the fields, and to evaluate the perturbations caused by two or three probes. Probes which were entirely enclosed within the evacuated experimental chamber were constructed. Additionally, as frequency response was a primary probe design parameter and strongly dependent upon the wire size used to wind the coils, i.e., smaller diameter wire increased the magnetic probe inductance an undersirable effect which degrades probe frequency response, numerous probe designs were tried before #28 enamel-coated magnetic wire was found to yield satisfactory results. Other probe design changes included the elimination of the double electrostatic shield, and the direct soldering of the probe coil to microdot or RG174 A/U cable. Figure 5 is a schematic drawing of the new probe design, minor changes being incorporated into each probe as it was constructed. Probe calibration was performed in the manner of Phillips and Turner

(Ref. 33) with carefully wound Helmholtz coils, whose radius and turn separation were 0.94 inch, and is discussed in some detail in Appendix B.

V. DATA REDUCTION AND ANALYSES TECHNIQUES

The raw data in this experiment were polaroid oscilloscope records of the magnetic probe signals. These signals, proportional to dB/dt via Faraday's law, were digitized, the probe response folded into the data, high frequency noise filtered out, and the signals integrated on a computer to obtain the magnetic field as a function of time.

The data obtained were not integrated directly with a simple R-C integrator for a number of reasons. First, integration by its nature is a smoothing process, and tends to eliminate the small effects of interest in this study, specifically, the ETS as compared to the SGMF signal which is of greater magnitude. Secondly, at high enough frequencies, a passive integrator becomes nonlinear, and will distort high frequency components of the signals. Thirdly, the signals' strengths obtained were on the order of volts, and after passing through the severe attenuation present in a passive integrator, which would correctly integrate the fast rising dB/dt signals present in the experiment, signal-to-noise would have presented serious problems. Active integrators, i.e., feedback amplifiers, were considered but available oscilloscope plug-ins with this capability had a maximum band pass of 13 MHz, which was insufficient for these studies.

The polaroid traces were digitized by the photo reduction branch of the computer software section at the AFWL, and

placed on magnetic tape. Straight line segments were used to represent the data, and typically between 60 and 130 points were read off each polaroid picture. Most traces were taken at 50 ns/division, with 10 divisions/picture. Therefore, an upper frequency which could be used in the data analyses program is given as $\frac{1}{2\Delta t}$ where t is the sampling time interval. Δt was typically 10 ns, so f_u was 50 MHz. The lower frequencies limit which one can "see" is $\frac{1}{2\Delta t'}$ where t' is the total trace time sweep. This was typically 500 ns, giving 1 MHz as the lower frequency limit.

The signals were computer-processed and the following information was available as output: maximum and mimimum dB/dt and B (t) values, a fourier series representation of the input data, corresponding times for these maximum and minimum values, a digital time history of B (t) and dB (t)/dt as functions of time after laser pulse arrival, and computer-generated plots of raw, and filtered, dB/dt and B (t) data.

Digital filtering of the data has been used to eliminate the high frequency noise present in the data. This noise is direct electromagnetic pick-up by the oscilloscope vertical amplifiers of signals generated by the laser power supply which was co-located in the experimental area. The digital filtering technique used was adapted for computer use by Ormsby (Ref. 34) in 1958. Appendix C presents the theory of this digital filtering technique, and an error estimate applicable to the specific filtering technique used in processing these data.

VI. DATA PRESENTATION AND DISCUSSION

The experimental data presented next are discussed and analyzed; estimates of pertinent plasma parameters are included where appropriate. This section is divided into four portions. The first is concerned with data from the Spacerays laser system. The second section presents and evaluates the data obtained on the K-1500 ruby laser system used in this investigation. The third section presents the pulse length dependence of the ETS and SGMFs. The fourth section is the presentation and discussion of the pressure dependence experiment performed with the Spacerays laser system, which provides additional insight into the electron emission and SGMF phenomena.

A. SPACERAYS TVR LASER MAGNETIC FIELD DATA -- 4 NS PULSE LENGTH

The following objectives were sought in gathering the data on the TVR laser system: (1) to map the ETS and SGMF in space and evaluate their magnitude and duration; and (2) to quantify the effects of laser pulse length and shape, and total energy output on the ETS and SGMF signals.

1. Magnetic Character and Symmetry of dB/dt Signals

To assure that the ETS and SGMF signals were not electrostatic pick-up, the magnetic probes were rotated between successive laser shots. The reversal of the signal polarity assured that the signals are magnetic, and not electrostatic as reported by others (Ref. 4). Shown in Figure 6 are two

data, redrawn for clarity, of dB/dt data taken with the probe oriented to detect the azimuthal component of B at 0° and then with the probe at 180°. The signal reversed, confirming the magnetic character of both the ETS and SGMF.

Another experiment was carried out to confirm the azimuthal magnetic symmetry of the magnetic fields produced in this experiment for the 4 ns FWHM pulse length. The magnetic probes were positioned at identical (r,z) positions, and then the 'r' coordinate was inverted, i.e., the probe was repositioned at (-r,z), and the magnetic probes signals were recorded. The results are shown in Figure 7, parallel those of previous investigators (Refs. 4, 5), and indicate that the fields are azimuthally symmetric.

These experiments verified that the ETS and SGMF signal were azimuthally symmetric about the target normal, and magnetic in nature.

2. Pre-lase Contribution to Magnetic Derivative (dB/dt) Signals

Pre-lase has been observed to contribute significantly to the measured dB/dt signals on the Spacerays laser system. The presence of these pre-lase effects is easily detected by subtracting the time delay introduced by the delay cables, and then noting that the magnetic field signals appear to begin before the Q-switched portion of the laser pulse is incident upon the target surface. Figures 8, 9, and 10 display the phenomenon for three different laser pulse shapes; the two laser pulses shown in Figures 9 and 10 were intensionally modified to display and evaluate the importance of the effect.

Note that the rise time of the laser pulse shape, f(t), and the dB/dt signal, can be put into a one-to-one correspondence on all three traces shown, in agreement with Stamper's early phenomenological model of the source term for the SGMFs, which related the dB/dt signals to the laser's temporal pulse shape, f(t). The explanation of this effect is that during the time in which the internal cavity photon density at the lasing wavelength is increasing, photon leakage from the laser oscillator cavity was sufficient to generate its own temperature and density gradients and, therefore, its own "spontaneous" magnetic field, before the main laser pulse arrived on target.

The significance of the effect is that the magnetic field rise time is lengthened in proportion to the amount of pre-lase which occurs. In the limiting case of no giant or Q-switched pulsed (Figure 10), the TVR laser operates as does a "conventional" Q-switched system, i.e., all the photons which reach and strike the target having "leaked" out the cavity's partially transmitting front mirror, in a pulse typically on the order of 30 ns FWHM. As the proportion of the energy in the giant TVR laser pulse increases, relative to that in the "foot" or pre-lase portion, the field rise time decreases and its absolute magnitude increases. In other words, the shape of the laser pulse incident upon a target directly affects the magnetic field rise time and intensity. Widner (Ref. 13) has proposed the use of a "foot" on laser pulses to decrease the maximum self-generated magnetic field intensities, for situations where such fields and their effects

are undesirable, as in laser fusion pellet experiments. His theoretical proposal is based upon the observation that such a "foot", operating as did the pre-lase in this experiment, generates a density gradient. Then, the magnitude of the SGMF signal, which is functionally dependent upon the product of the temperature and normalized density gradients as

$$B \propto \frac{1}{ne} \frac{T_e}{L_T} \frac{n}{L_n} \approx \frac{T}{eL_T L_n} \qquad (20)$$

where L_n and L_T are the density and temperature scale lengths respectively, would be decreased when the main Q-switched pulse arrived on target because the pre-lase effectively increases L_n. The effects of pre-lase are also important in situations where thin foils or pellets are to be used as targets. Malozzi, for example, observed that his thin foil targets were completely vaporized by pre-lase before the Q-switched pulse ever arrived at the target (Ref. 35). In summary, the effect of pre-lase was observed to directly influence the rise time and magnitude of the SGMF signals obtained with Q-switched lasers.

3. SGMF and ETS Spatial Mapping -- Spacerays TVR Laser

The radial and axial location of the magnetic probes used in this work, relative to the focal spot of the laser beam, were systematically varied to map the spatial and temporal characteristics of the SGMF and ETS. The target normal and the incident laser beam formed the plane in which these magnetic probes were placed in gathering these data. For this reason, when (r,z) positions are referred to, the "r"

coordinate, though strictly defined as the square root of the sum of the squares of the x and y coordinates, is very nearly the value of the x coordinate. Figure 11 is a schematic of the coordinate system with respect to which probe positions are referred. The scan data were obtained with the laser operated in the 4 ns FWHM mode. A 28-cm meniscus lens was used to focus the 3/4" laser beam to a focal spot diameter of approximately 150 microns, at a 45° angle of incidence (relative to the target normal), onto a 20-mil copper target. Figure 12 is a schematic of the (x,z) plane as seen from above showing the locations of the axial and radial scan lines and the extent of the mapping.

4. Axial and Radial Scan Data Presentation

The SGMF and ETS derivative data obtained in this mapping were integrated to produce magnetic field intensity. Figures 13 through 15 are these maximum ETS and SGMF intensities plotted as functions of spatial locations (axial and radial) for the laser parameters and pressures indicated. A single pressure of 50 mTorr was selected because it was sufficiently high to produce easily detectable SGMF signals. Radial scan information is presented at 2, 6, 10 and 15 mm from the plane of the target surface in Figures 13 and 14, the target normal being taken as origin (Figure 12). Axial scan data have been obtained and are presented at distances of 1.5, 4, 9, and 22 mm from the target normal, in Figures 15 and 16, where the target surface is now taken as the origin for each scan. The closest axial scan for which ETS data are available is 4 mm

(Figure 15) because for "r" values less than 4 mm, no discernible ETS was present.

The ETS and SGMF data are both plotted on Figures 17 (radial scan) and 18 (axial scan) to display the spatial rates of decay of the two signals. Figure 19 shows the extrapolation of the measured maximum magnetic field intensity back to the focal spot, for the two scans "r" = 1.5 mm, and "z" = 2. mm.

5. Axial and Radial Scan Data: General Characteristics

An important observation which is characteristic of all the dB/dt data must first be presented before the scan results can be correctly interpreted. This observation is that to within the ±4 ns timing accuracy of the arrival of the laser pulse on target, relative to the beginning of the dB/dt signal, the ETS occurs simultaneously at all probe locations, and that its time extent of $\tilde{\sim}$12-15 ns varied less than 30%. Secondly, though it reached its maximum value significantly later in time, the SGMF data obtained with the Space-rays laser began within 10 ns of the time that the peak of the laser pulse arrived on the target. There also was no time delay in the arrival of the SGMF as the probe was moved further from the laser focal spot. In other words, there is no increase in the magnetic field rise time for either the ETS or SGMF, as the probe was moved out from the laser focal spot, either radially or axially, simply a decrease in the value of the peak intensity of the magnetic fields. One exception needs to be noted here, that being a somewhat longer time duration SGMF signal which was measured near the target

normal ("r" = 1.5 mm scan). However, even in this case no increase in the field half width occurs as the distance from the laser focal spot is increased.

6. Estimation of Laser Plasma Parameters

To adequately interpret the magnetic field data presented in Figures 13 through 19, estimates of the basic parameters characterizing the laser plasma produced in this experiment are necessary. These include the plasma temperature and expansion velocity, its electron density, the electron current responsible for the ETS, the Debye length, the magnetic field diffusion time, and the magnetic Reynold's number in the laser plasma. These parameters can now be estimated using a theoretical model of the production and expansion of laser produced plasmas, and data from previous investigations of similar laser-produced plasmas.

An estimate of the temperature of the plasma which has been generated with the Spacerays laser requires a knowledge of the number of atoms in the laser plasma. The mass vaporized from a metal target by a 1.0 joule, 4 ns Spacerays laser pulse has been measured to be 50.0 micrograms (Ref. 36). Then, if a 1% degree of ionization (Ref. 4) and a 1% conversion of the laser energy to electron temperature (Ref. 37) is assumed, 4.7×10^{15} atoms share 10 millijoules of energy, and a temperature of 12.5 e.V. is obtained for the plasma. This temperature is comparable to that estimated by McKee (Ref. 4), where he then further assumed an average charge state of 2.3. Using this average $\bar{z}$, the plasma electron number is given by

$\bar{z} \times N_{ionized} = 2.3 \times 4.72 \times 10^{15} = 1.08 \times 10^{16}$ electrons. Using a plasma radius of 4.75×10^{-2} cm (see next page) results in an electron density of 1.2×10^{19} e/cm^3.

The plasma expansion velocity has been determined by many investigators of laser plasmas to be on the order of 10^7 cm/sec at early times in the expansion process (Ref. 7). In a background gas density of 50 mTorr (1.8×10^{15} atoms/cm^3), for time scales of hundreds of nanoseconds, the expanding plasma has been observed to decelerate to velocities of the order of 10^6 cm/sec (Ref. 39). However, since the processes under investigation for the ETS occur very early in the laser plasma formation process, the larger figure of 10^7 cm/sec will be used to characterize the plasma.

To estimate the current responsible for the ETS, a relationship between current and magnetic field intensity is required. Here, the relationship used is that for a long straight wire -- the current is assumed to flow from the focal spot outwards in a cyclinder, parallel to the target normal. In this approximation, the return current path is assumed to be at infinity, while in reality it is known to occur in the background gas which has been photoionized by the U-V radiation from the laser plasma. Inherent, then, in this calculation is the assumption that the probe is inside the return current sheath, otherwise the signal is partially shielded from the probe. The formula relating current and field intensity in this situation is the Biot-Savart Law and given by

$$B = 2i_s/cr \qquad (21)$$

The current then, which generates a 10 gauss magnetic field at a distance of 1.0 cm from the target normal (symmetry axis) is given as $I_S = Bcr/2 = 50$ amperes. To evaluate the ability of a thermionic source to generate this current, an expression for the electron emitting area of the plasma is necessary (see equation (10a)), as is an estimation of the space charge potential limiting the electron current drawn from the plasma. The plasma radius used to estimate the current which can be drawn from such a source is that obtained at the end of the 4 ns laser pulse using the initial 75 micron focal spot radius (Ref. 38) and the final plasma radius of 4×10^2 microns, obtained assuming $r = vt$, where $v = 10^7$ cm/sec, and t = laser pulse length of 4 ns. The resulting value of $\bar{R}$ is 4.75×10^{-2} cm. To evaluate the maximum current from a non-space charge limited thermionic source, Equation 9 is used. Inserting numerical values of T = 12.5 e.V., $\bar{R} = 4.75 \times 10^{-2}$ cm, and $n = 1.2 \times 10^{19}$ e/cm^3 yields $i_e = 6.4 \times 10^5$ amperes. The observed fields, then, can be readily produced by a thermionic source.

If we return to Equation (10a), the retarding potential, U_S, can be evaluated. Inserting $i_S = 50$ amperes, and $i_e = 6.4 \times 10^5$ amperes, U_S is calculated as 118 volts, a value in agreement with those calculated by Andrev, et al, in their study of thermionic electron emission from laser plasmas (Ref. 11).

The Debye length in this laser plasma is a function of temperature and density and given as (Ref. 15)

$$\lambda_D = 6.9 \times 10^{-2}\ T^{1/2}\ n_e^{-1/2} \qquad (22)$$

for T in °K and n_e in number/cm^3. For the plasma herein produced, the Debye length is 7.28×10^{-7} cm, or 73 Å. The magnetic field diffusion time was defined and an expression derived for its value in the theory section, as equation (7).

$$t_o = \frac{4\pi\sigma L^2}{c^2} \qquad (7)$$

The value of the scale length, L, applicable here is evaluated by noting that the temperature and density gradients responsible for the SGMF signals occur at the outer edge of the plasma over a distance less than or equal to the total plasma thickness; the value of this plasma thickness used is the thickness of the plasma and equal to 4.75×10^{-4} m. The conductivity used is from Spitzer (Ref. 15), assuming an average charge state $\bar{Z}$ of 2.3 (Ref. 4) as

$$\sigma = 2.62 \times 10^{-4}\ \frac{T^{3/2}\ \gamma_E}{\bar{Z}\ \ln \Lambda} \qquad (23)$$

$$= 3.5 \times 10^{2}\ \text{mho/cm}$$

Inserting this value into Equation (7) yields a diffusion time of 10^{-8} sec, comparable to the full width of the laser pulse.

In other words, in this experiment conditions were such that the diffusion time is so short that the self-generated magnetic fields began to dissipate appreciably in magnitude before the laser shuts off. This conclusion is born out in a computer simulation of the generation, propagation, and decay of SGMFs made by Widner (Ref. 39). In this work, the general conclusion drawn is that for T $\lesssim$ 100 e.V., magnetic diffusion is significant, and for T $\lesssim$ 10 e.V., it is certainly very dominant.

To evaluate the magnetic Reynold's number, as defined in equation (8) as

$$R_m \equiv \frac{4\pi LV\sigma}{c^2} , \qquad (8)$$

values of plasma expansion velocity, conductivity, and scale length are inserted to yield $R_m = 1.1$. This value of R_m describes the situation in which the diffusion and convection terms in Equation (5) are of the same order of magnitude, and so of approximately equal importance. Note that the values used in evaluating R_m were those applicable at the time the laser pulse is over. After this time, the conductivity σ, and plasma expansion velocity V decrease, while L increases; the parameters of σ and V decrease more rapidly than L increases, so R_m grows smaller with time, and magnetic field diffusion increases in importance.

7. Interpretation of Radial and Axial Scan Data

The simultaneous occurrence of the SGMF signal in the magnetic probe network at all probe locations, indicates that

the field transport is not convectively dominated (see Equation (5), Theory Section), for if it were, a time lag corresponding to the transit time of the laser plasma from the target to the probe location should be observed. No such delay was observed in this experimental investigation. The similar simultaneous appearance of the ETS signal poses a different problem, which is explained as follows. The ETS electron emission occurs in a forward peaked cyclinder or cone, with a return current path which closes through the background gas. The propagation velocity of the emitted electrons will be of the order of 10^8 cm/sec or greater, beyond the experimental resolution of this experiment. The electrons arrive at the probe location in several nanoseconds, whereupon they induce a potential in the probe, since they constitute a time varying current.

Figure 13 is the ETS radial scan data, at axial z values of 6, 10, and 15 mm. No ETS data along the z = 2 mm scan are plotted, since only at a position r = 26 mm could the ETS be clearly discerned from the SGMF signal. The maximum magnetic field intensity for the three scans presented occurs at larger and larger radial coordinate values, as one moves the probe to larger and larger axial coordinate values. This indicates that the source of the early field is not a collimated electron beam, but one which diverges in moving further from the target. At larger axial locations, weaker fields are observed, indicating that the field dissipates with distance, or that the probe has moved outside the current loop. Estimating a conical beam half angle from the location of the peak

magnetic field intensity for the 6 mm scan yields $\theta = 45°$, at 10 mm, $\theta = 37°$; at 15 mm, the location of the maximum field is not clearly defined, and a 5 - 6 fold decrease in the maximum field intensity is evident.

Figure 14 is the axial scan ETS data at positions of r = 4, 9, and 22 mm. Here no ETS data are evident inside a radius of 2 mm from the target normal, though SGMFs of up to 25 gauss were measured along the r = 1.5 mm scan line at z values of up to 20 mm. The most noticeable feature on this figure is the movement of the peak in the ETS intensity toward larger axial locations, as the "r" scan location moves further from the target normal. For a collimated electron beam, the radius at which the maximum ETS intensity occurs would be independent of the axial location, since the location of this maximum corresponds to the radius inside which all the electron current would flow. Experimentally, this position increases with increasing values of z. This is explicable if the electron stream is conical since for a conical beam the position of maximum intensity should increase with z, i.e.,

1. cylindrical beam: $r(B_{max}) = \text{constant}$
2. conical beam: $r(B_{max}) \propto z$

The conical emission may be a result of the complex multiple lobed structure observed by Langer (Ref. 10), or to a space charge repulsion within the emitted electron beam itself. A third possible explanation is that the return current which flows within the ambient background plasma screens the magnetic

probes from an increasingly larger portion of the electron current as they are moved further from the target.

The radial SGMF data are plotted for z values of 2, 6, 10, and 15 mm in Figure 15. Superimposed thereon are two spatial scaling laws which have been previously observed in SGMF studies (Refs. 2, 4, 6): $B \propto R^{-1}$ and $B \propto R^{-3}$. One should note that these scaling laws are only directly applicable to the z = 2 mm scan, since only it can be properly extrapolated back to the focal spot, all other scans being referenced to the target normal as the r = 0 location. This fact is responsible for the turnover and fall off in the measured intensities as the radial coordinate is decreased, since by symmetry the fields must vanish along the target normal. Note also on this plot that the curves for the various axial locations gentle in slope from near -3 at z = 2 mm toward -1 at z = 15 mm.

Figure 16 displays the SGMF data at values of r = 1.5, 4, 9, and 22 mm. Again, a spatial scaling law previously observed (Refs. 2, 4, 6) is overplotted on this figure. The data at r = 1.5 and 4 mm are fit reasonably well by this spatial dependence, but as one moves outward to the r = 9, and 22 mm scans, a flattening or localized bump is observed.

On Figure 17, the ETS and SGMF data from the r = 9 mm scan are plotted; on Figure 18, the ETS and SGMF data from the z = 6. and 10. mm scans are plotted. Note that the e-folding length or spatial rate of decay of the two fields is very similar indicating that the collisional decay of the currents

responsible for the magnetic fields are the same for both field components, and is evident on these figures as similar slopes. This implies that the observed SGMF data are diffusion dominated, which in turn explains why all the dB/dt data possess a similar shape, and fail to display the time delay corresponding to plasma transit time previously observed in studies of SGMFs (Refs. 4, 5, 6).

The conclusion drawn from: (1) the similarity in slope or decay rate, and (2) the constant rise time of both signals at all probe locations, is that diffusive field transport is dominant for SGMF produced with the Spacerays laser. Supporting this conclusion are the two computer studies of the SGMF performed at Sandia Laboratories by Wright and Widner (Refs. 13, 39). Their results indicate that for temperatures less than 100 e.V., magnetic diffusion is the dominant mechanisms of field transport. Recall that in this experiment, the plasma temperature is estimated at 12.5 e.V. significantly below the temperature where convection is predicted to dominate.

8. Extrapolated Focal Spot Magnetic Fields

Figure 19 displays the results of extrapolating the peak SGMF data from the z = 2 mm radial scan, and the r = 1.5 axial scan back to the focal spot. As can be seen on the graphs, values of approximately 10^3 gauss are obtained for both scans, significantly less than predictions made by the various groups who have modelled the SGMF mechanism using a computer (Refs. 13, 20, 21, 26). Widner has derived a formula applicable for laser intensities above 10^{12} watts/cm^2 which relates laser

intensity, beam diameter and target parameters to the maximum SGMF which can be produced neglecting magnetic field diffusion and convection. His expression is given by

$$B_{max} = 7.8 \times 10^{-6} A^{-1/2} Z^{-5/14} \left\{ \frac{I \ln \Lambda}{\delta_E} \right\} r_{fs}^{-6/7} \ln \left(\frac{t + t_o}{t_o} \right) \quad (24)$$

When the applicable parameters for this experiment are inserted, a value of $B_{max} = 13.1 \times 10^6$ gauss is obtained, orders of magnitude beyond what has been experimentally measured. A second estimate of the maximum focal spot magnetic field is obtainable directly from the source term in equation (5). First, neglect diffusion and convection, and approximate the left-hand side of equation (5) as

$$\frac{\partial B}{\partial t} \approx \frac{B_{max}}{\tau_L} \quad (25)$$

Approximate the right-hand side of equation (5) as

$$\frac{k}{ne} \nabla T_e \times \nabla n \approx \frac{k T_{max}}{e L_n L_T} \quad (26)$$

Combining (25) and (26)

$$B_{max} \approx \frac{\tau_L k T_{max}}{e L_T L_n} \quad (27)$$

For the Spacerays laser, this results in $B_{max} = 1.68 \times 10^5$ gauss. The large disparity between measured and calculated fields is explained by noting that in the above estimations,

convection and diffusive field losses have been ignored, and an ideal, pre-lase free, laser pulse was assumed. As seen in Equation 27, B_{max} decreases with the increase in the scale length of the density gradient L_n which occurs when pre-lase preconditions the target. Secondly, both convection and diffusion remove magnetic fields from the focal spot during the laser pulse, effectively increasing the values of L_T and L_n, and decreasing B_{max} accordingly. Thirdly, the probe used to detect these fields is located at large distances from the regions in which SGMFs are generated. As they are moved in closer to the focal spot to measure such fields, they seriously perturb the laser plasma.

The conclusion drawn from the disparity in magnitudes between the magnetic fields which have been extrapolated to exist at the focal spot (Figure 19), and those calculated to exist at the focal spot with a computer assuming a nonparallel temperature and density gradient source term, is that such extrapolation is not in general valid. In other words, the magnetic probe signals and magnetic fields inferred from them are not necessarily representative of those which may be generated at very early times in the formation process of the laser plasma.

B. K1500 RUBY LASER SYSTEM -- DATA PRESENTATION AND INTERPRETATION

The second laser system similar to that used in prior investigations of SGMFs is a K1500 Korad laser. With this system, 5 joules were delivered on target in a pulse length which

varied from 40 to 50 ns FWHM at a wavelength of 6943Å. To evaluate the spatial SGMF decay rate using this laser pulse, which was an order of magnitude longer than that of the Spacerays laser, a scan was performed at a radial distance of 5 mm for axial coordinate values of 4 to 15 mm. The horizontal plane, as with the Spacerays data, was that in which the probes were located and the laser radiation polarized. Table II summarizes the results of that study.

TABLE II

K1500 RUBY LASER MAGNETIC FIELD AND PLASMA EXPANSION VELOCITY DATA

(Measured at r = 5. mm, z = 4. - 15. mm)

$\bar{R}$ (mm)	z	t_d (ns)	V (x 10^6 cm/sec)	B_{SGMF} (max) (gauss)	B_{ETS} (max) (gauss)
6.6	4	90	7.3	35	9.
8.7	8	170	5.1	43	6.5
11.3	11	200	5.7	25	1.9
15.9	15	370	4.3	14	0.4

$\bar{R} = \sqrt{z^2 + r^2}$

Figure 20 compares the spatial rates of decay of the Korad K1500 data with that from the Spacerays laser system. The significant difference evident when the data obtained on the K1500 ruby laser system are compared to those obtained on the Spacerays laser is displayed as a delay in the time at which the maximum SGMF occurred, as the magnetic probe is moved outwards along the scan line at r = 5 mm. The column entitled t_d in Table II is this measured time delay, from

when the laser pulse arrived on target to the time of the peak magnetic field from which the data in the velocity column in Table II were obtained. The presence of a propagation velocity for the magnetic field implies that $R_m \tilde{>} 1.$, i.e., that convection is significant for the K1500 laser generated SGMFs when compared with those produced by the Spacerays laser, where $R_m << 1$.

The ETS time duration for the longer laser pulse is on the order of 50-80 ns, or 1-1.6 times the laser pulse width -- the corresponding values on the Spacerays laser are 1-4 depending upon background gas pressure, but still related to the laser pulse length. Secondly, as occurred on the Spacerays laser, the ETS half width remained constant as the probe was moved further from the target. Thirdly, the peak ETS magnetic field intensity was characterized by an e-folding length different than that of the Spacerays ETS. The explanation is that for the K1500 laser system, the electron emission process into the background gas occurs during the longer laser pulse length. When the laser pulse is over, collisional dissipative effects predominate and the electron current responsible for the ETS rapidly decay away. The effect of this decay is the direct correlation between the laser pulse length and ETS time duration.

The explanation for the SGMF peak field intensity occurring at a larger axial distance for the Korad laser is related to the fact that $R_m \tilde{>} 1$ for the experiments performed with the Korad laser system. In this case, the field was

partially frozen into the plasma, traveled with it as it expanded preferentially out along the target normal and, therefore, remained more intense at larger distances. In other words, the SGMFs generated with the Spacerays laser dissipated by diffusive processes from their inception at a rate proportional to R^{-a}, where $a \gtrsim 3$ (geometric volume expansion) as shown on Figures 12-17. On the Korad K1500 laser, the field was convectively carried along the target normal before diffusive (collisional) and geometric dissipation effects predominated. The result was that maximum SGMF intensity occurred further axially from the target for the Korad laser than for the Spacerays laser data. Secondly, because the laser pulse which generated and maintained the gradients responsible for the SGMFs was temporally longer on the K1500 laser, the plasma expanded and occupied a larger volume at the time the laser pulse was over, and the effects of geometric dissipation were correspondingly less in the case of the K1500 laser system.

C. PULSE LENGTH DEPENDENCE OF SGMF AND ETS -- ALL LASER SUMMARY

Pulse shape has previously been shown to be important in determining the characteristics of the SGMF signals, in the discussion of the effect of pre-lase on the magnetic signals measured using the Spacerays laser. Pulse length, and laser pulse rise time is also significant in determining the characteristics of the SGMF and ETS from laser-produced plasmas, as shown in Figure 21. The corresponding laser pulses are displayed in Figure 22. Two distinct data groupings are evident: those from the Spacerays laser, for three pulse

lengths, and those from the other laser systems, with their differing pulse lengths, shapes, and wavelengths. The one characteristic of the Spacerays data, which differs from that on the other systems, is the four-nanosecond laser pulse rise time. This faster rise time results in a faster rate of deposition of energy into the target, a corresponding decrease in the time at which the maximum temperature in the laser plasma is reached, since the temporal dependence of the temperature is similar to and dependent upon the laser pulse length, and a faster cooling rate in the expanding laser plasma.

The effect on the SGMFs is that for two laser pulses, differing only in pulse length, the longer produces a stronger longer-lasting SGMF, as the temperature gradient responsible for these SGMFs is longer-lasting and generates magnetic field for a correspondingly longer period of time.

D. PRESSURE DEPENDENCE OF THE ETS AND SGMF

1. Experimental Data

The dependence of the peak ETS and SGMF intensities at a position (1.5,6,6) mm has been measured over the pressure range 5×10^{-6} - 10^{+1} Torr of air. These results are displayed in Figures 23 and 24. Overplotted on Figure 23 is the measured dependency of the electron emission current from a laser plasma as measured by Arifov [Ref. 8]. Over the pressure range 10^{-5} - 10^{-3} Torr, Isenor [Ref. 9] measured a linear dependence upon gas pressure, i.e., $i \propto AP^{+1}$; Arifov measured a P^a dependence of the emission current on pressure, $0.5 < a < 0.7$, with

pressures of 10^{-6} to 10^{-2} Torr. At higher pressures, Arifov measured a steep drop of the emission current. Overplotted on Figure 24 is the measured dependence upon pressure of the peak SGMF intensity, as measured by McKee and Bird (Refs. 4, 5).

2. Discussion and Interpretation

a. SGMF

On Figure 24, good agreement is obtained with the data of McKee and Bird relating the ambient background gas pressure at a given probe position to the peak measured SGMF intensity.

The explanation of this dependence, as given by Bird (Ref. 5), is that the increased background pressure inertially confines the expanding laser plasma, and increases the normalized axial density gradient, $\frac{\nabla_z n_e}{n_e}$, in proportion to the (1/3) power of the pressure. Then, as $B \propto \frac{1}{n_e} \nabla_z n_e$, the dependence of the magnetic field is

$$B \propto \frac{\nabla_z n_e}{n_e} \propto p^{1/3} \qquad (28)$$

This dependence was shown by Bird to agree well up to about 0.25 Torr, where a fall-off in intensity of B_{max} is observed. The high pressure fall-off is attributed to the re-thermalization of the expansion energy of the laser plasma, and the generation of reverse field at the front of the laser plasma. The algebraic cancellation of the two fields then account for the decrease in B_{max} above 250 mTorr. In this work, no further

theoretical work on this SGMF pressure dependence has been attempted, but the experimental results in Figure 24 are in full agreement with Bird's thesis.

b. ETS

The pressure dependence of the ETS, as plotted in Figure 23, is seen to be quite different from that measured for the SGMF signal, which is displayed in Figure 24. The most striking difference is the difference in pressures at which the two signals reach their maximum values, at $1 - 2 \times 10^{-3}$ Torr for the ETS, and 80×10^{-2} Torr for the SGMF signal. The differences, however, are not unexpected, when the data are considered in light of the theory developed earlier in this work, since the ETS pressure dependence is the result of different processes than those responsible for the increase in SGMF peak intensity.

A curve fit to the low pressure dependence data of the form $B = a P^{\beta}$ (see equation (16)) over the pressure range of 5×10^{-5} to 10^{-3} Torr yields for a and β, $a = 8.1 \times 10^{2}$, and $\beta = 0.71$ when P is in Torr, and B in gauss. An estimate of T_2 is obtained by solving equation (16) for T_2. If the plasma temperature, T_1, is taken to be 12.5 e.V., a background plasma temperature of 6.5 e.V., is evaluated, in reasonable agreement with values obtained in a similar experiment and measured by other means [Ref. 40].

Next, we apply this value of beta, 0.71, to the high pressure data, i.e., to the pressure-dependent data above 10^{-3} Torr, using a functional form, $B = a' P^{\beta-1} = a' P^{-0.29}$.

By curve fitting this experimental data at the end points, i.e., at 5 Torr and 10^{-3} Torr, a value of a' = 0.81 is obtained with the same units for B and P as given above. These calculated dependencies are replotted along with the experimental data in Figure 25.

This agreement between experiment and theory strengthens the arguments made earlier that thermal electron emission modified by space charge effects are responsible for the ETS and its corresponding pressure dependence.

3. ETS Pressure Dependence -- Calculation of Space Charge Potential

Using the just calculated values of the background plasma temperature and equation (11), a value of the expected space charge potential at the peak of the ETS pressure dependence curve can be obtained, and compared with that obtained from the measured peak magnetic field. Values of electron density are chosen as 1.2×10^{19} for n_1, 3.54×10^{13} for n_2 (corresponding to a pressure of 10^{-3} Torr), $T_1 = 12.5$ e.V. and $T_2 = 6.5$ e.V. Inserting these values, a value of 131 volts is obtained for the space charge potential, which agrees within 10% with that value obtained from the experimentally observed peak ETS magnetic field.

VII. ERROR ANALYSIS

The error bars shown on the data were obtained by estimating the individual error components involved in this experiment, as listed in Table III, and assuming a worst case, i.e., all errors cummulatively adding.

Error estimates for the other experimental parameters are:

(1) the chamber pressure is estimated to be accurate to within the rated accuracy of the thermocouple gauging system used in the experiment ±20%, while pressures lower than 1 mTorr are believed to lie within confidence limits of 5%, the ionization gauge accuracy,

(2) the probe locations presented have an estimated uncertainty of 1 mm; this estimate was obtained by measuring a probe location multiple times and averaging the results,

(3) the laser output energy is known to within 15%, the instrumental accuracy of the calorimeter used for calibration,

(4) timing of the arrival of the laser pulse relative to the beginning of the magnetic signal is estimated at 4 ns.

The above is an appraisal of the errors involved in this experiment; most are instrumental in nature and relatively insensitive to improvement except by the replacement of equipment.

TABLE III

ERROR SOURCES AND THEIR ESTIMATED MAGNITUDES

Error Source	Absolute Error	% Error	Comments
1. Oscilloscope nonlinearity	----------	3.	Value from USAF calibration.
2. Digitization of data	1/5 division in 8	2.5	Finite width of oscilloscope trace.
3. Trapezoidal integration (ETS)	----------	5.	
4. Numerical filtering -- computer integration	----------	5. - 10.	Estimated from averaged fourier series using analytic functions -- may include some of Item 2 above.
5. Probe calibration	2/5 division in 8	5.	Finite scope width for two signals.
6. Delay cable timing	1/5 division in 10	2.	Finite scope trace width.

VIII. CONCLUSIONS

In the previous sections, the results of the experimental investigation of electron emission and self-generated magnetic fields in laser-produced plasmas have been presented, analyzed, and discussed. Characteristics of both phenomena have been investigated, and their significance discussed. Here, conclusions concerning the ETS are collated. Secondly, the characteristics of the SGMFs which have been investigated are summarized.

A. ELECTRON EMISSION -- ETS

The ETS investigated in this thesis has been shown to be magnetic in character, and has been attributed to energetic electrons emitted by the laser plasma into the ambient background plasma during the time period in which the laser pulse is incident upon the metallic foil targets.

Its spatial characteristics have been shown to indicate that the electron emission process is anisotropic, the emitted "beam" being conical in cross section with a cone half-angle of $\tilde{\sim}$ 40°. It is estimated that the electrons travel with a velocity of about 10^8 cm/sec, a value comparable with the thermal velocity of the laser plasma electrons. The near instantaneous arrival of these electron currents at the probe location is explicable since the currents responsible for the ETS flow through all the background gas, so no propagation is necessary for the ETS to be detected on the magnetic probes. Note that such propagation is required for the SGMF signal,

which is initially confined to the interior of the laser-produced plasma. The electrons responsible for the ETS close their current loops within the photoionized background plasma. The number of emitted electrons is limited by a space charge potential which is built up while between the laser plasma and the background plasma. Immediately after the laser pulse is over, the currents responsible for the ETS are rapidly collisionally damped, resulting in the measured correlation between the time duration of the ETS and that of the incident laser pulse.

From a relatively unsophisticated theoretical treatment of such electron emission processes, it has been shown that 6.4×10^5 amperes could be drawn without space charge effects being included. The presence of such a space charge potential has been interpreted to reduce the emission to that inferred from experimental data of 50 amperes. Using equation (10a), and these numerical values, an estimate of this space charge potential of 118 volts has been obtained, comparable to previous investigators results for times late in the laser plasma expansion process (Ref. 11). A theory of the pressure dependence of the ETS has been formulated, and used to obtain an estimate of the space charge potential expected theoretically under the experimental conditions. The calculated value of 131 volts compares well to the above experimentally inferred voltage. The results display nearly the same dependence on pressure as those obtained by Arifov using electrostatic charge collectors, but do differ in the pressure at which the maximum electron

current flows. This disagreement is attributed to a number of effects, including probe shielding by return currents, inaccuracies in pressure sensing equipment, differing electron emission energies and space charge potential effects.

The ETS half width, or temporal duration has been observed to be directly dependent upon the laser pulse length, and a function of the laser pulse rise time, increasing with an increase in pulse length, though not always in a linear manner. This conclusion has been drawn from the Spacerays data, when compared with that from the Korad laser data. A further example of this can be seen in Appendix D, wherein the data from the CO_2 and Nd glass lasers are presented, and this pulse length/rise time -- ETS time duration correlation is readily observable.

B. SGMFs

The effects of the variation of the laser parameters of pulse length, rise time, and shape, and those of background gas pressure on the magnetic field intensity have been observed in this work. Different laser pulse shapes have been generated with the Spacerays laser system by varying the amount of prelase present in the laser pulses incident upon the metallic foil targets. This prelase generated its own internal plasma with nonparallel temperature and density gradients, and in turn, its own magnetic fields. The effect reduced the magnitude of normalized density gradient scale length L_n. Therefore, as can be seen from equation (24), the peak magnetic field intensity will be reduced in proportion to the increase in the

normalized density gradient. In this experiment, the magnetic field rise time was observed to increase in direct proportion to the amount of pre-lase present during an experiment. The conclusion drawn from these observations is that the laser pulse shape directly influenced the SGMFs peak intensity by modifying the normalized density gradient, $\nabla n_e/n_e$ in just the same manner as does the residual gas pressure.

That is, the presence of a pre-existing density gradient produced by the pre-lase portion of the laser pulse, has the effect of lengthening the magnetic field rise time by effectively increasing the laser pulse length. Therefore, since the source term of the magnetic field is linearly dependent on the normalized density gradient, less intense peak magnetic fields are produced because the scale length over which the density gradient occurs is increased by the pre-lase. This direct influence of laser pulse length has been observed in this experimental investigation, as shown in Figure 21, where data from all the laser systems used herein are presented.

As proposed in their initial report on SGMFs, Stamper's phenomenological model relating laser pulse length to magnetic field duration has been observed. The fact that the Spacerays laser pulse length is significantly shorter than that of the Korad laser system allows the laser plasma to cool more rapidly earlier in time, since it is the laser pulse which maintains the temperature gradient, ∇T_e, in the source term for the SGMFs.

The dominance of diffusion as the primary magnetic field transport mechanism for the SGMFs generated with the Spacerays

laser system is evident from the lack of the increase in magnetic field rise time as the probe is moved farther out from the laser focal spot, and the unreasonably high convective velocities implied by these experimental results if the field is transported by convective processes. Such results are to be expected for the experimental conditions which occur in this experiment, and have been shown to correlate well with computer simulations of similar experiments (Refs. 13, 14).

The pressure dependence of the SGMF signal for the short pulse laser system has been evaluated and found to agree within experimental errors with that observed by McKee and studies subsequently by Bird (Refs. 4, 5).

Further experimental results have been collated in Appendix D, where several ancillary experiments on two other laser systems are discussed and their significance mentioned.

IX. FUTURE EXPERIMENTS — PROPOSALS

Though the original questions asked in this investigation have been answered, as is the case more often than not, other questions have been raised. More experimentation is required to adequately understand the generation and propagation of both the SGMF and ETS. The following are proposals for several appropriate experiments designed to answer some of the questions which have arisen in this work.

A. At the AFWL, a K1500 ruby laser has been converted to operate either in a conventional Q-switch or TVR mode. With this laser system, the relative importance of the convection and diffusion terms in the equation governing the magnetic field signals (Equation 5) can be more fully investigated than has been possible in this and previous studies of SGMFs.

B. The possible use of an optical diagnostic technique to study the strong focal spot fields is under consideration at NRL, LASL, and the AFWL. In such an experiment perhaps using the Faraday rotation of an incident laser probe beam by the SGMFs, peak magnetic fields near the focal spot could be measured and the computer simulations presently available improved with the experimental scaling laws derived from such experiments.

C. Holography and shadowgraphy can be used to correlate the position and magnitude of the plasma electron density and density gradients at various times after laser pulse arrival at the target with the measured peak fields at the same times. Such experiments should conclusively show whether the field transport is either diffusive or convective, depending upon the relative profiles of the magnetic field and the electron density.

D. By beam splitting, or the use of multiple lasers, two or more laser pulses can be made to impinge upon a target with a variable time interval. Such an experiment should re-confirm or deny the claims made by LASL (Ref. 6) that they have effectively reversed the roles of temperature and density gradients and produced a reverse polarity magnetic field.

APPENDIX A

TVR LASER

The Spacerays Time Varying Reflectivity (TVR) laser system used to obtain the major portion of the data in this experiment is Q-switched in a different manner from either the CGE VD640 Nd glass laser which uses a rotating prism, or the K-1500 ruby laser which uses a Pockel's cell in the "conventional" manner.

The technique used in a TVR laser is one of varying the reflectivity of the laser oscillator's front optical element from 0 to 100% and then back to 0% using a Pockel's cell and birefringent calcite polarizer. It is accomplished on this system as seen in Figure 26. During the initial flash lamp pumping of the ruby rod, no voltage is applied to the Pockel's cell so that the spontaneously emitted, horizontally polarized, ruby photons are allowed to pass through the birefringent calcite prism and out the front of the laser. The vertically polarized photon flux is totally internally reflected by the calcite and 100% dielectric mirror, whereupon it returns through the rod and is dumped from the system by the glan-thompson polarizer at the rear of the ruby rod. To a photon flux polarized in the horizontal plane, then, the system appears as a resonant rear reflector.

At the time of peak population inversion, the Pockel's cell is activated with a voltage from a charged transmission

line which rotates the plan of polarization of the photon flux passing through it by $+\pi/2$ (half wave voltage). In essence then, for the time the voltage is applied to the Pockel's cell, the horizontally polarized photon flux is allowed to build up in the cavity by spontaneous and stimulated emission but is totally contained by the 100% reflectors at either end of the cavity. At the time of maximum internal photon flux, the front reflector is returned to a condition of 0% reflectivity by turning the Pockel's cell off; the photons pass out the front in a pulse whose duration is determined by the cavity length, the pulse width being equal to the round trip transit time for the photons in the cavity. In practice, the shape is triangular because the rise and fall time of the Pockel's cell voltage is not infinitely sharp.

If the oscillator voltage is not carefully regulated, the total pulse shape can be significantly different because the change in charging voltage causes a temporal shift in the optimum time at which the Pockel's cell should be activated, and no provision is available for such a shift as a function of oscillator voltage. In essence, one Q-switches the cavity at a nonoptimum time and most of the output energy appears on target, not in the giant pulse but rather in a longer temporally diffuse leakage pulse. The Pockel's cell then acts like a "conventional" Q-switched laser front reflector, and a 30 ns FWHM pulse is obtained. More information is available on such TVR lasers in References 41 and 42.

APPENDIX B

PROBE RESPONSE AND CALIBRATION -- EXPERIMENT AND THEORY

In addition to evaluating the angular response of the magnetic probes which were constructed in this work, the measured magnetic probe frequency response was compared with a simplified theory where the probe was represented as an R-L circuit. Since the probe resistance of 0.5 - 1.1Ω is much less than the co-axial cable resistance, 50Ω, there is no significant frequency dependence in the probe until ωL_p becomes comparable to that of the co-axial transmission line (RG 58 cable). At this point, i.e., $\omega L_p \tilde{\sim} 50\Omega$ a partial signal integration, or roll off in frequency response is to be expected, similar to that observed in calibration curves shown in Figure 27. However, since the roll-off frequencies calculated for the probes and the measured values differ as much as they do, as shown in Table IV, other effects are involved.

One source of response degradation is the bandwidth of the oscilloscopes used for calibration, though this is insufficient in itself to account for the roll-off frequency being so much lower than predicted. A second source of error is the simple model used to predict this roll-off frequency where capacitive effects are neglected.

TABLE IV

PROBE DESIGN DETAILS AND CHARACTERISTICS

Probe No.	No. of Wire Turns	Wire* Size (mm)	Roll-Off Frequency Measured (MHz)	Roll-Off Frequency Calculated (MHz)	Effective Area (m^2)
7	5	0.0799	50	425	1.6
9	5	0.0799	**	939	1.5
19	4	0.0799	33	485	4.3
22***	5	0.3211	33	267	90.
23	5	0.3211	37	103	43.
L***	3	0.3211	****	------	400.

* #40 magnet wire and #28 magnet wire used.

** resonance measured at 40 MHz; no roll-off detected to at least 50 MHz.

*** coil interior free of glue and epoxy.

**** coil too large to fit into Helmholtz coil; area calculated theoretically.

To assess the possible influence of a nonazimuthal magnetic field component on a probe signal when the probe was situated in a manner to detect an azimuthal field, a quantity termed the extinction ratio (E.R.) was measured for each probe. This quantity is simply the response of the probe when the normal to the magnetic probe area was oriented parallel to the magnetic field, divided into the response when it was perpendicular, i.e.

$$E.R. = \frac{V_{max(\parallel)}}{V_{max(\perp)}} \qquad (B.1)$$

It was found that this ratio varied from approximately 20 to 100, depending upon frequency, being larger at lower frequencies. The explanation lies partially in the fact that at high frequencies (>15 MHz), there is a direct pickup in the cables and oscilloscope amplifiers which is larger in proportion to the total signal in the parallel arrangement than it was when the probe normal and the magnetic field were perpendicular to one another.

Also, probes were routinely checked for the expected cosine response as a function of angle between the magnetic field and probe vector area. Such a cosine behavior was found to be an adequate description of the probe behavior for all probes constructed.

To determine the magnetic field intensity from the voltage induced in a diamagnetic loop, the effective area of the loop must be known. One of the simplest techniques for evaluating this area is to use Helmholtz coils to produce a spatially uniform, time varying, magnetic field which in turn is used to excite the probe coil. Knowing the magnetic field in the Helmholtz coil and the induced voltage in the probe, the area of the probe can be evaluated.

The magnetic field intensity in a Helmholtz coil, which has the coil separation equal to the coil radius, is given in MKS units as

$$B = \frac{0.72\ Ni\mu_o}{d} \qquad (B.2)$$

where: i = current

N = number of turns

d = radius of coil

A time varying field is required to induce a potential in the probe. Such a field of variable frequency and amplitude was generated from a GR180A signal generator.

The voltage across the Helmholtz coils can also be obtained by considering it as a pure inductive load so that

$$V_{coil} = L_c \frac{di}{dt} \tag{B.3}$$

Combining (B.2) and (B.3), after differentiation with respect to time, yields:

$$\frac{dB}{dt} = \frac{0.72\ N\mu_o\ V_{coil}}{dL_c} \tag{B.4}$$

The potential across the probe leads is obtained from Maxwell's equation after integration over the area dA via

$$\int \nabla \times E \cdot dA = \int E \cdot dl = \frac{\partial}{\partial t}\int B \cdot dA \tag{B.5}$$

$$\int E \cdot dl = V_p = \frac{\partial}{\partial t} BA_p = A_p \frac{dB}{dt}$$

if B is assumed not to vary over the probe area. Then combining (B.4) and (B.5) yields:

$$\frac{dB}{dt} = \frac{V_p}{A_p} = \frac{0.72\ N\mu_o\ V_{coil}}{d\ L_c} \tag{B.6}$$

The voltages V_p and V_{coil} are read directly off on oscilloscope, and the other parameters are known; L_{coil} was obtained from experimental measurements as described below. Then

$$A_p(\omega) = \frac{K_{coil}\ V_p(\omega)}{V_{coil}(\omega)} \tag{B.7}$$

where

$$K_{coil} = \frac{dL_c}{0.72\ N\mu_o} \tag{B.8}$$

when the frequency dependence is explicitedly shown.

The inductance of the coils, four of which were constructed, was measured by measuring the ringing frequency of an L-C circuit of which the L was the coil. Calibrated capacitors were used, and the square wave calibration pulses from an H-P 180E oscilloscope were used to excite the circuit. L was then obtained from the approximate expression

$$2\pi f = (LC)^{-1/2};\quad L = \frac{C}{(2\pi f)^2} \tag{B.9}$$

where the circuit resistance was assumed to be 0, and where f is the ringing frequency of the damped sine wave which is produced by this circuit. Table V summarizes the characteristics of the coils constructed.

TABLE V

CALIBRATION COIL PARAMETERS

N No. of Turns	L Measured Inductance (μH)	K_{coil} (m^2)	Frequency Range (MHz)
1	0.47	0.0125	0.05 - 50
2	1.38	0.0187	1 - 5
5	6.61	0.0351	5 - 15
10	26.42	0.0702	0.1 - 1.0

By amplifying the few millivolt signal obtained from the single turn coil with an H-P 641A wide band amplifier, only a single Helmholtz coil was found necessary to cover the frequency range of 0.1 to 50 MHz over which the probes were calibrated. The use of the single coil for calibration additionally yielded calibration data with significantly less scatter than that obtained with the separate coils for their respective frequency ranges.

APPENDIX C

NUMERICAL DIGITAL FILTERING OF dB/dt DATA

In the attempt to remove very high frequency noise which is present in many of the data traces obtained in this experiment, and to be able to assess the importance of high frequency components in the data itself, a fourier analysis code and a time domain digital filtering code have been obtained, modified, and used in reducing the digitized magnetic signals. The routine employed uses a linear nonrecursive technique of digitally filtering the data.

If one passes an input signal, X(f), through a network (probe, signal cable, and oscilloscope), the signal which is recorded, Y(f), is different than the input because of the filtering action of the network through which it passed. This filtering can be described by the use of a transfer function, H(f), which may be defined in terms of the two signals described above via

$$H(f) = \frac{X(f)}{Y(f)} \qquad (C.1)$$

This definition, however, is not operationally useful as it requires both the input and output signals to be known; in general, one is trying to obtain the input signal, X(f), given the output signal, Y(f), and some idea of the transfer characteristics of the network in the frequency domain, while

A straightforward fourier analysis is required to obtain H(t) from H(f), i.e.,

$$H(t) = \int_{-\infty}^{+\infty} e^{i\omega t} H(2\pi f)\, d\omega \qquad (C.2)$$

One can alternately think of H(t) as the unit impulse (delta function) response function.

In this time domain the input and output functions are related via

$$Y(t) = \int_{-\infty}^{+\infty} H(t')\, X(t - t')\, dt' \qquad (C.3)$$

This is the equation that is approximated numerically in the form

$$Y_i(t) = \sum_{k=1}^{m} H_k(f)\, X_{i+k}(t) \qquad (C.4)$$

where $H_k(f)$ contains the Δt terms from C.3, and is referred to as filter weights. The remaining problem then is to obtain these filter weights.

In the work herein, the filter function used is specified in the frequency domain as a step function with unit amplitude between 0 and a frequency f, and then a linear fall-off to amplitude 0 in a frequency range of .1f (Figure 28). This filter shape is referred to as a P=1 Ormsby filter (Ref. 34). In his original work, Ormsby allowed the linear portion of

the filter to roll off at a higher power than 1, but the P=1 case is deemed sufficient for this work. The frequency range, 0 to 1.1f, in this work was chosen as 50 Mhz which is also the range of the probe calibration; it is sufficiently high in frequency that no data are observed at frequencies greater than this.

One advantage of this type of filter, in addition to its intuitive nature, is that there is analytic expression available from which one can estimate the maximum numerical error introduced by filtering the raw experimental data. The error in per cent, arising from using N_f fourier terms to represent the filter function in the frequency domain is given by an empirically derived constant A = 1.2, and L_r, where $L_r = (f_\mu - f_L)/f_\mu$

$$\text{Error } (\%) = \frac{1.2N_f}{L_r} \qquad \text{(C.5)}$$

The number of terms used in this work is 20, while L_r is fixed at 0.1, so that an upper bound on the purely numerical error introduced by this numerical filtering technique is one per cent, within the estimated error arising from digitizing the raw polaroid traces.

The FORTRAN filtering routine used in this work was derived and computer coded in 1968 by Mr. Robert Conley of the AFWL, and was modified in 1972 to operate on the data obtained from magnetic probes. Though not included herein, it has been

shown that the technique which he used in obtaining the h_k filter weights is equivalent to Ormsby's result.

One should note here that in addition to the low pass Ormsby filtering used, that the nature of the magnetic probe response is that of a similarly shaped filter whose roll-off frequency is approximately 20 - 25 MHz. In essence then, the probe filters the data (i.e., magnetic field signals) with a roll off at frequencies of 25 to 35 MHz; the numerical filter eliminates HF noise picked up directly in the oscilloscope, or the co-axial cable linking the probes with the oscilloscopes, with a frequency roll-off point of approximately 45 MHz. As a practical matter, it has been found from parametric studies that without such a digital filtering routine, the effects of the probe response, the digitizing of the data, and the limited number of fourier terms in the expansion, caused undesirable high frequency components to be magnified and introduced nonphysical oscillations in the resulting data. The solution was the use of the numerical filtering routine.

APPENDIX D

Nd AND CO_2 LASER WAVELENGTH EFFECTS AND TARGET MATERIAL STUDY

A. SGMF AND ETS DATA -- OTHER LASER SYSTEMS

To investigate the effects of laser pulse length, laser wavelength, and total laser energy input to the laser plasma on the magnetic signals obtained from such plasmas, a CGE Vd-640 Nd doped glass laser, and an electron beam pumped CO_2 laser have been used. The Vd-640 system laser pulse possess the same temporal characteristics of 30 ns FWHM as that used by previous investigators of SGMFs (Ref. 2, 4, 5). The pulsed CO_2 system operates at 10.6 microns, a wavelength not before used to generate SGMFs and ETS.

1. Nd Glass Laser -- Experimental Data

Experimental magnetic signal data were gather using the CGE Vd-640 Nd glass laser. Twelve to fifteen joules were delivered at a wavelength of 10,600 Å to 2 mil mylar and 5 mil copper targets at 0° and 45° incidence angles, in a 30 ns FWHM pulse. Only a limited number of data shots were available using this laser system. No timing data were available though, with which the relative arrival times of the laser pulse and magnetic probe signal could be evaluated. Figures 29 - 31 are dB/dt data, redrawn for clarity, obtained on this system. Figure 29 includes a typical laser pulse, displaying the complex structure which is generated by the rotating prism Q-switch used in this laser system, as well as four data measured with

magnetic probes at different background gas pressures. Figure 30 displays the multiple pulse structure evident in nearly all the data obtained on the Nd glass laser system. Figure 31 is a comparison of the magnetic probe signals obtained when the laser was incident upon 2 mil mylar and 5 mil copper targets. Note that both McKee (Ref. 4) and Stamper (Ref. 2) used hydrocarbon (lucite or mylar) targets in their investigations of SGMFs.

2. Nd Glass Laser Data -- Discussion and Interpretation

In Figure 29, a number of features should be noted: (1) the magnetic probe signal rise time is on the order of 150 ns, a factor of two to three larger than that observed on the Spacerays system; (2) there is a small ETS present and identifiable; (3) the half-width of the SGMF signals is 250 - 300 ns, comparable with the results of previous investigators. The most intense SGMF measured in this experiment is that shown in Figure 29C. The magnetic intensity, B, was 750 gauss, at a probe location of (0,7,5). The multiple pulse structure shown in Figures 30a and 30b is definitely magnetic because as shown, it reverses upon probe rotation by 180°. Its orgin however, is less clear. It was not observed when the background pressure is raised to values of 400 and 750 mTorr in agreement with Stamper's results (Ref. 2) obtained at pressures of 250 mTorr of N_2, where smooth rise and falls of the dB/dt signals were reported.

In Figure 31, where two target materials were used, the thick metallic target magnetic probe signal is longer

lasting, and does not display the double pulse structure evident on that obtained with the mylar target. A hole was bored through the plastic target, while there was only surface damage occurring on the copper foil target. No further study of SGMFs and ETS was done on the Nd glass laser.

The conclusions drawn from this work, however, are the following. First, the presence or absence of the ETS is much less evident on the Nd glass data than in that obtained on the Spacerays system. Secondly, the multiple spike phenomena shown in Figure 30 was present only for thin mular targets, and occurred near the peak (maximum) of the integrated B(t) traces (or zero point of the dB/dt data). Thirdly, the limited Nd glass data does imply that the SGMFs measured using this laser are carried by the plasma. This conclusion was drawn because the magnetic field data obtained further from the focal spot reached a maximum later in time than did data obtained nearer to the target. Fourthly, in comparison with the data obtained on the Spacerays laser system, the longer pulse length of this system, and the increased energy on target both have been found to contribute to the different temporal characteristics of the SGMF signals which were observed. The effect of the total energy on target was to increase the plasma temperature and, therefore, the importance of convective field transport; the effect of the longer pulse length is to increase the volume which the plasma occupies and in which SGMFs exist and, therefore, the rise time of the magnetic signals, since the laser was incident upon the target for times during which the

laser plasma increased its volume nearly 50-fold. The corresponding volume increase for the Spacerays laser system was approximately a factor of four.

3. CO_2 Laser -- Experimental ETS and SGMF Data

The fourth laser system used in this experiment was a cold cathode electron beam pumped CO_2 laser, recently developed at the AFWL (Ref. 43). In the configuration used for the experiments herein, an unstable ring coupled cavity resonator was used. Approximately half of the 30 joules of laser energy is emitted in a self-mode locked 80 ns FWHM spike, while the other half of the energy is delivered in a two to three microsecond trailer pulse.

The data obtained on the CO_2 electron beam pumped laser was at normal incidence on 20 mil aluminum and copper targets. Two significant results have been obtained with this system and are reported here. Figure 32 is a dB/dt data, redrawn for clarity, recorded at a position (40,30) mm from the focal spot, Figure 33 contains two dB/dt data which are discussed below.

4. Discussion and Interpretation of ETS and SGMF Data- CO_2 Laser

Note first that in Figure 32, the ETS has a half-width on the order of 80 - 100 ns, a factor of 1.0 - 1.2 times the initial laser pulse width. Secondly, the rise time of the SGMF is on the order of several microseconds several times that observed with the 40 - 50 ns ruby or 30 ns Nd glass laser, and an order of magnitude larger than that observed with the

Spacerays laser. Thirdly, the magnetic field intensity at the probe location, 50 mm from the laser focus, is 35 gauss, almost two orders of magnitude larger than previously reported field strengths at or near this distance (Ref. 2). These are effects resulting from the laser pulse shape. The trailing pulse continuously creates plasma from the target surface, and because of the λ^{+3} dependence on photon wave length (Ref. 15) of the inverse bremsstrahlung absorption coefficient, effectively heats the expanding laser plasma for time scales far longer than for the other laser systems used in this experiment. Assuming a plasma expansion velocity of 10^7 cm/sec, the laser beam is still incident on the plasma (and target) when the leading edge of the laser plasma passes the probe location of (40,30) mm.

The two data on Figure 33 were obtained for magnetic probe orientations of 0° and 180°, verifying the magnetic character of the ETS and SGMF signals for the CO_2 wavelength.

5. Magnetic Field Data Characteristics -- Summary and Wavelength Dependence

An intercomparison of the SGMF and ETS magnetic field data obtained with each laser system is displayed in Figure 22; the corresponding laser pulses are displayed in Figure 21. The magnetic probe location for these data is (7,5) mm, except in the case of the CO_2 data. For the CO_2 laser, the data presented was obtained at the position (13,9) mm, which was as close to the focal spot as data were gathered on the CO_2 laser.

From the data obtained in this experimental study, the lasing wavelength appeared not to cause any significant

differences in the ETS or SGMF signals -- those differences which can be observed on Figures 22 are attributed to the differing pulse shapes and lengths shown in Figure 21.

6. Ancillary Experiments Concerning ETS and SGMFs

A study of the characteristics of the ETS and SGMFs on an ancillary experiment has been performed using the Spacerays laser to evaluate the effects of differing target materials on the ETS and SGMF signals.

a. Material Study -- Experimental Data

The dependence of the magnitude and character of the ETS and SGMF signals were evaluated in the four nanoseconds FWHM mode. The range of atomic number covered was then 26 - 82; background gas pressures of 1, 20, and 200 mTorr were used to investigate the effect that background gas pressure had on the ETS and SGMF for these target materials. Two probes, located at different spatial locations, were used for each data shot. Figures 34, 35, and 36 present the material study results for the three pressures as a function of Z, the atomic number. Additional material variation data were obtained at the longer 16 ns FWHM pulse length on the Spacerays laser and similar results to those presented here were obtained.

b. Material Study -- Interpretation and Discussion

A number of conclusions can be drawn from Figures 34 - 36. First, the ETS and SGMF magnitudes vary significantly as a function of target material and background gas pressure. Secondly, the higher the background pressure, the more intense the SGMF, while at this probe position the ETS reaches a peak

near a pressure near 2×10^{-2} Torr, somewhat higher than that measured at a position (1.5,6,6) and reported in an earlier section of this paper.

An adequate explanation of the relative magnitudes of the peak intensity of the ETS and SGMFs as a function of target material is as yet lacking as the attempt has been made unsuccessfully to correlate the above experimental results with the obvious parameters of first - fourth ionization potentials, metallic conductivity, atomic weight, atomic number, metallic reflectivity, and melting point, to enumerate a few.

FIGURE 1 CONCEPTUAL VISUALIZATION OF SGMF AND ETS GENERATION

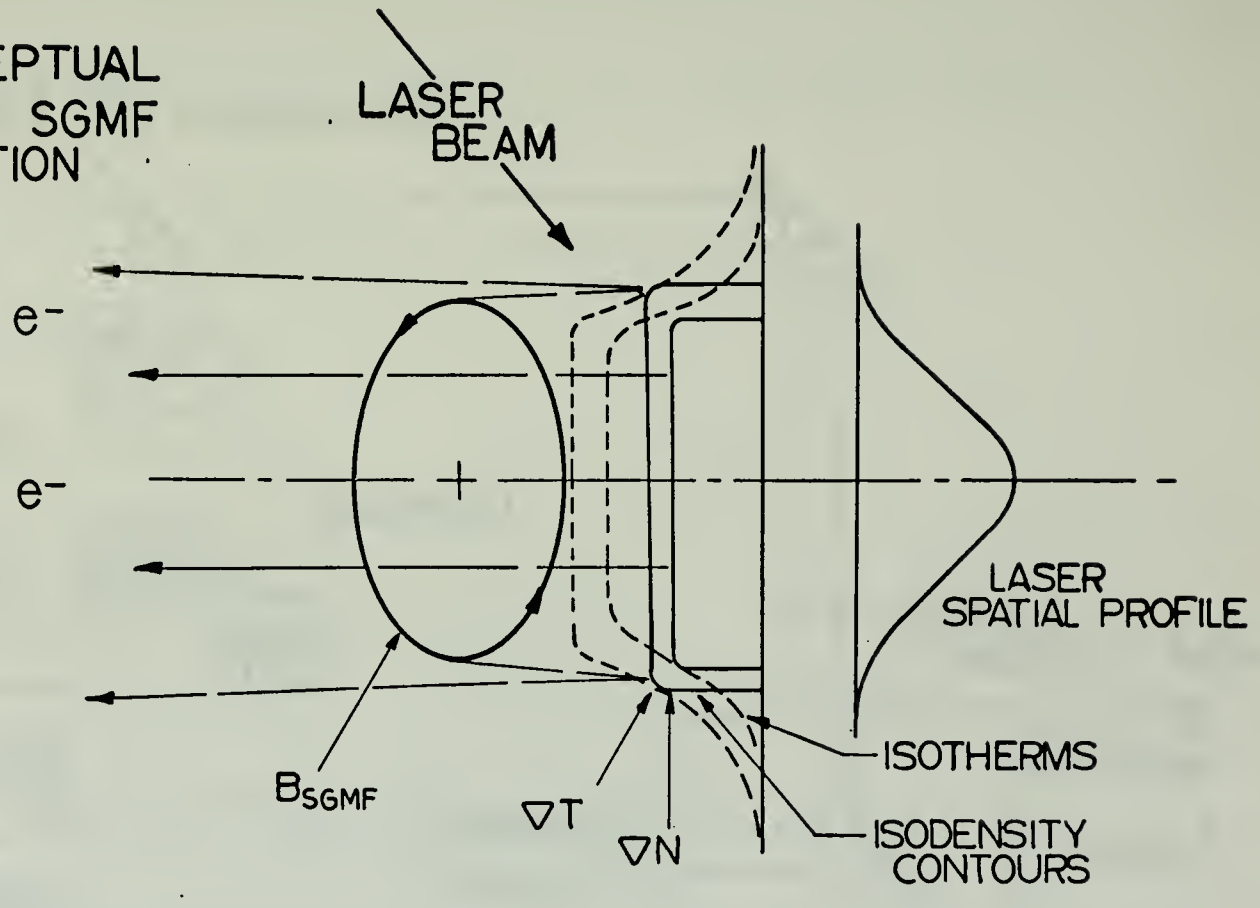

NOTE: MAGNETIC FIELD GENERATION OCCURS AT FOCAL SPOT EDGES WHERE ∇T AND ∇N ARE NON-PARALLEL

FIGURE 2
Experimental Arrangement

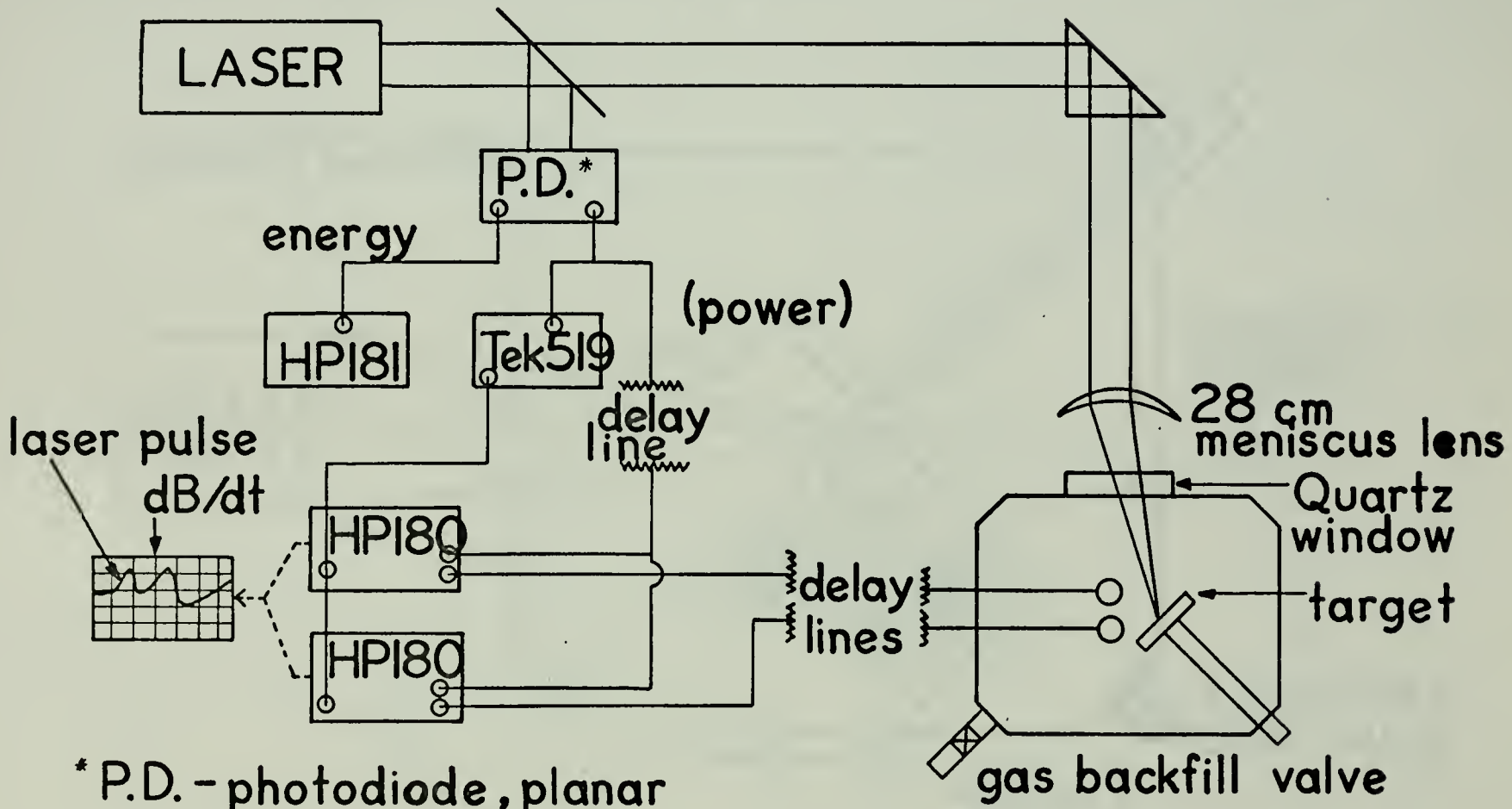

* P.D. - photodiode, planar
ITT type S24

FIGURE 3 VACUUM CHAMBER AND FIELD MAPPING REGION

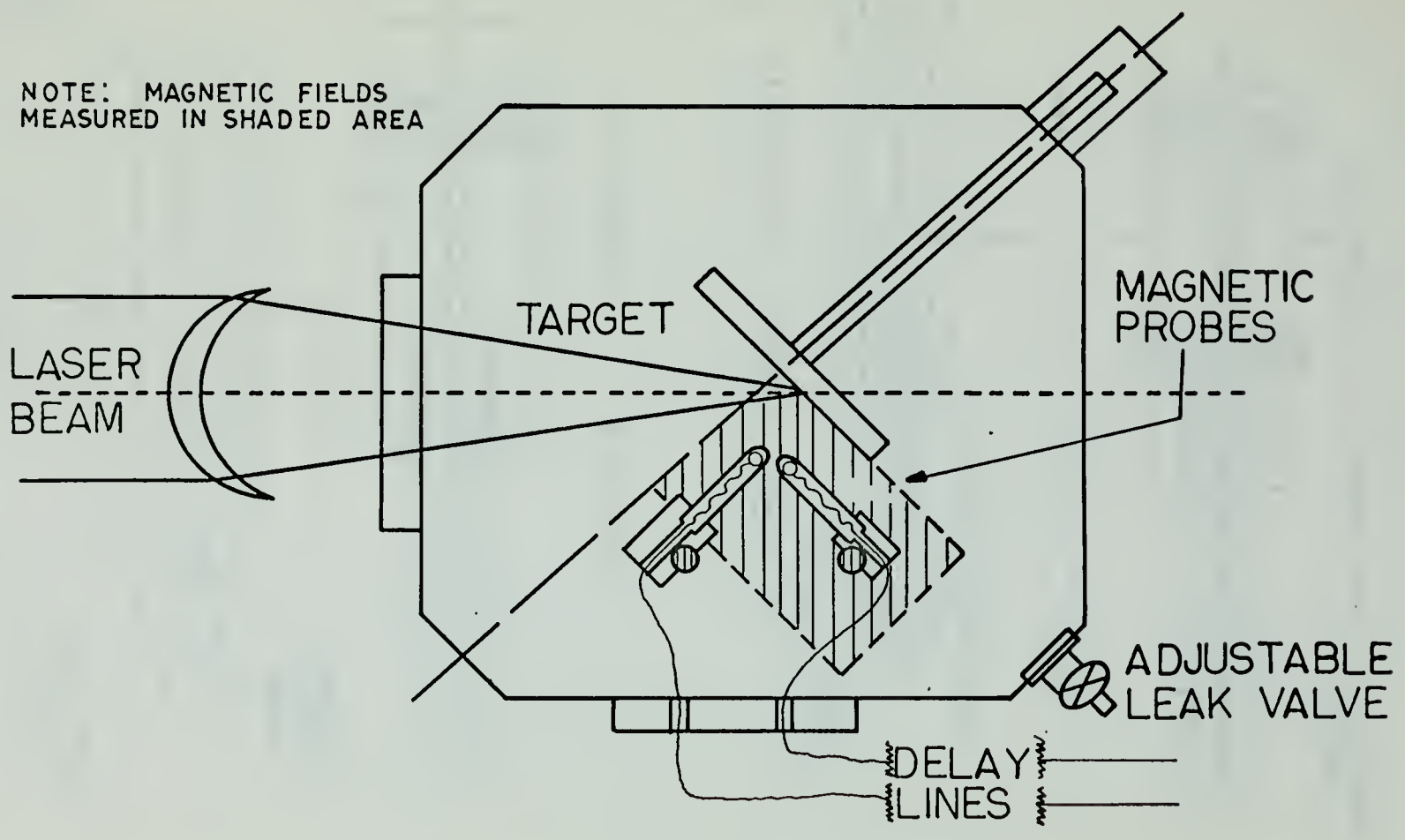

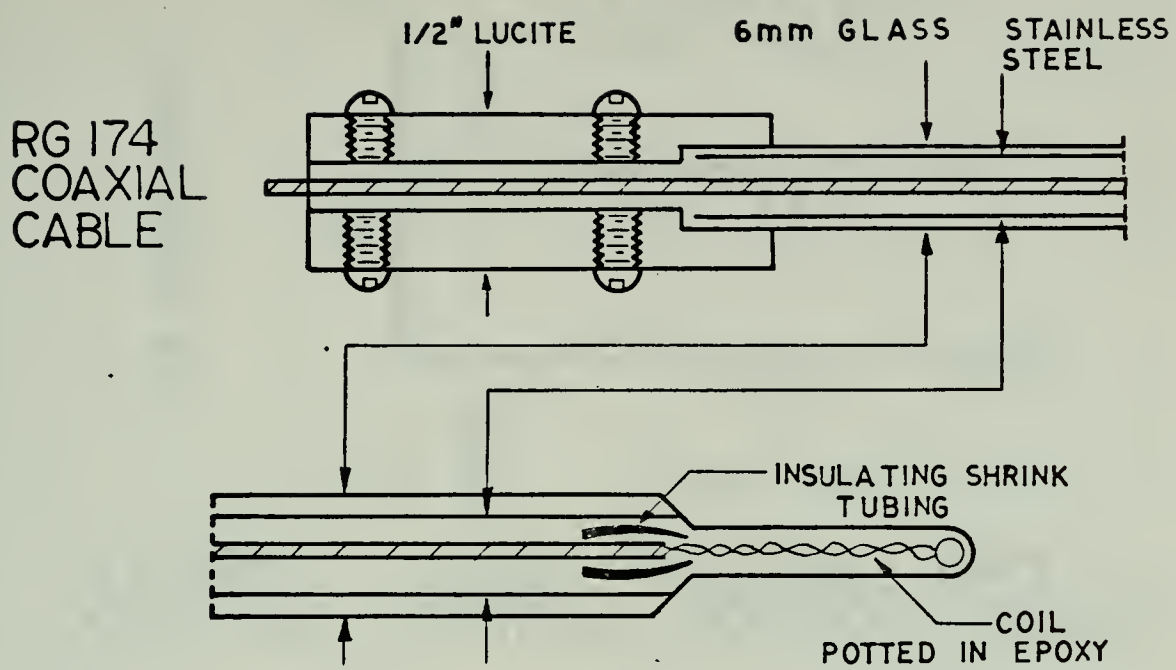

FIGURE 4 MAGNETIC PROBE DESIGN

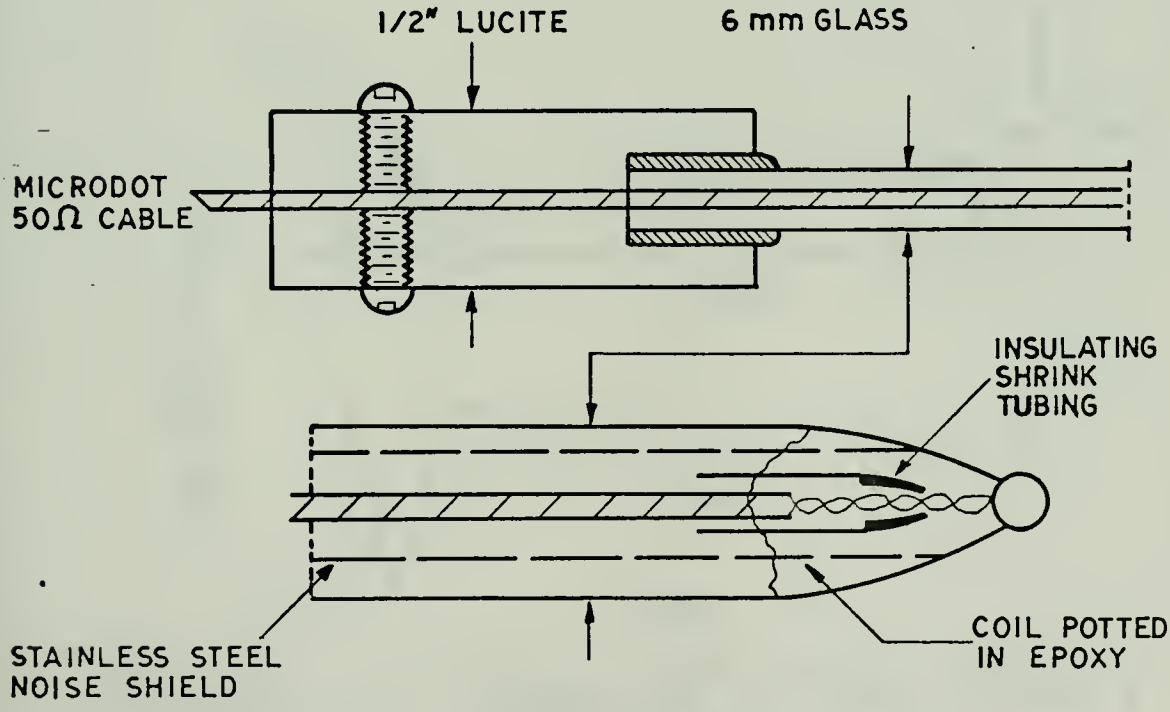

FIGURE 5 MINIATURIZED PROBE DESIGN

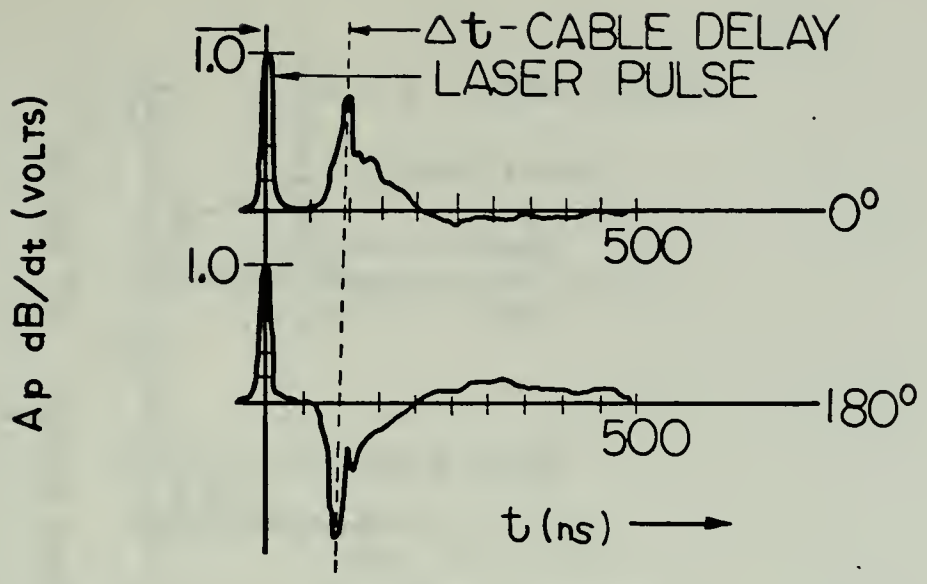

FIGURE 6 SIGNAL REVERSAL UPON COIL AXIS ROTATION POSITION (20,0,15)

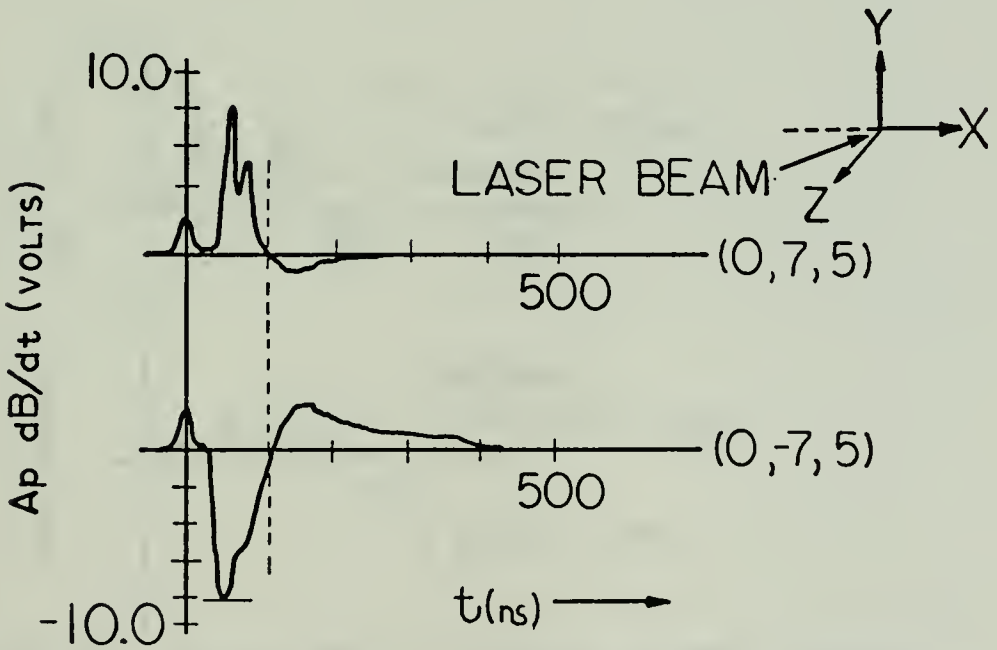

FIGURE 7 SIGNAL REVERSAL UPON Y COORDINATE REVERSAL

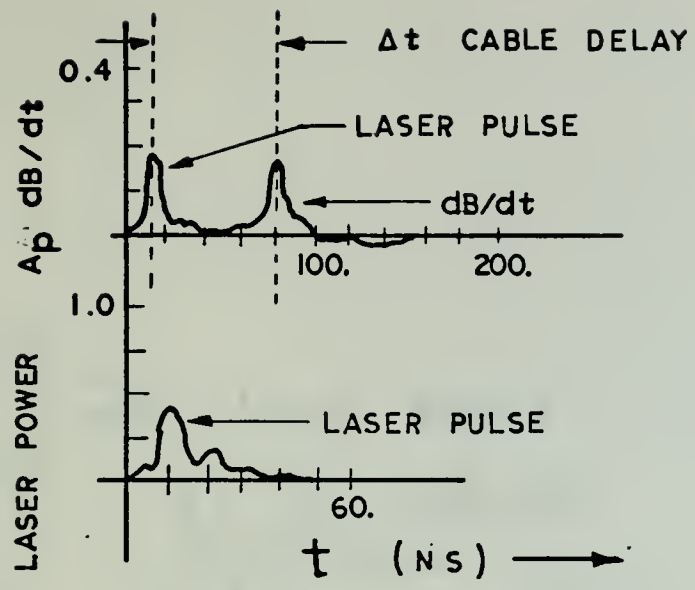

FIGURE 8 PRELASE CONTRIBUTION TO MAGNETIC SIGNAL AT POSITION (3.5,0,2) FOR 4NS PULSE ON Cu AT 50 MTORR OF AIR

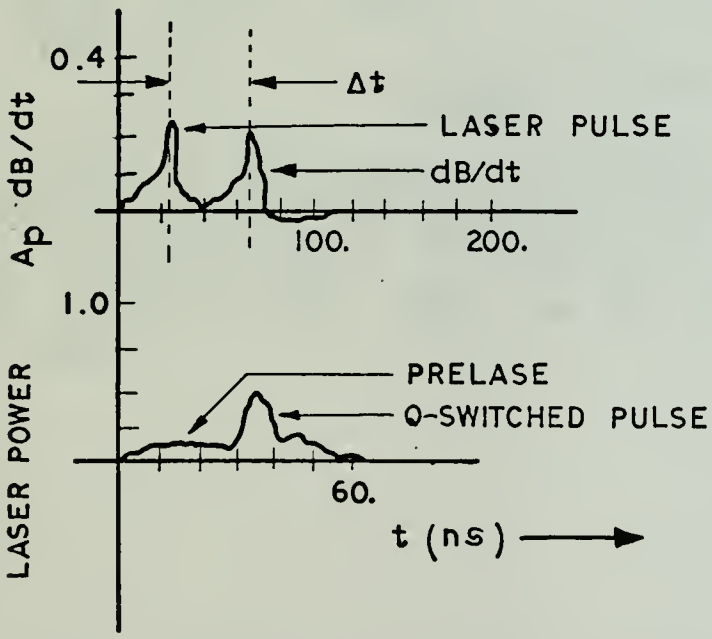

FIGURE 9 MAGNETIC SIGNAL WITH SOME LASING CAVITY LEAKAGE AT (3.5,0,2) FOR 4ns PULSE ON Cu;50 MTORR OF AIR

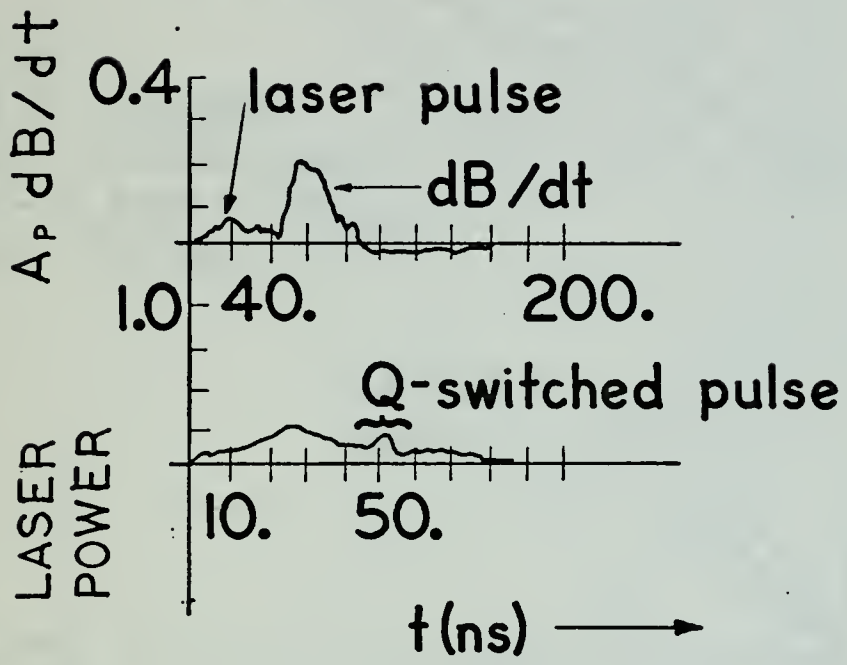

FIGURE 10 MAGNETIC SIGNAL FOR 'NO' Q SWITCHED PULSE AT (3.5, 0, 2) FOR 4NS PULSE ON Cu AT 50 mTORR OF AIR

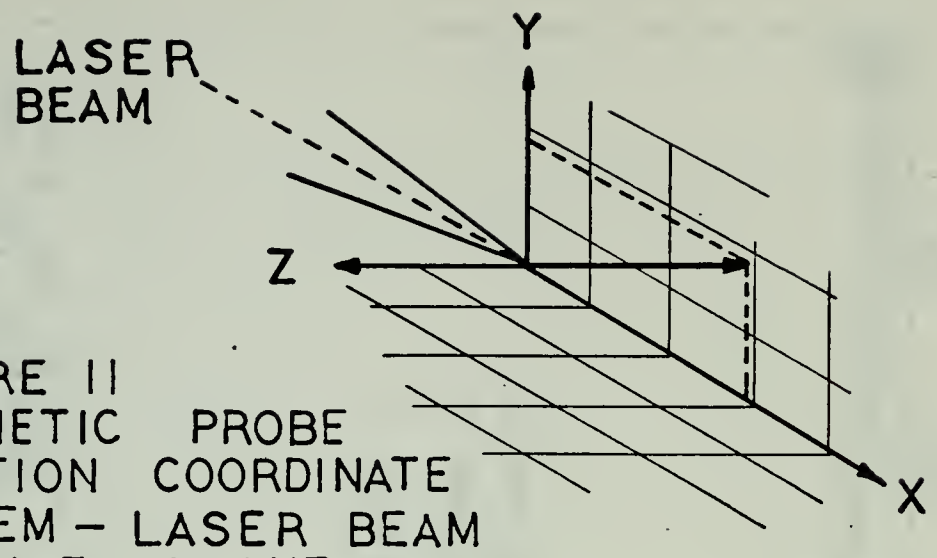

FIGURE 11
MAGNETIC PROBE
POSITION COORDINATE
SYSTEM – LASER BEAM
IN X–Z PLANE

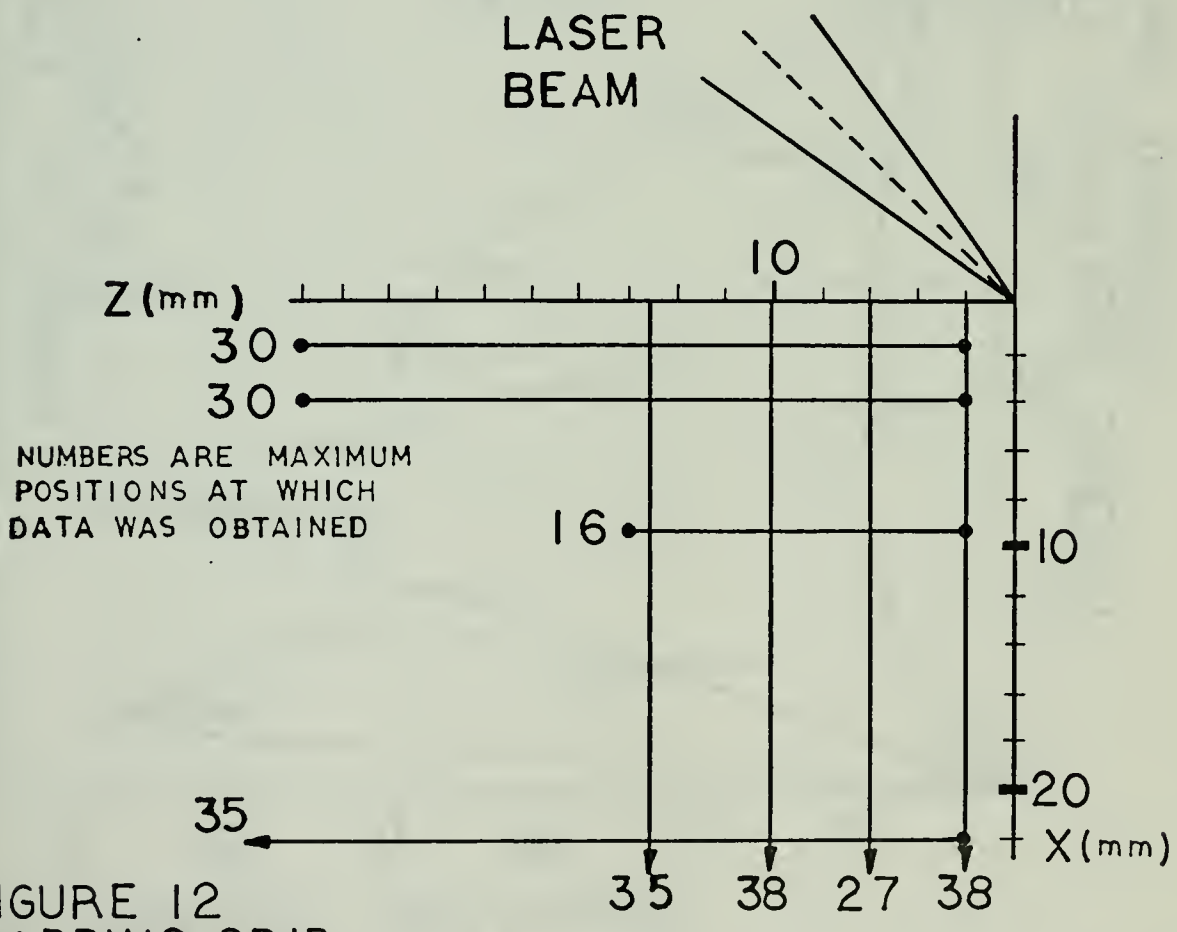

FIGURE 12
MAPPING GRID

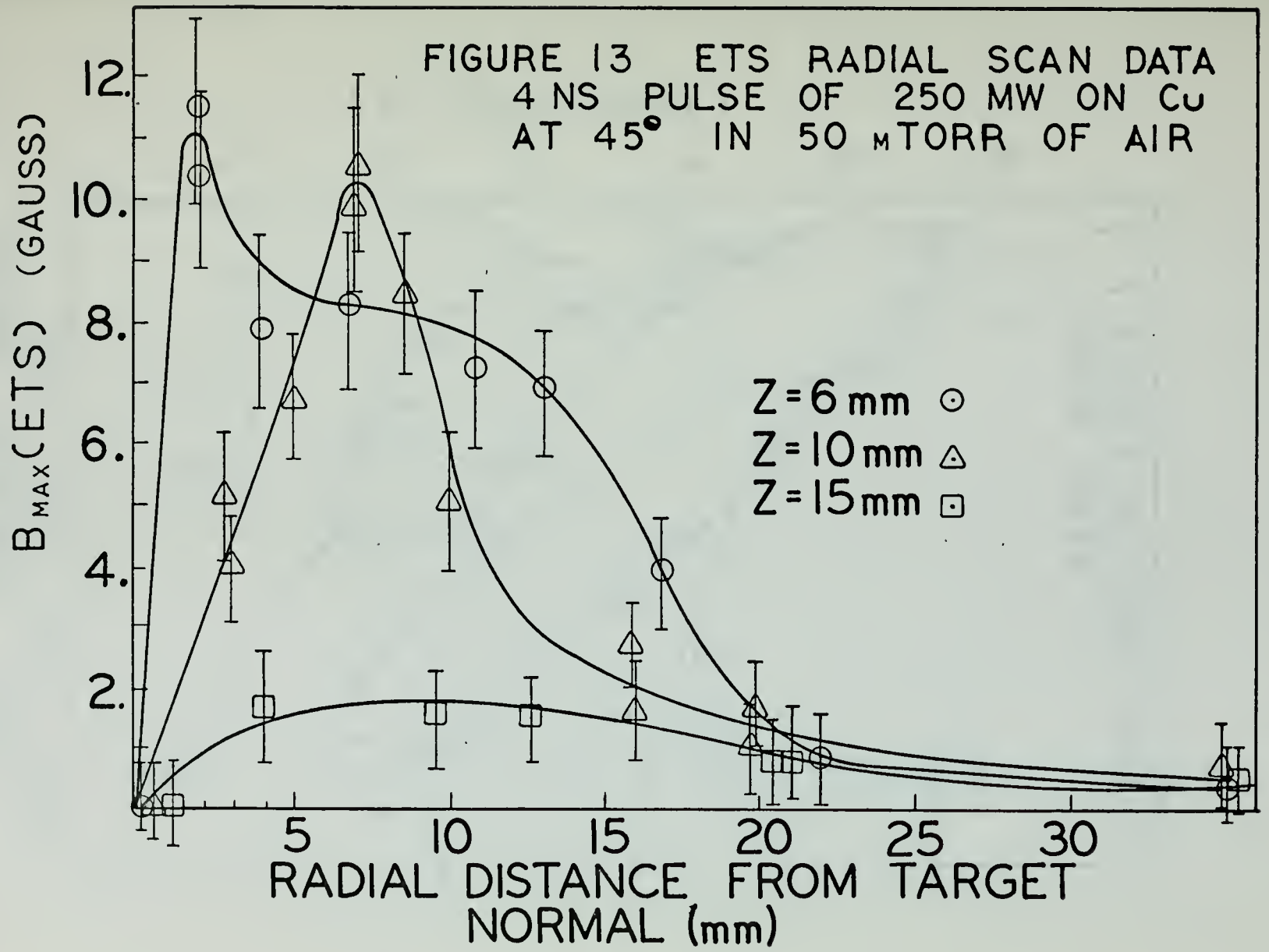
FIGURE 13 ETS RADIAL SCAN DATA
4 NS PULSE OF 250 MW ON Cu
AT 45° IN 50 mTORR OF AIR
Z = 6 mm
Z = 10 mm
Z = 15 mm
B MAX (ETS) (GAUSS)
12.
10.
8.
6.
4.
2.
5
10
15
20
25
30
RADIAL DISTANCE FROM TARGET
NORMAL (mm)

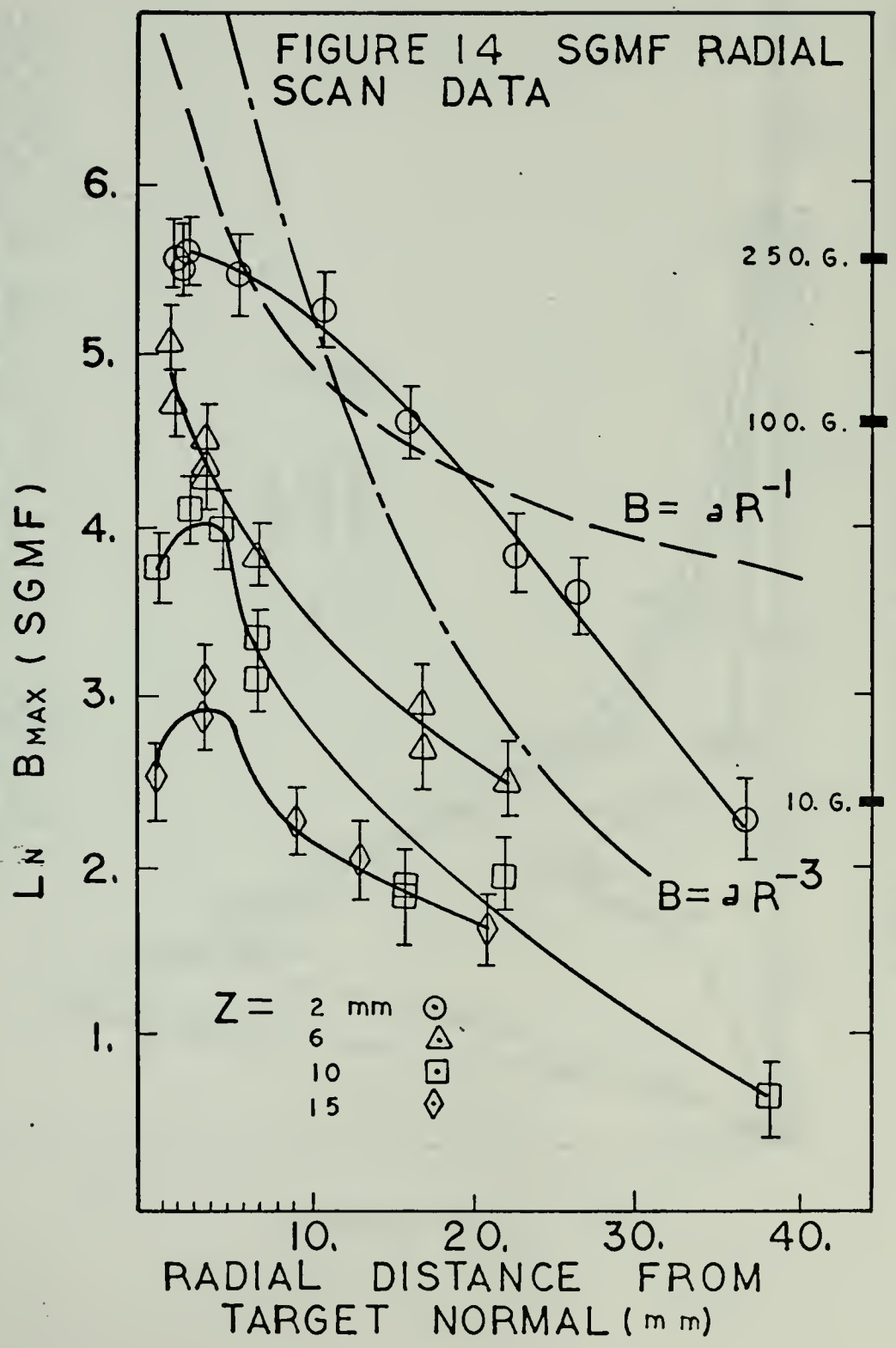
FIGURE 14 SGMF RADIAL SCAN DATA
6.
5.
4.
3.
2.
1.
250. G.
100. G.
10. G.
B= aR^-1
B= aR^-3
Z= 2 mm
6
10
15
LN BMAX (SGMF)
10.
20.
30.
40.
RADIAL DISTANCE FROM TARGET NORMAL (mm)

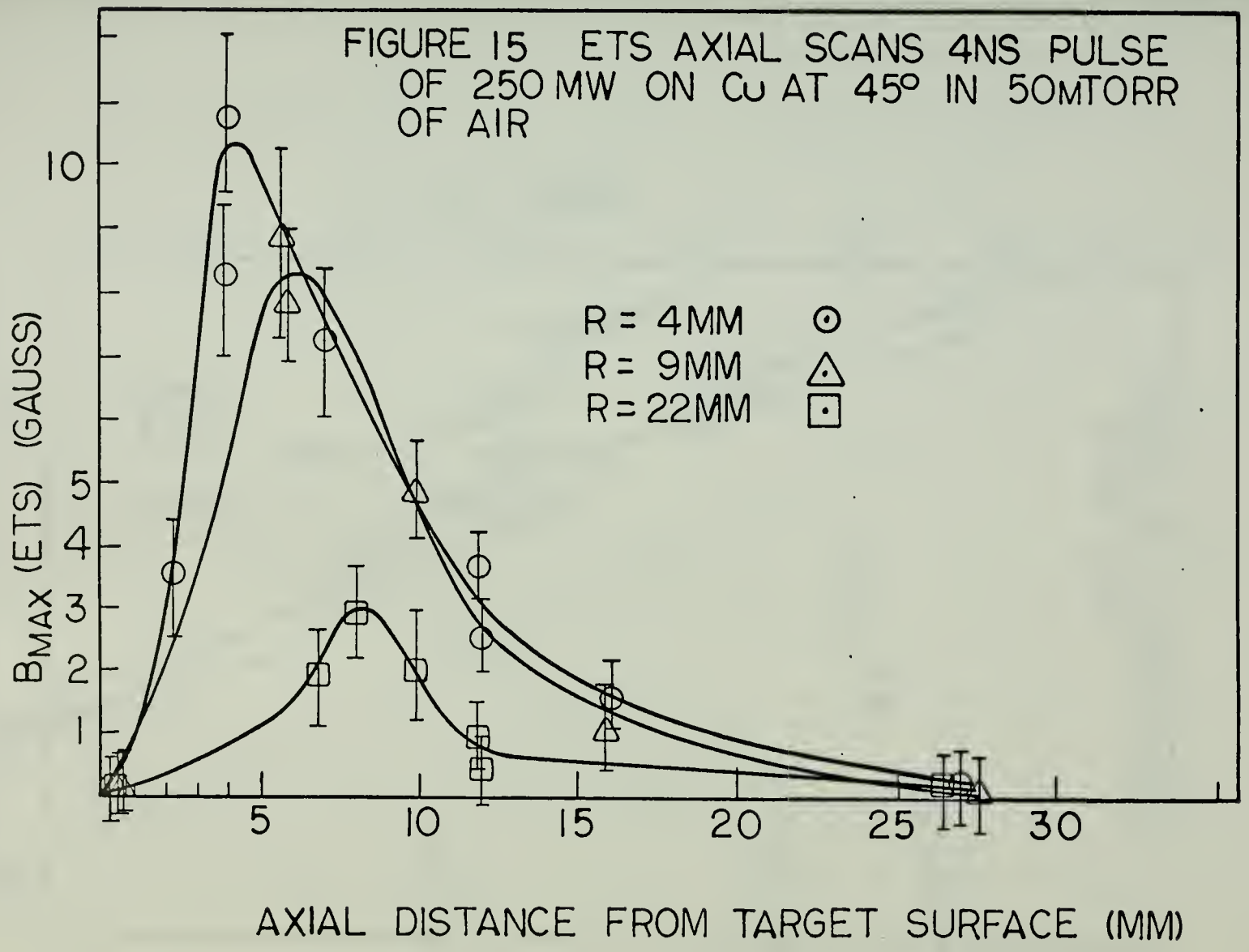
FIGURE 15 ETS AXIAL SCANS 4NS PULSE OF 250 MW ON Cu AT 45° IN 50MTORR OF AIR
R = 4MM
R = 9MM
R = 22MM
B_MAX (ETS) (GAUSS)
1
2
3
4
5
10
5
10
15
20
25
30
AXIAL DISTANCE FROM TARGET SURFACE (MM)

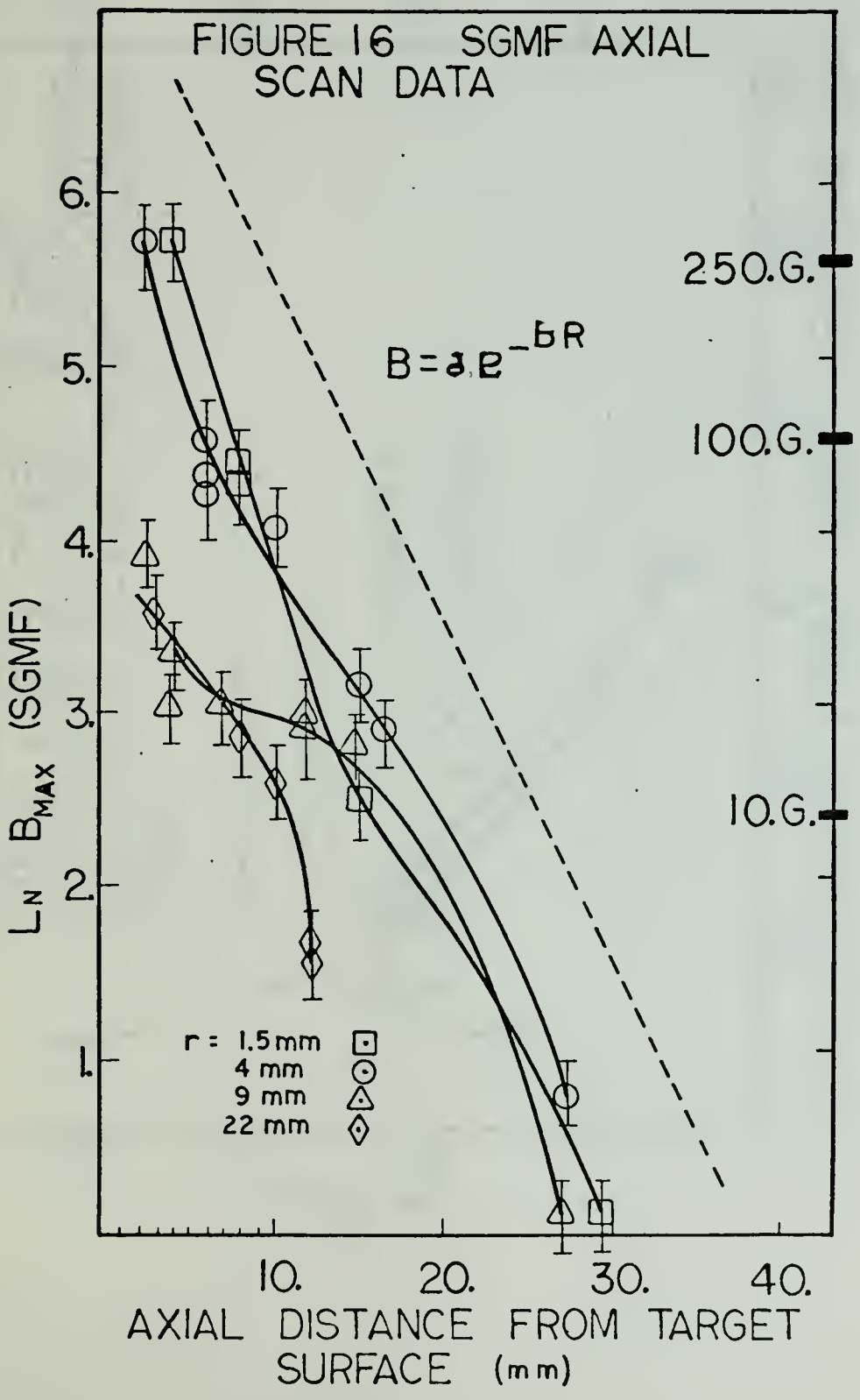
FIGURE 16 SGMF AXIAL SCAN DATA
$B = a e^{-bR}$
250.G.
100.G.
10.G.
$L_N B_{MAX}$ (SGMF)
6.
5.
4.
3.
2.
1.
r = 1.5mm
4 mm
9 mm
22 mm
10.
20.
30.
40.
AXIAL DISTANCE FROM TARGET SURFACE (mm)

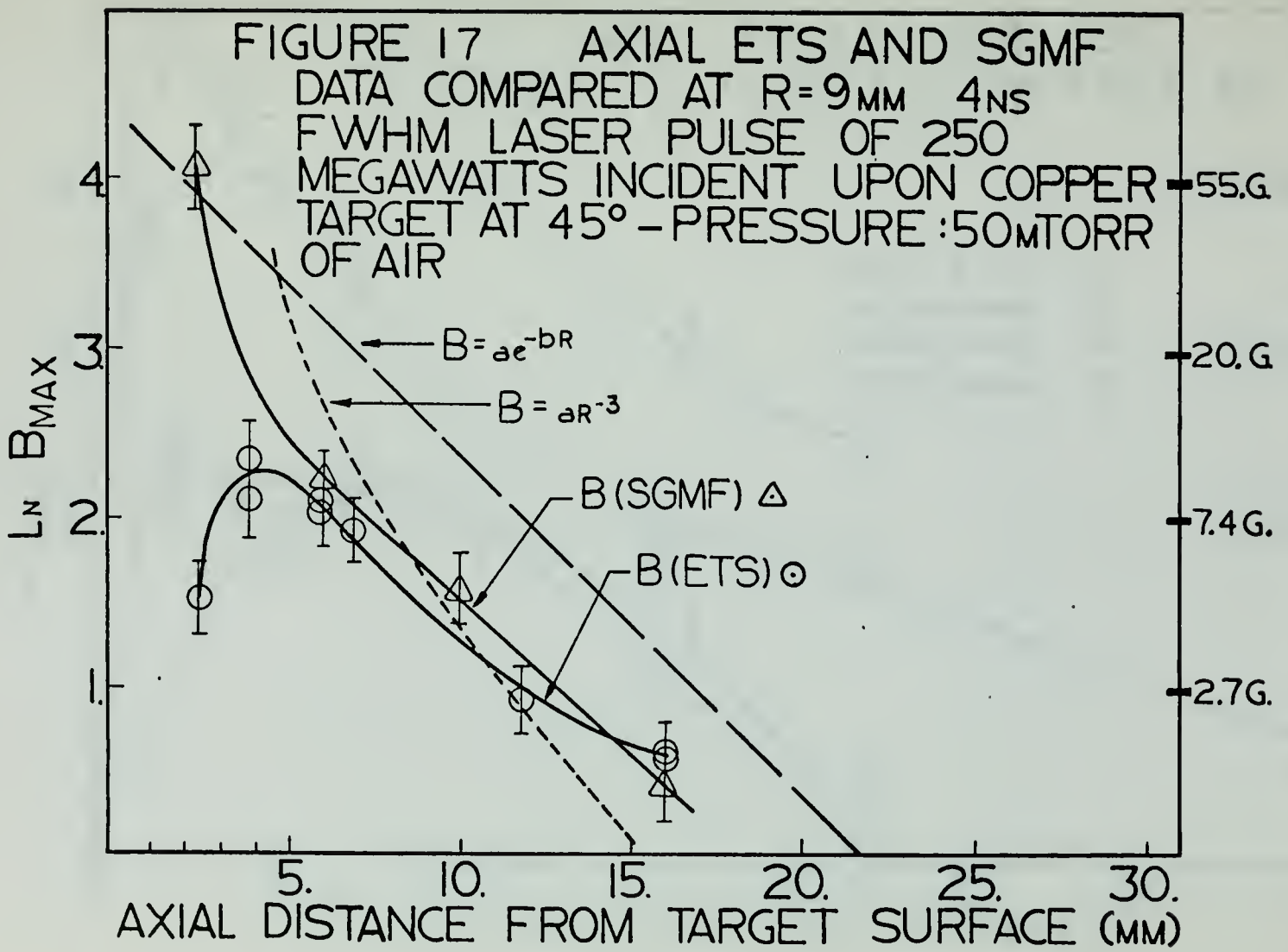
FIGURE 17 AXIAL ETS AND SGMF DATA COMPARED AT R=9MM 4NS FWHM LASER PULSE OF 250 MEGAWATTS INCIDENT UPON COPPER TARGET AT 45° - PRESSURE: 50MTORR OF AIR
B = ae^-bR
B = aR^-3
B (SGMF) △
B (ETS) ⊙
LN BMAX
4
3
2
1
55.G.
20.G
7.4G.
2.7G.
5.
10.
15.
20.
25.
30.
AXIAL DISTANCE FROM TARGET SURFACE (MM)

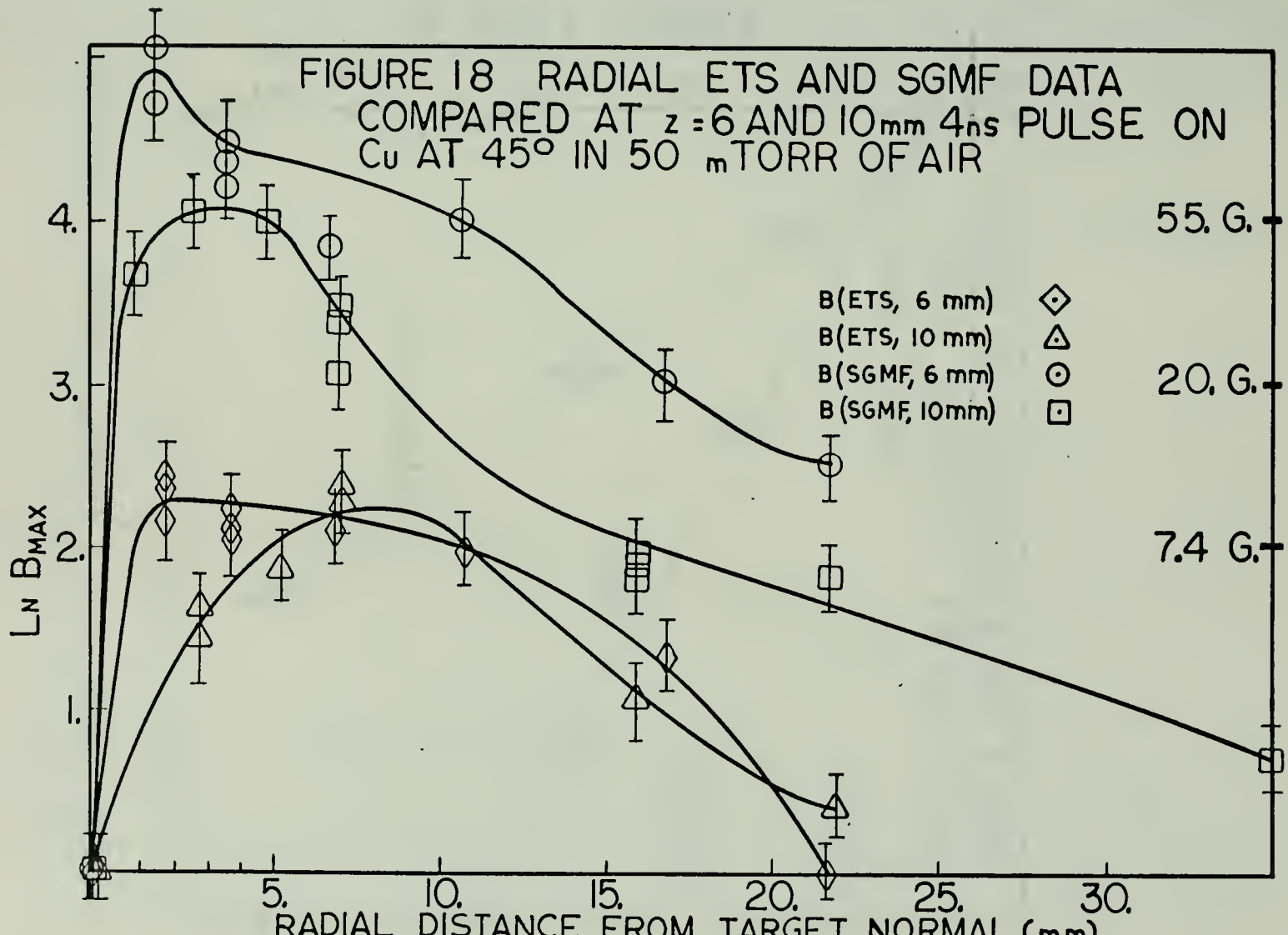
FIGURE 18 RADIAL ETS AND SGMF DATA
COMPARED AT z = 6 AND 10mm 4ns PULSE ON
Cu AT 45° IN 50 mTORR OF AIR
B(ETS, 6 mm)
B(ETS, 10 mm)
B(SGMF, 6 mm)
B(SGMF, 10mm)
55. G.
20. G.
7.4 G.
LN BMAX
4.
3.
2.
1.
5.
10.
15.
20.
25.
30.
RADIAL DISTANCE FROM TARGET NORMAL (mm)

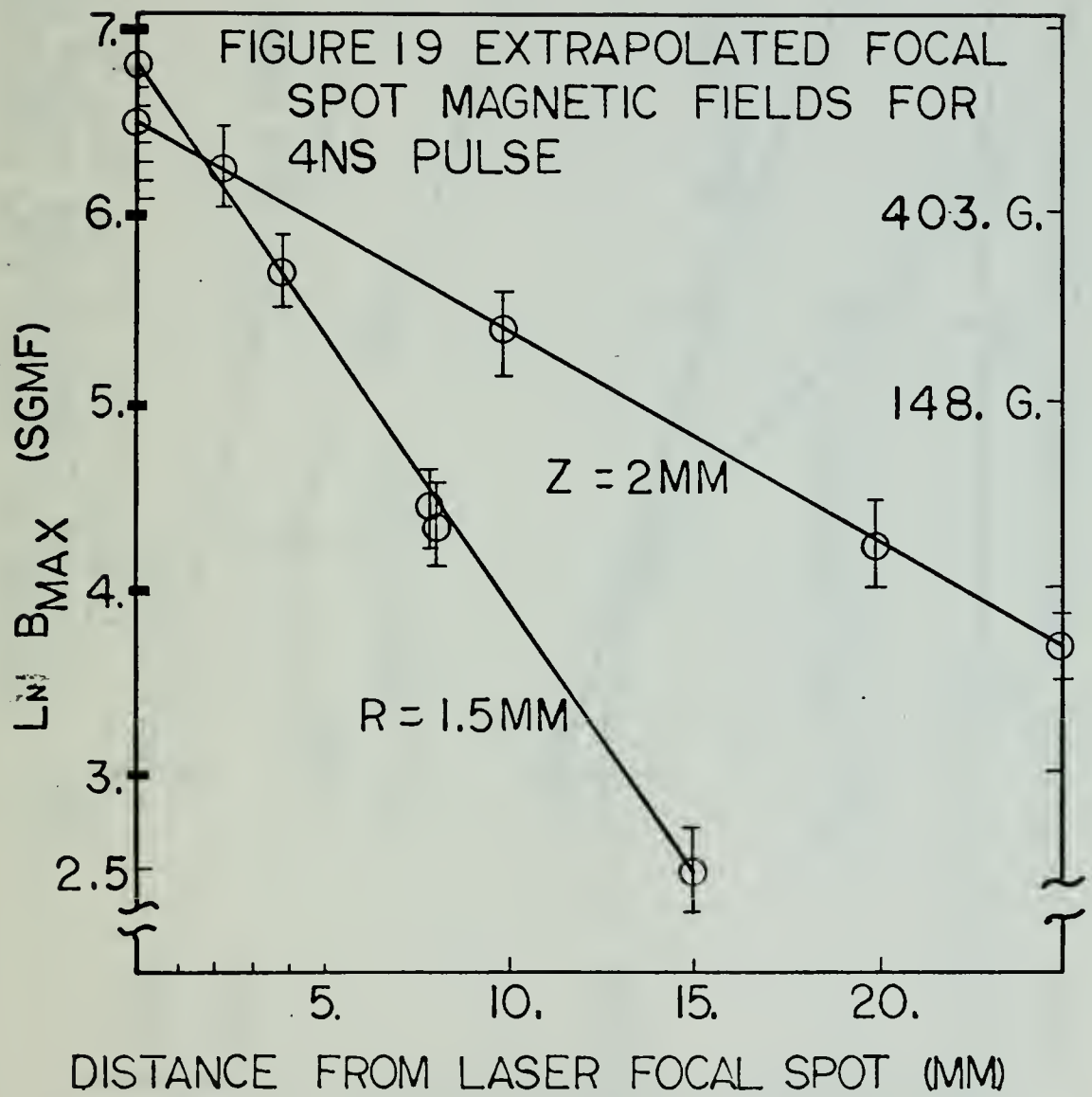
FIGURE 19 EXTRAPOLATED FOCAL SPOT MAGNETIC FIELDS FOR 4NS PULSE
403. G.
148. G.
Z = 2MM
R = 1.5MM
LN B MAX (SGMF)
7.
6.
5.
4.
3.
2.5
5.
10.
15.
20.
DISTANCE FROM LASER FOCAL SPOT (MM)

FIGURE 20 K1500 AND SPACERAYS LASER DATA COMPARISON – 40ns AND 4ns LASER PULSES ON Cu AT 45° IN 50 mTORR OF AIR

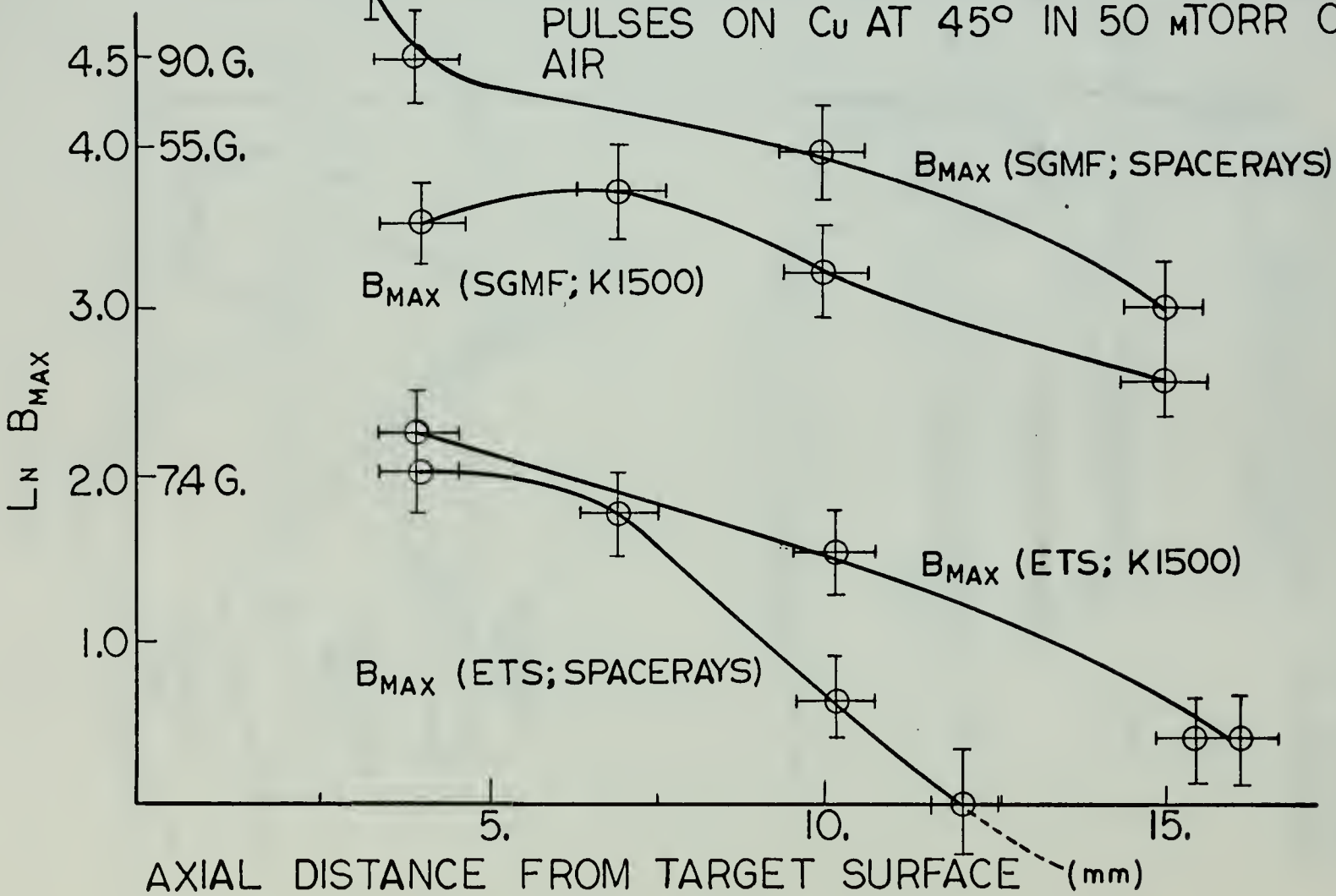

FIGURE 21 TYPICAL dB/dt DATA FROM ALL LASER SYSTEMS FOR 50 mTORR OF AIR AT POSITIONS: CO_2-(13,0,9)- ALL OTHERS (7,0,5)

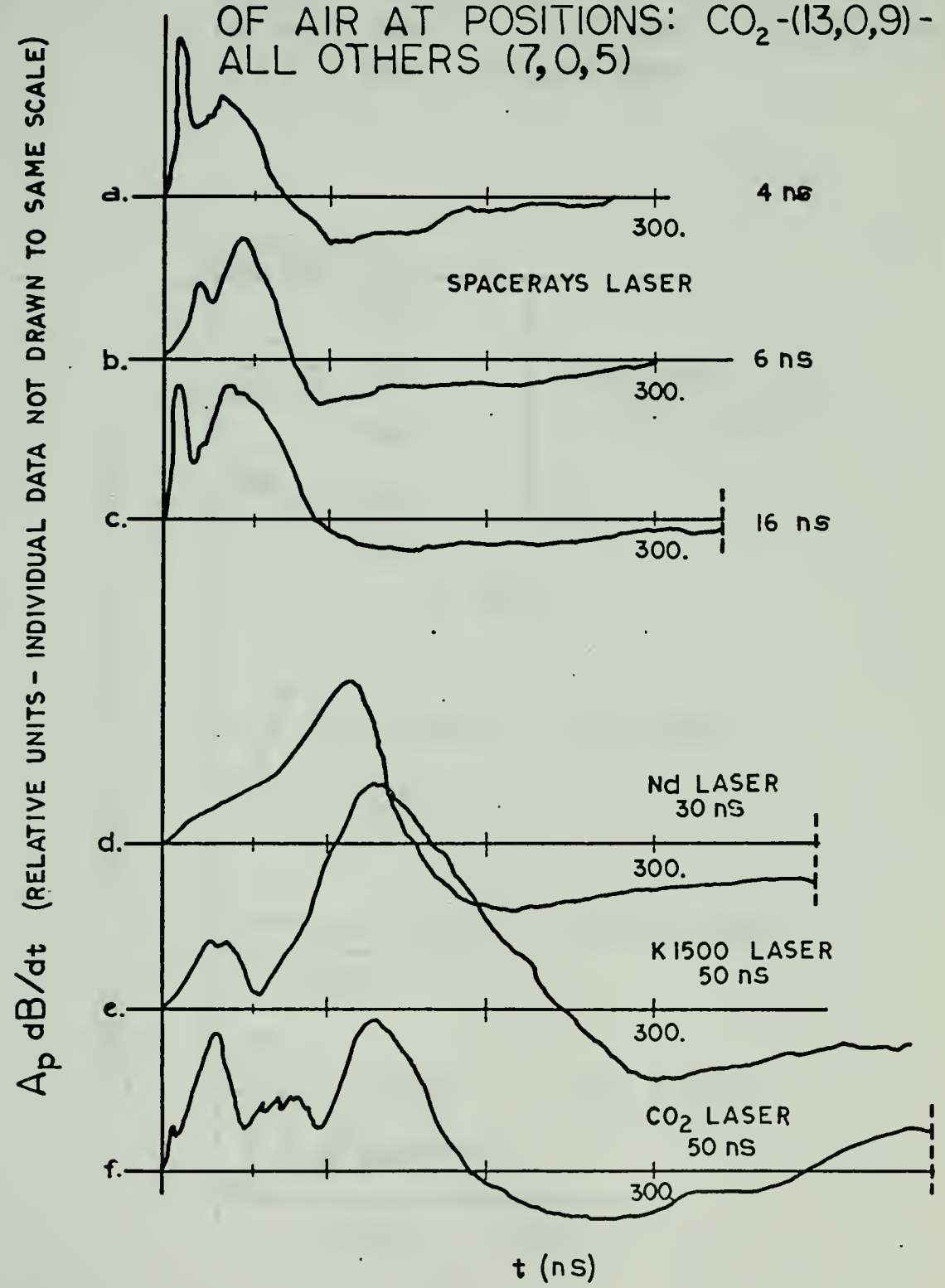

FIGURE 22 LASER PULSE SHAPES FOR ALL LASER SYSTEMS AT: (a) 250 MW, (b) 400 MW, (c) 200 MW, (d) 500 MW, (e) 150 MW, (f) 300 MW

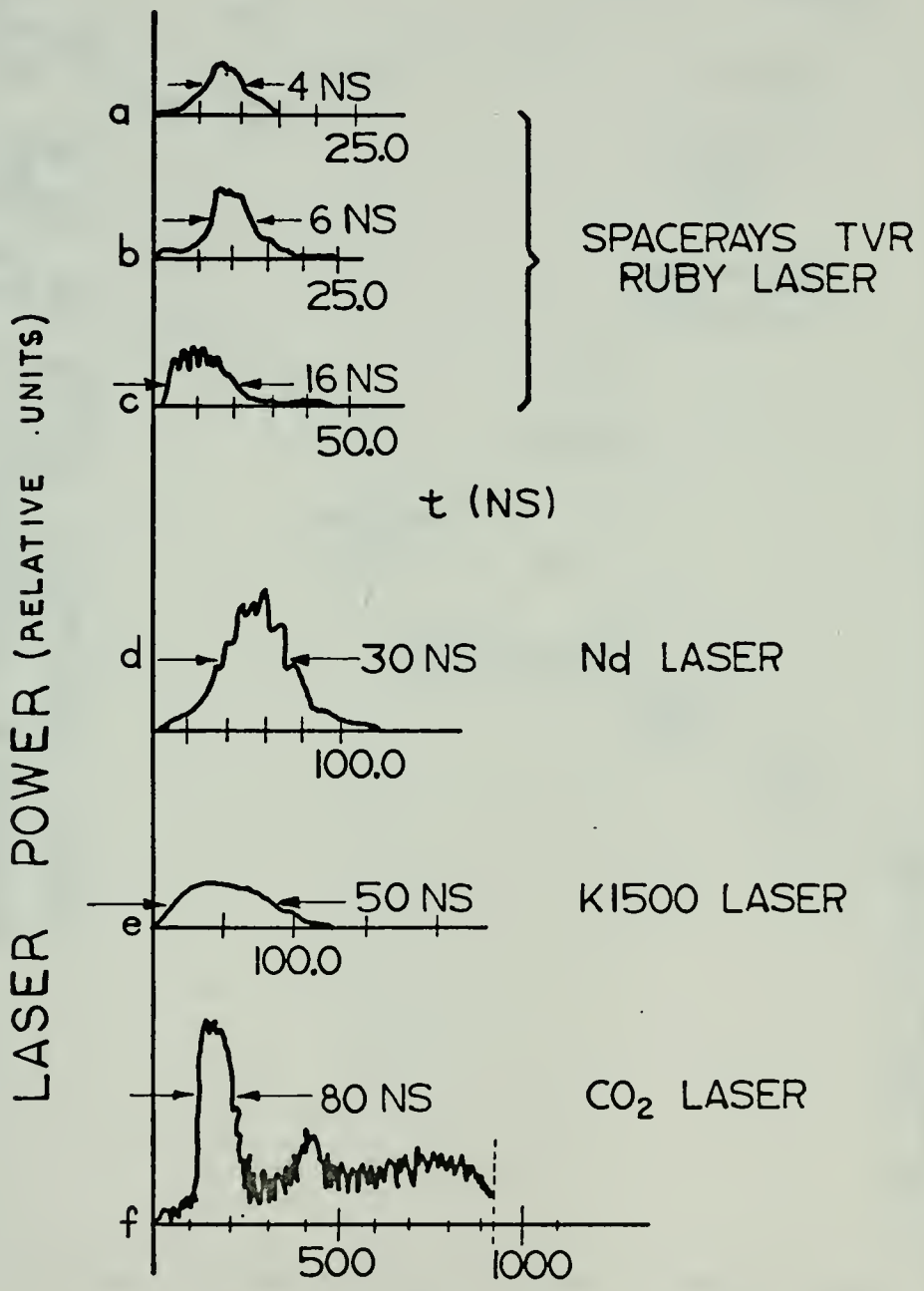

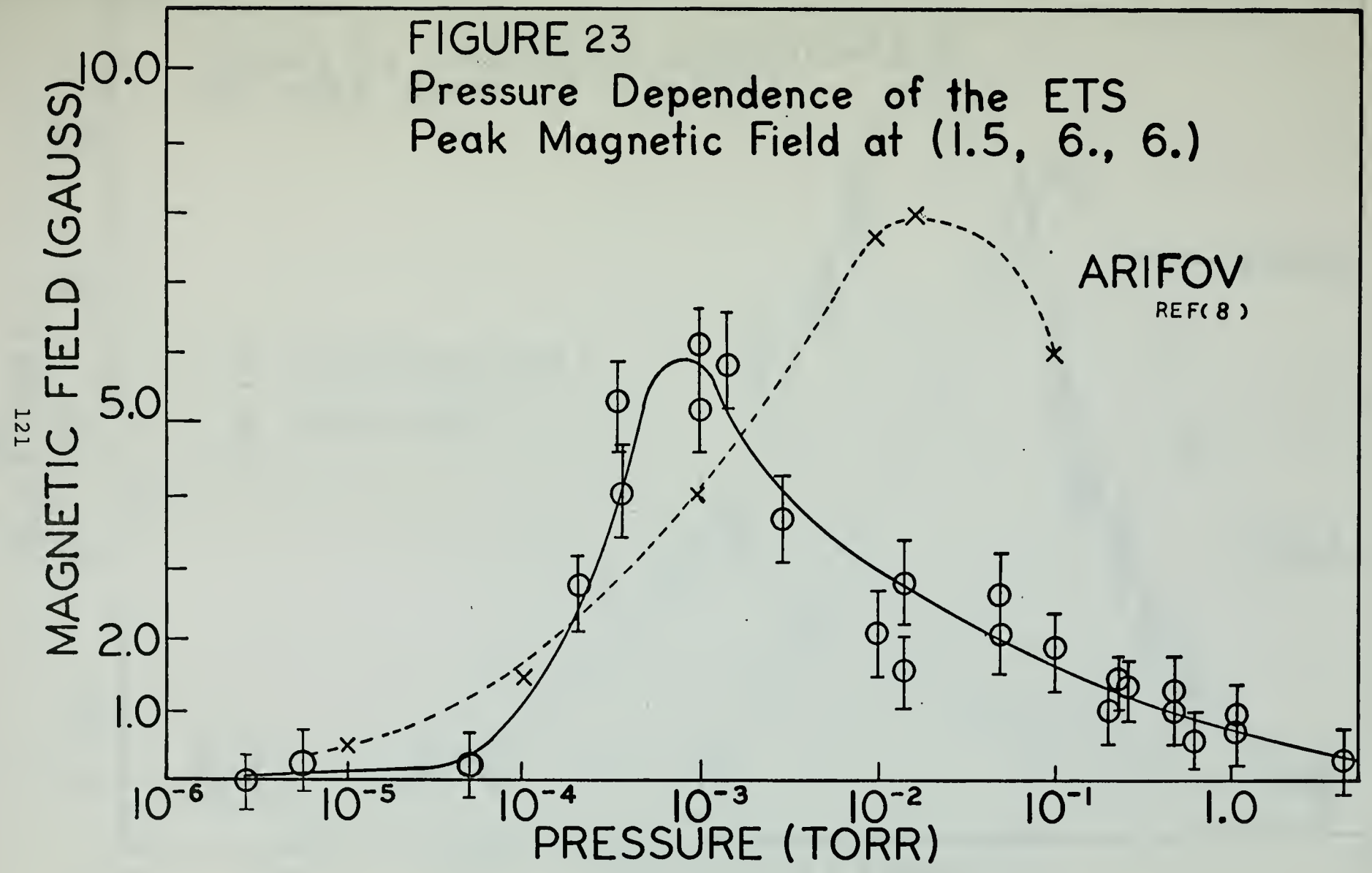
FIGURE 23
Pressure Dependence of the ETS
Peak Magnetic Field at (1.5, 6., 6.)
ARIFOV
REF(8)
MAGNETIC FIELD (GAUSS)
10.0
5.0
2.0
1.0
10^{-6}
10^{-5}
10^{-4}
10^{-3}
10^{-2}
10^{-1}
1.0
PRESSURE (TORR)

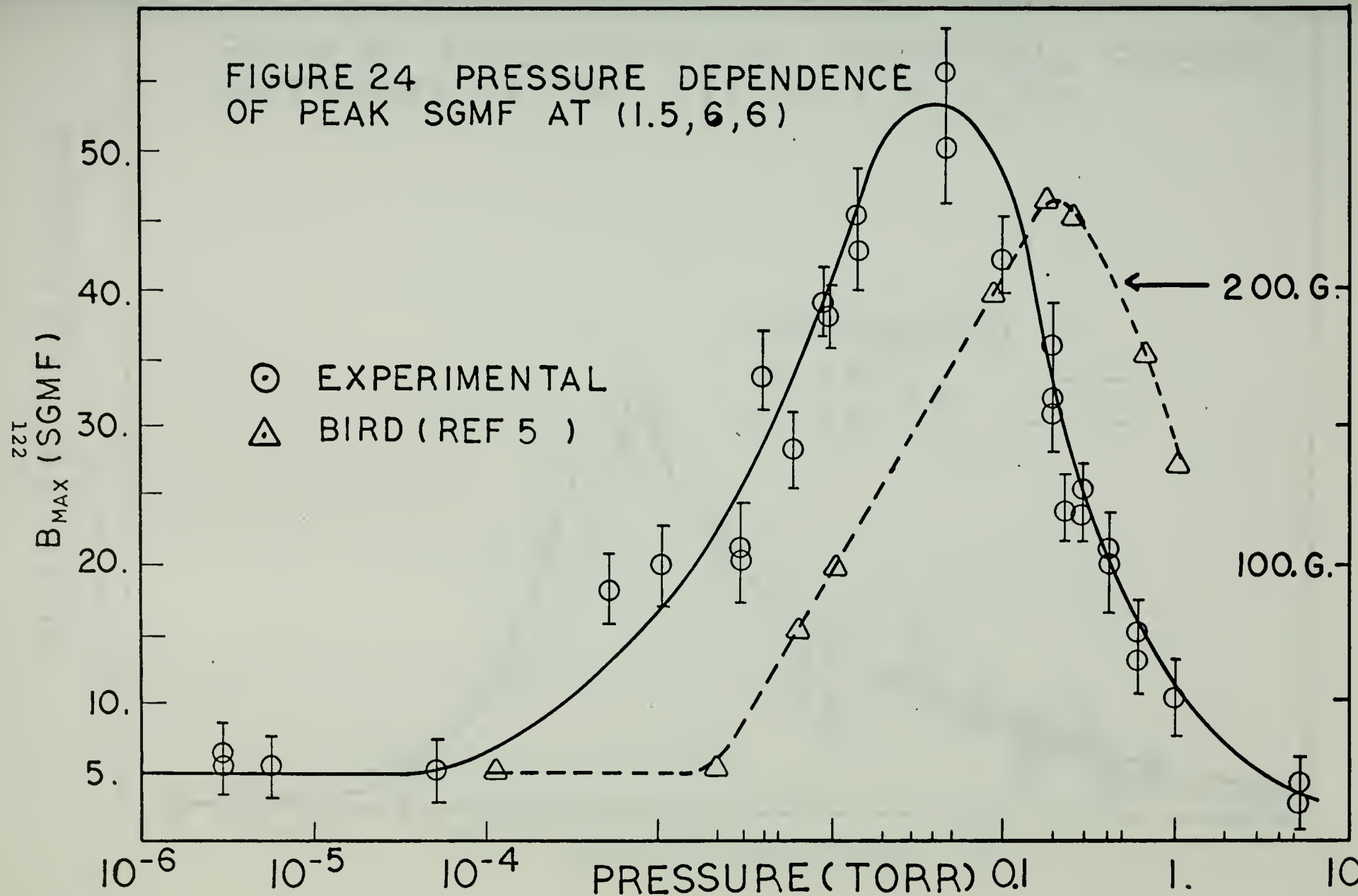
FIGURE 24 PRESSURE DEPENDENCE OF PEAK SGMF AT (1.5,6,6)
50.
40.
30.
20.
10.
5.
B_{MAX} (SGMF)
EXPERIMENTAL
BIRD (REF 5)
200. G.
100. G.
10^{-6}
10^{-5}
10^{-4}
PRESSURE (TORR)
0.1
1.
10.

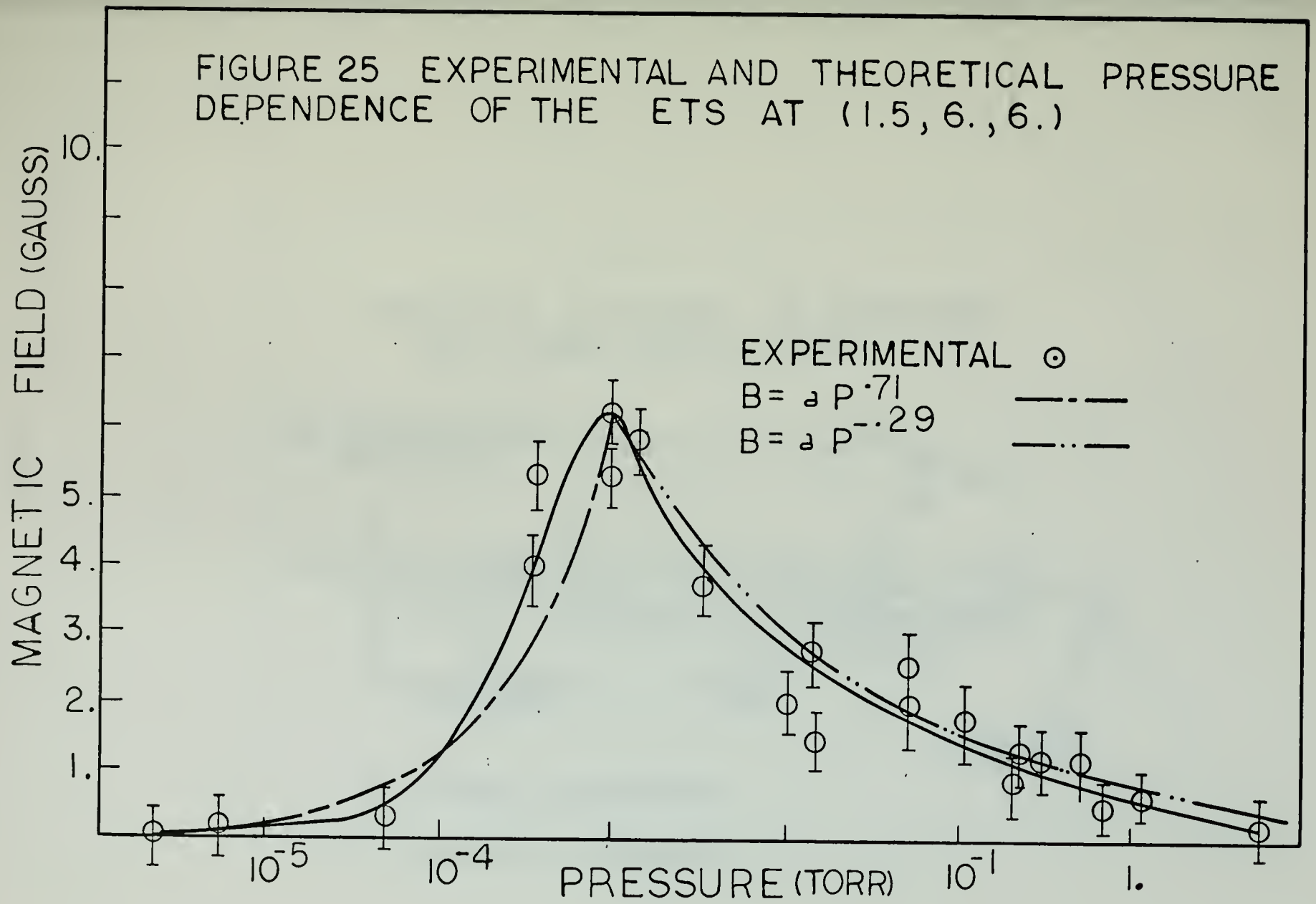
FIGURE 25 EXPERIMENTAL AND THEORETICAL PRESSURE DEPENDENCE OF THE ETS AT (1.5, 6., 6.)
MAGNETIC FIELD (GAUSS)
10.
5.
4.
3.
2.
1.
EXPERIMENTAL ⊙
B = a P^.71
B = a P^-.29
10^-5
10^-4
PRESSURE (TORR)
10^-1
1.

FIGURE 26 SCHEMATIC OF SPACERAYS TVR LASER OSCILLATOR

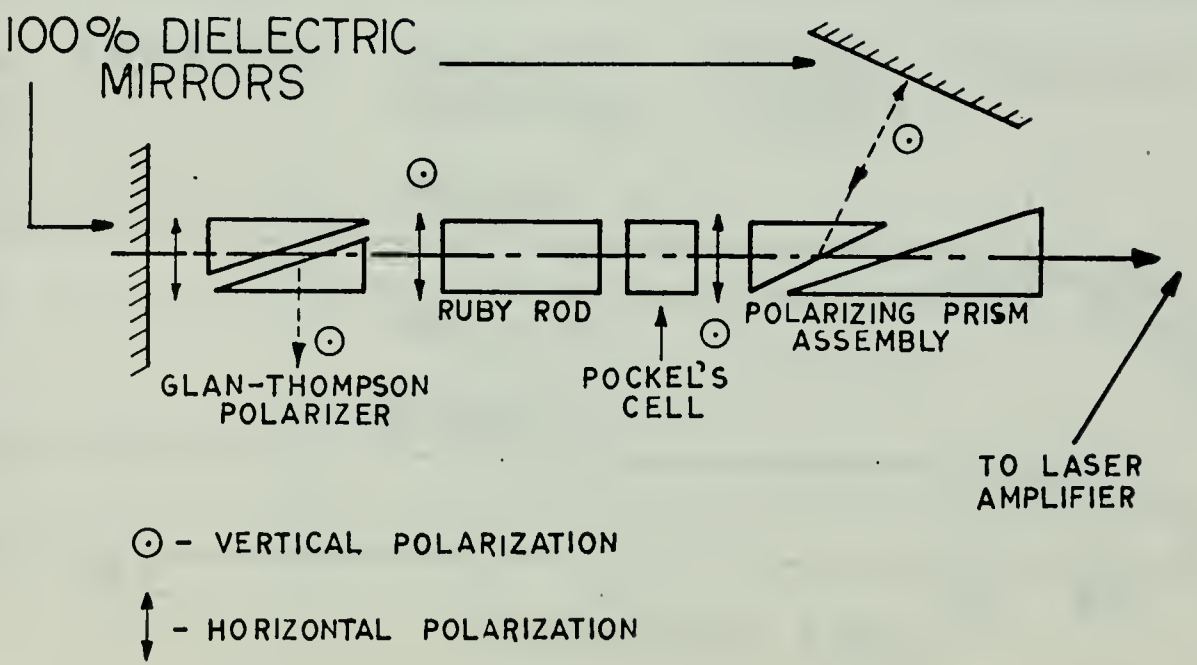

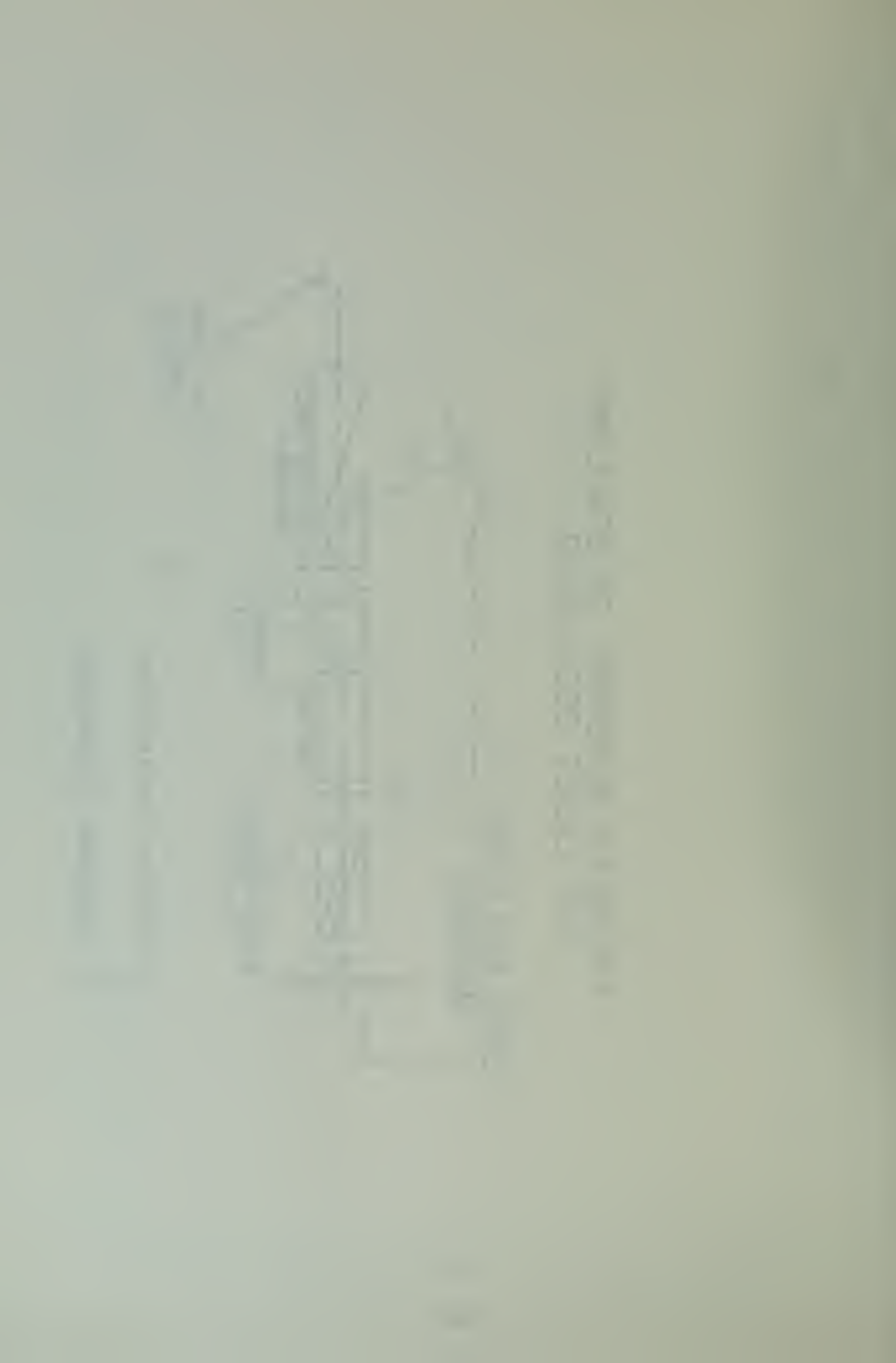

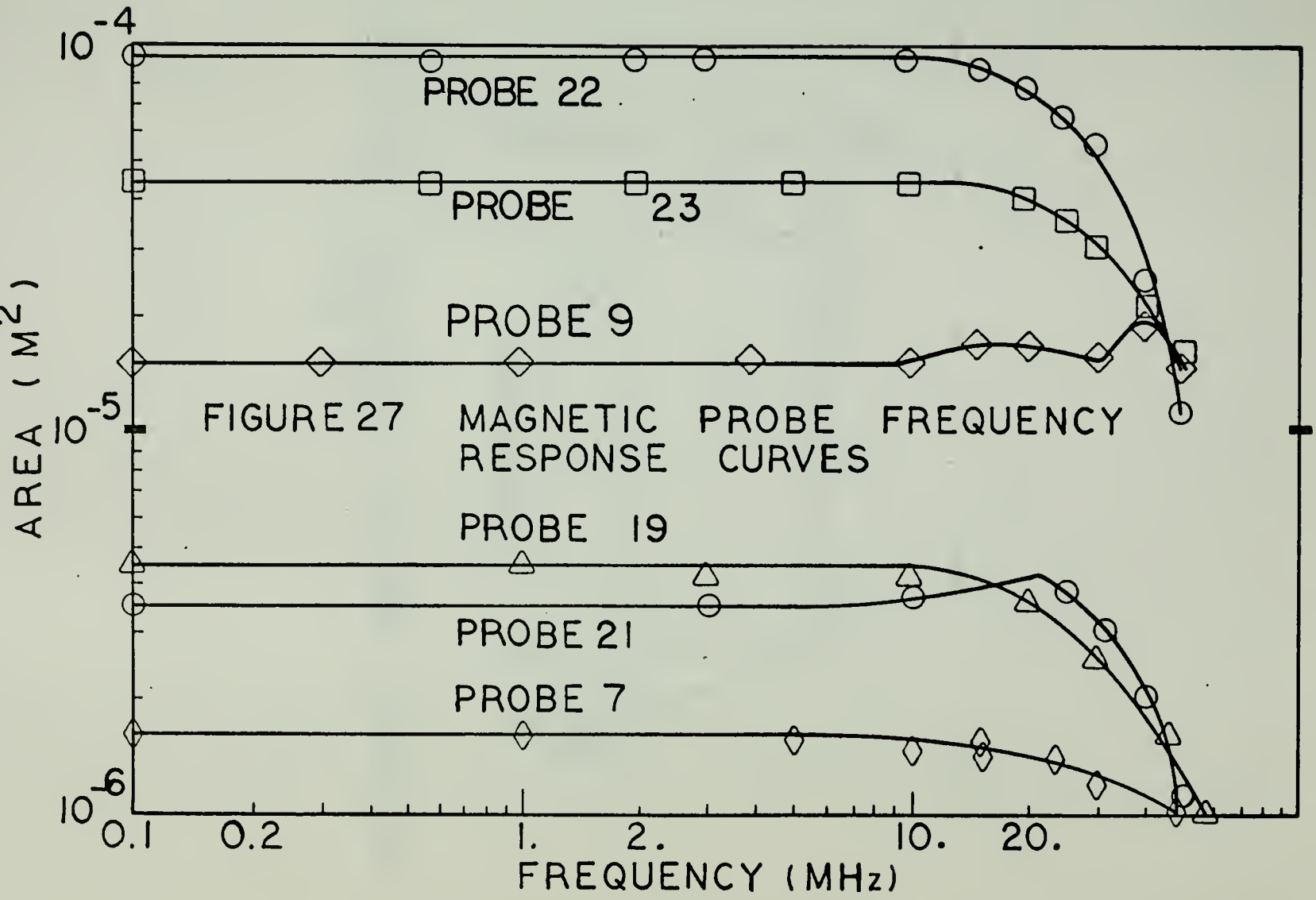

FIGURE 27 MAGNETIC PROBE FREQUENCY RESPONSE CURVES

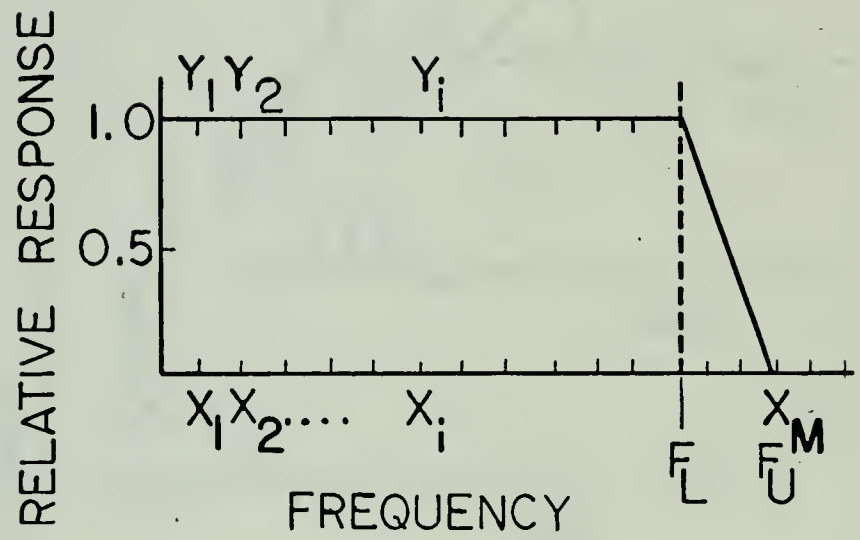

FIGURE 28 NUMERICAL FILTERING RESPONSE FUNCTION

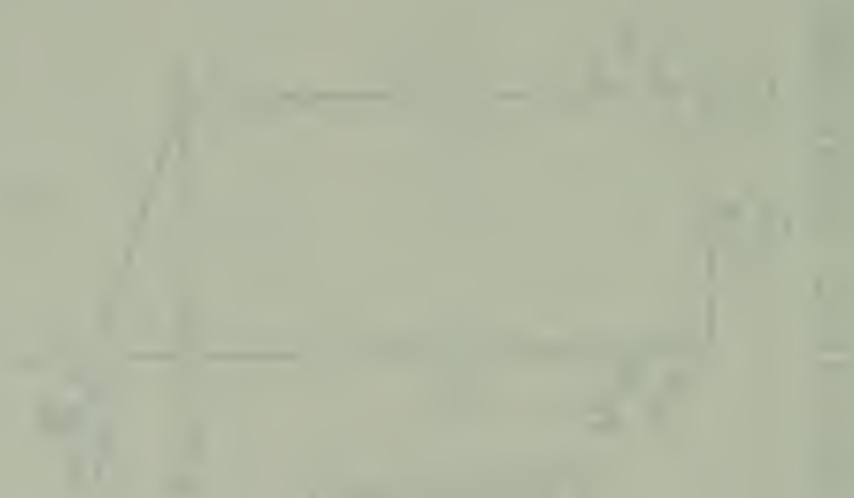

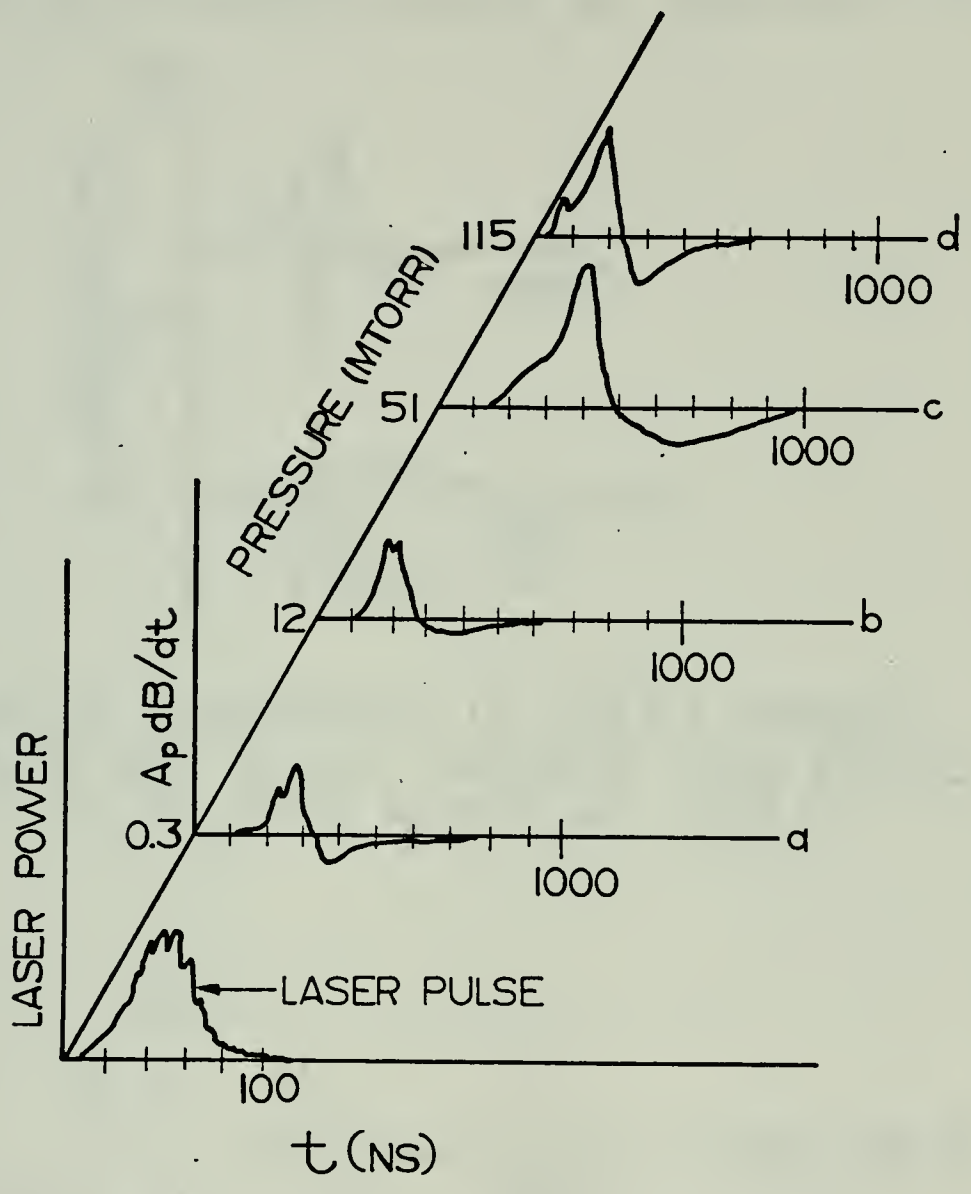

FIGURE 29 Nd GLASS LASER PULSE AND TYPICAL dB/dt DATA AT 4 PRESSURES AT (7,0,5)

FIGURE 30 MULTIPLE PULSE DATA FROM Nd LASER ON 0.002" MYLAR - 30 NS PULSE AT 0° IN 10 MTORR OF AIR AT (10,0,5)

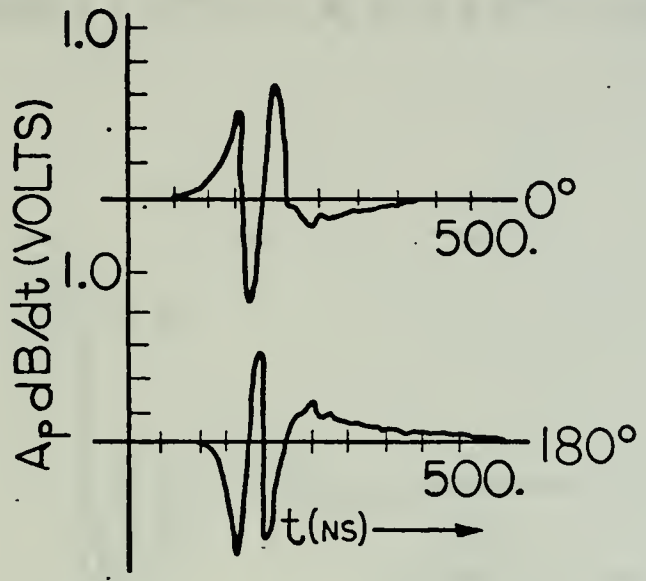

FIGURE 31 COMPARISON OF dB/dt SIGNALS FROM Cu AND MYLAR TARGETS - 30 NS PULSE AT 0° IN 25 MTORR OF AIR AT (10,0,5)

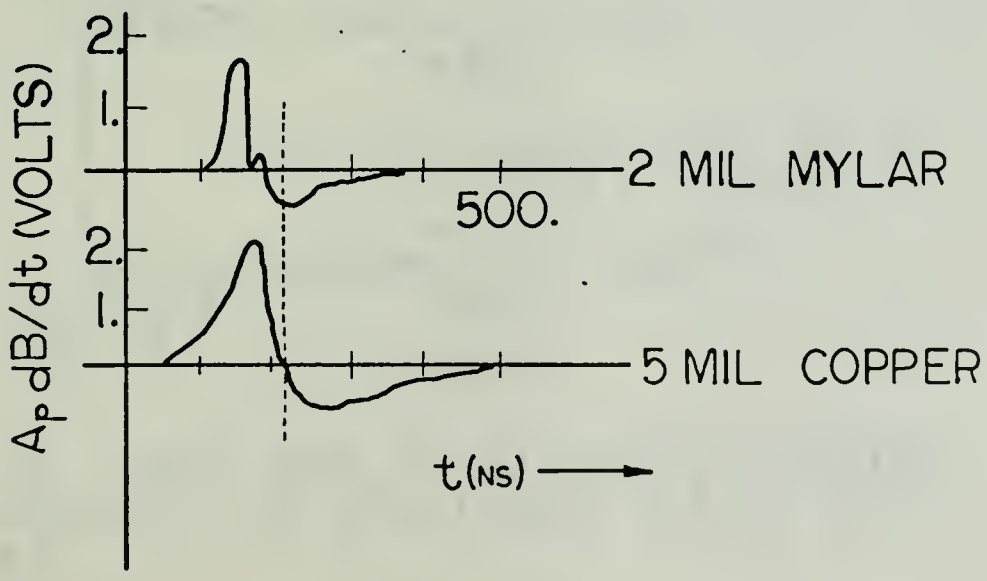

FIGURE 32 dB/dt CO_2 DATUM AT (40,0,30) MM
CO_2 LASER ON Cu AT 0° IN 2.5 MTORR OF AIR
B_{MAX} (SGMF) = 35 G. ; $v_\tau = 6 \times 10^6$ CM/SEC

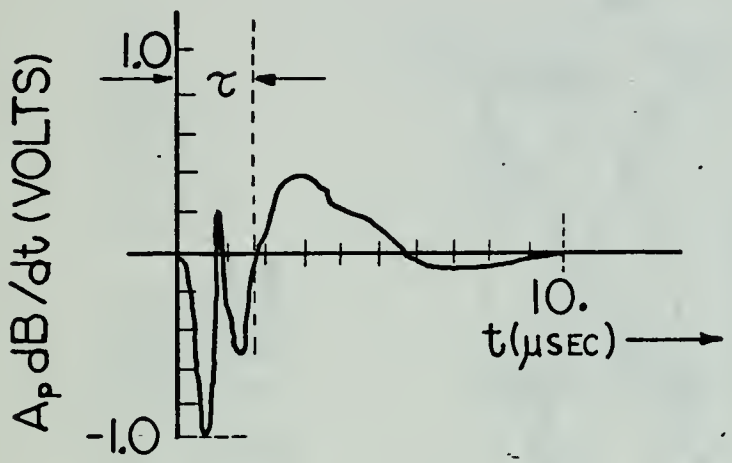

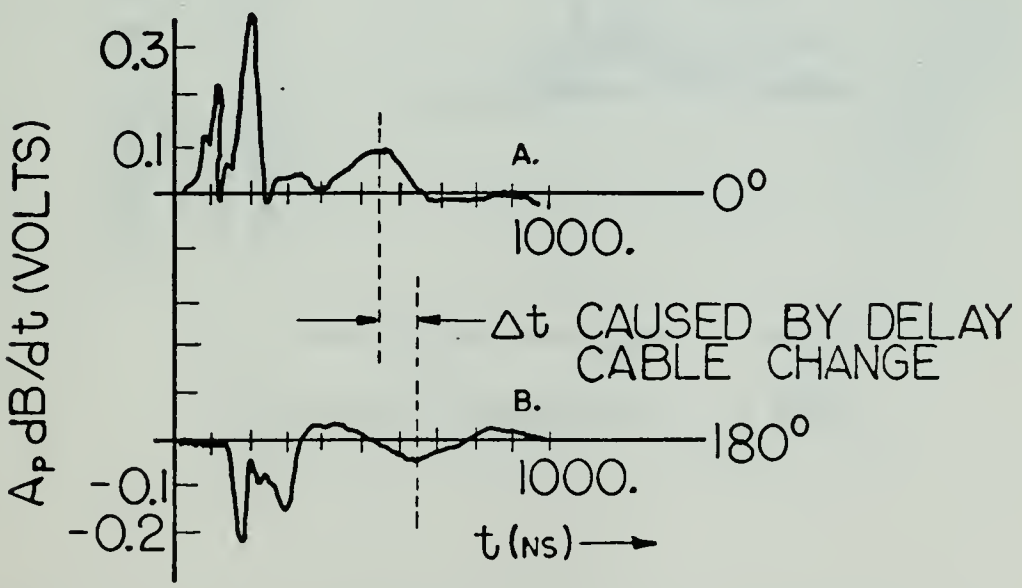

FIGURE 33 dB/dt DATA AT (A) (15,0,9) (B) (13,0,9) IN 2.5 MTORR OF AIR 80 NS LASER PULSE ONTO Cu TARGET.

FIGURE 34 MATERIAL STUDY AT
1 mTORR 4 ns LASER PULSE
PROBE 1 : (5.4, 0, 6.5) mm
PROBE 2 : (5., 0, 7.5) mm

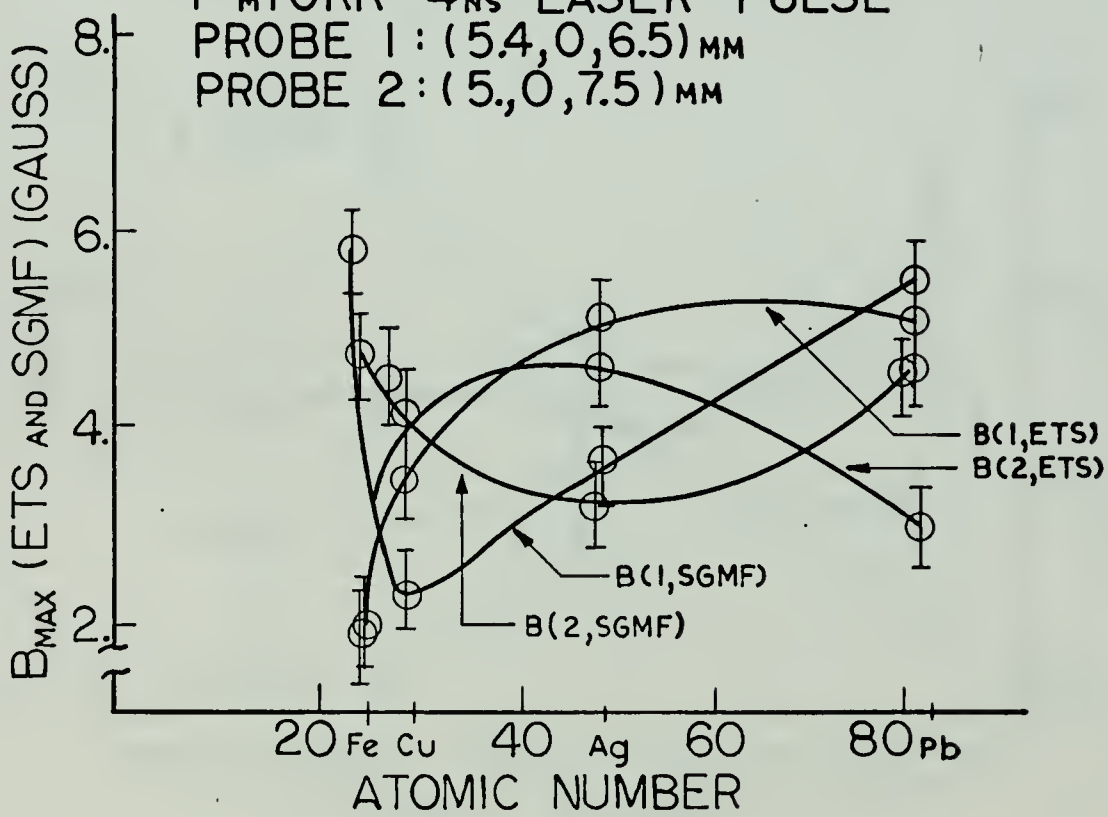

FIGURE 35 MATERIAL STUDY AT
20 mTORR 4ns LASER PULSE
PROBE 1: (5.4, 0, 6.5) mm
PROBE 2: (5., 0, 7.5) mm

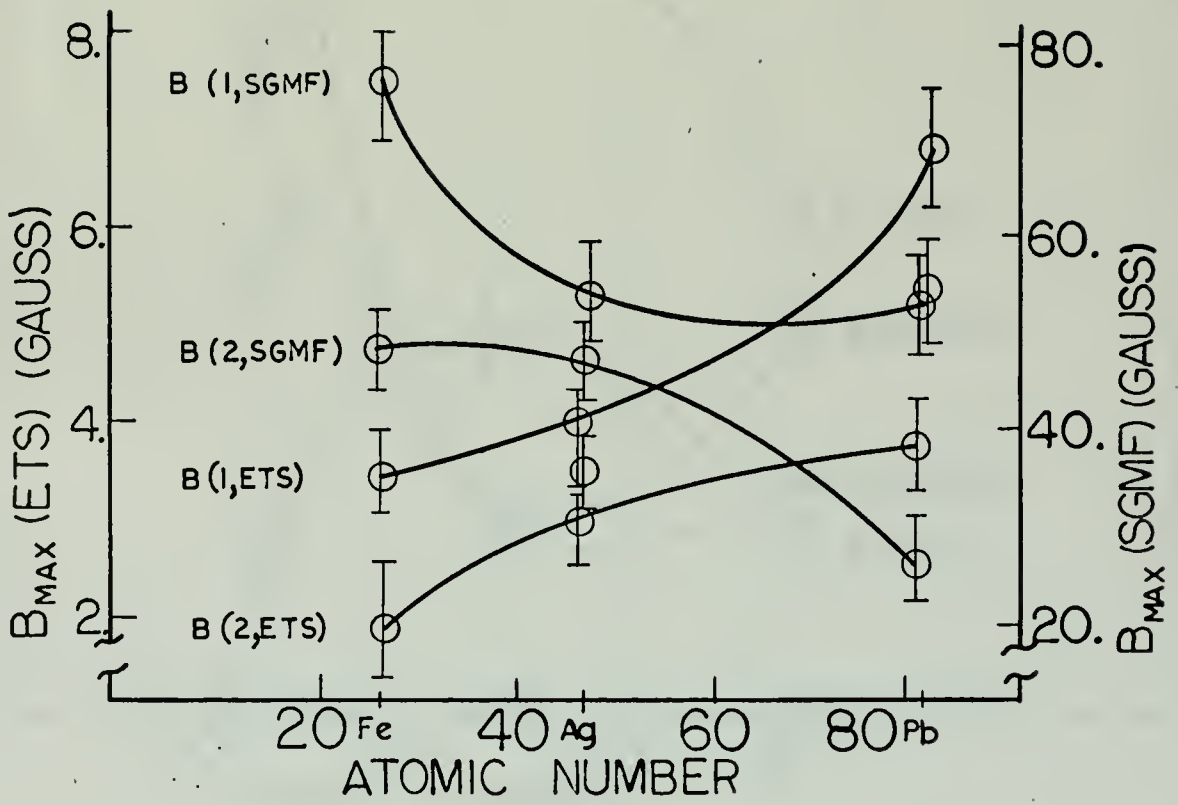

FIGURE 36 MATERIAL STUDY AT 200 mTORR 4ns LASER PULSE
PROBE 1: (5.4,0,6.5) mm PROBE 2: (5.,0,7.5) mm

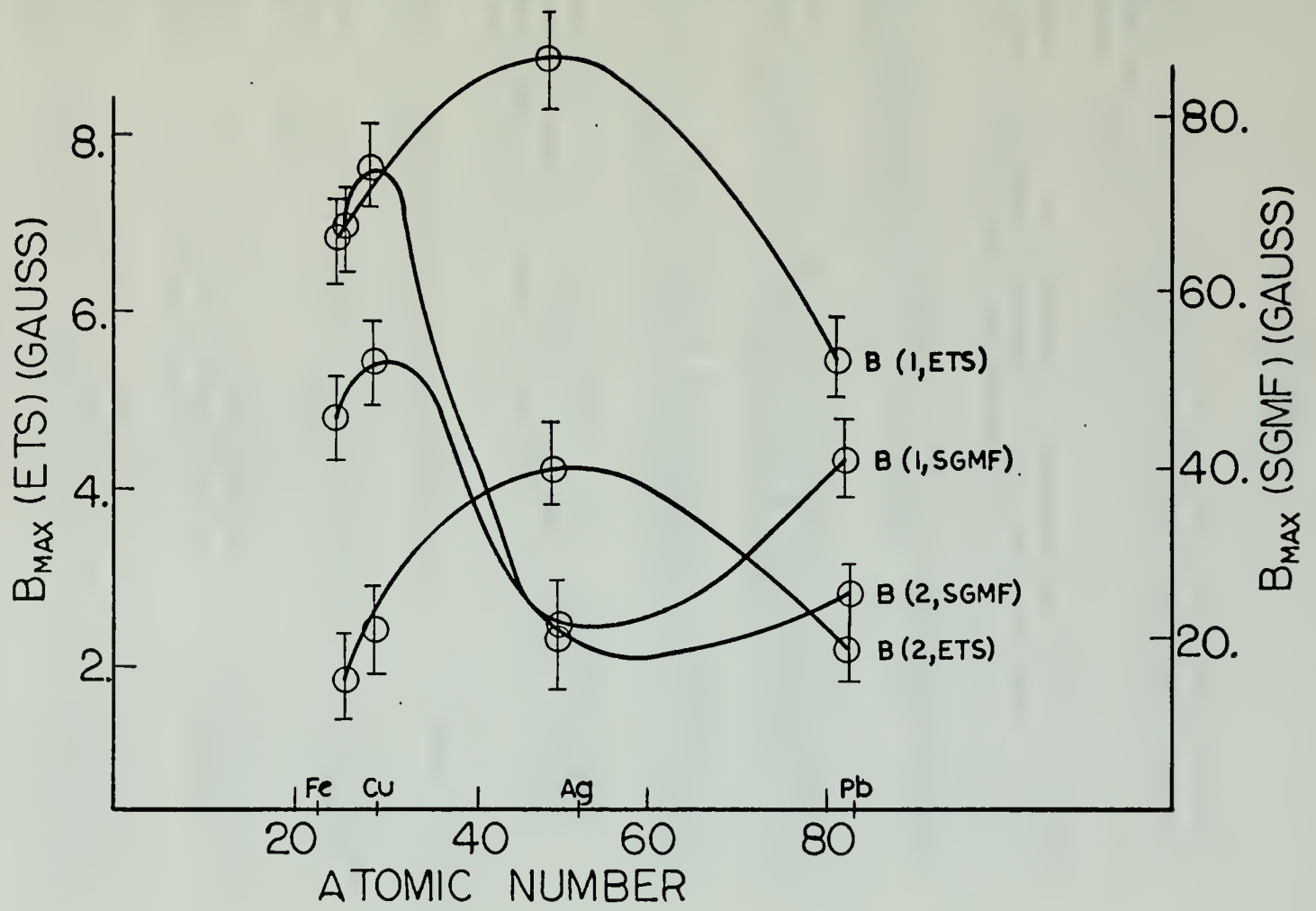

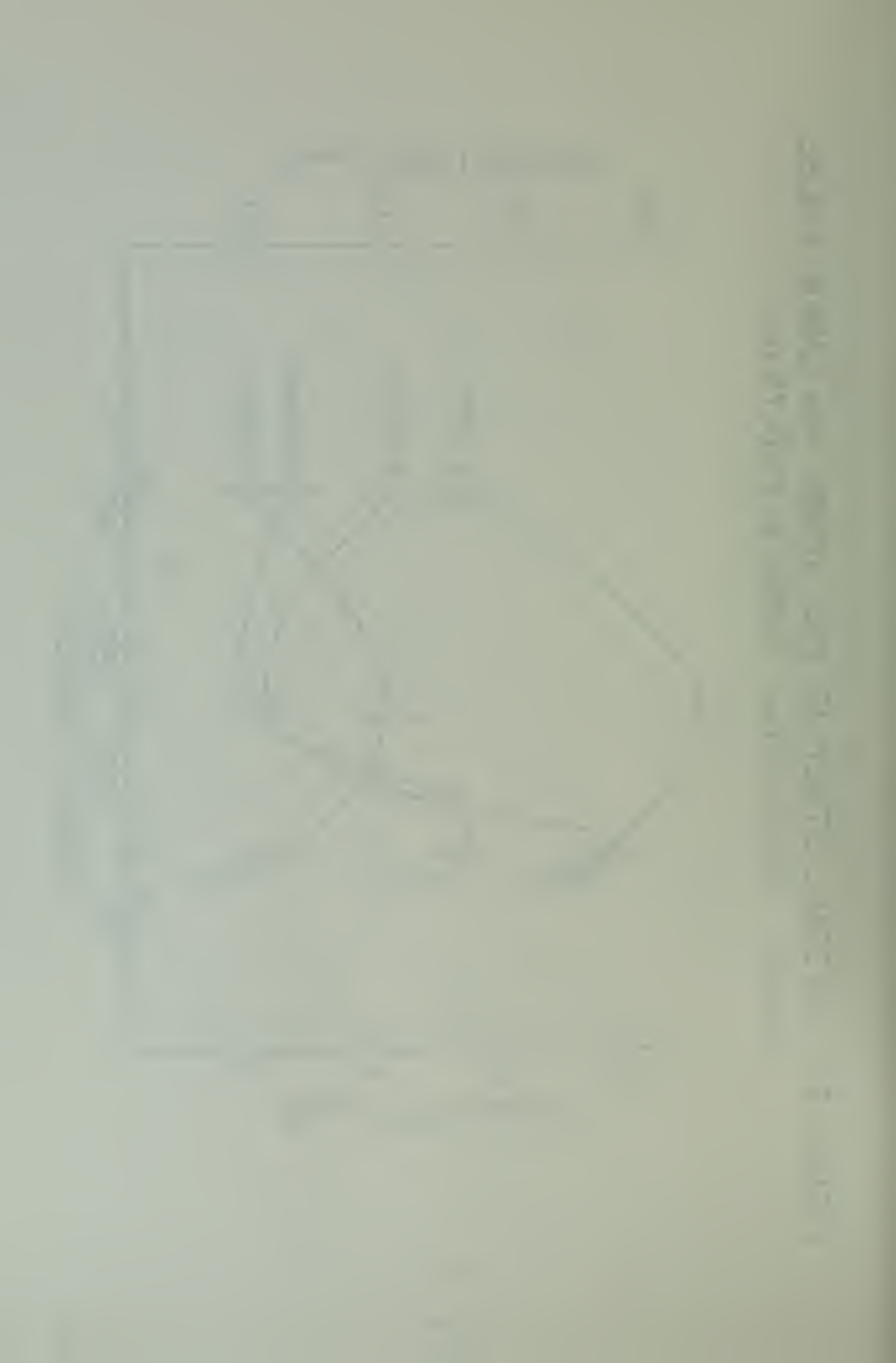

BIBLIOGRAPHY

1. Korobkin, V.V., and Serov, R.V., "Investigation of the Magnetic Field of a Spark Produced by Focusing Laser Radiation", JEPT Letters, v.4, no. 3, pp 103-106, 1 August 1966.

2. Stamper, J.A., and others, "Spontaneous Magnetic Fields in Laser Produced Plasmas", Phys. Rev. Letters, v.26, no. 17, pp 1012-1015, 26 April 1971.

3. Davis, L.J., Self-Generated Magnetic Fields Produced by Laser Bombardment of a Solid Target, MS Thesis, Naval Postgraduate School, 1971.

4. McKee, L.L., III, An Investigation of the Self-Generated Magnetic Fields Associated with a Laser Produced Plasma, Ph.D. Thesis, Naval Postgraduate School, 1972.

5. Bird, R.S., The Pressure Dependence of Spontaneous Magnetic Fields in a Laser Produced Plasma, Ph.D. Thesis, Naval Postgraduate School, 1973.

6. Giovanielli, D.V., and McCall, G.H., "Spontaneously Generated Magnetic Fields in a Laser Driven Plasma", unpublished Los Alamos Scientific Laboratory Report, February 1973.

7. Effects of High Power Laser Radiation, J.F. Ready, editor, chpt 4, Academic Press, 1971.

8. Arifov, T.U., and others, "Laser Induced Current Pulses from a Target in a Gas", JETP, v.28, no. 2, pp 201-203, February 1969.

9. Isenor, N.R., "Effect of Background Gas on Laser Induced Electron Emission from Metal Surfaces", J. Applied Physics, v.36, pp 316, 1965.

10. Langer, P., and others, "Laser Induced Emission of Electrons, Ions, and X-rays from Solid Targets", IEEE J. of Quantum Electronics, v.QE-2, no. 9, pp 299-512, September 1966.

11. Andreev, S.I., and others, "Thermionic Emission and Expansion of a Plasma Formed by Focussed Single Pulse Laser Radiation on a Solid Target", Soviet Physics-Technical Physics, v.13, no. 5, pp 657-662, November 1968.

12. Siller, G., and others, "Intense Electron Emission for Laser Produced Plasmas", in Laser Interaction and Related Plasma Phenomena, H. Hora and H. Schwarz, editors, Plenum Press, 1972.

13. Widner, M.M., and Wright, T.P., "Alternating Direction Implicit MHD Code for Simulating Laser Plasmas", Sandia Laboratories Report SC-DR-72-0733, January 1973., and Widner, M.M., "Self-Generated Magnetic Fields in Laser Produced Plasmas, Sandia Laboratories Report SLA-73-5161, 1973.

14. Wright, T.P., "Some Geometrical Effects on the Source of Spontaneous Magnetic Fields", Bulletin of the APS, November 1972, pp 1027 (paper presented at the Monterey Meeting of the APS Division of Plasma Physics, November 13-16, 1972).

15. Spitzer, L., Physics of Fully Ionized Gases, 1st Edition, pp 21, Interscience Publishers, 1956.

16. Tanenbaum, B.S., Plasma Physics, pp 348, McGraw Hill Book Company, 1967.

17. Ashmarim, I.I., and others, "Pulsed Hologram Investigations of Gas Breakdown in Front of a Laser Produced Plasma", Soviet Physics - Technical Physics, v.16, no. 11, pp 1881-1887, May 1972.

18. Soo, S.L., Analytical Thermodynamics, pp 315, Prentice Hall Book Company, 1962.

19. Boyd, R.L.F., "Langmuir Probes on Spacecraft", in Plasma Diagnostics, North Holland Publishing Company, Amsterdam, 1968.

20. Zimmerman, G.B., and others, "Self-Generated Magnetic Fields and Nonthermal Electrons in Laser Produced Plasmas: Simulation Techniques and Calculational Results", Bulletin of the APS, November 1972, pp 1035, (paper presented at Monterey meeting of the APS Division of Plasma Physics, November 13-16, 1972.).

21. Clark, R.W., and Book, D.L., "Interaction of Laser Produced Plasma with a Magnetic Field", Bulletin of the APS, November 1972, pp 1035, (paper presented at the Monterey meeting of the APS Division of Plasma Physics, November 13-16, 1972.).

22. Papadoupolous, K., and others, "Heating of Counter Streaming Ion Beams in an External Magnetic Field", Physics of Fluids, v.14, no. 4, pp 849-857, April 1971.

23. Cobine, J.D., Gaseous Conductors, pp 81, McGraw Hill Book Company, 1941.

24. Stamper, J.A., "Laser Induced Sources for Magnetic Fields", NRL Report 7411, June 16, 1972.

25. Widner, M.M., Private Communication, 13 April 1973.

26. Windsor, N., et. al., A Laser Target Model, Bulletin of the APS, October 1973, pp 1317. (Paper presented at the Philadelphia meeting of the APS Division of Plasma Physics, October 30 - November 3, 1973).

27. Askar'yan, G.A., and others, "Currents Produced by Light Pressure When a Light Beam Acts on Matter", ZhETF Pis'ma, v.5, no. 4, pp 116-118, 15 February 1967.

28. Basov, N.G., and others, "Heating and Decay of a Plasma Produced by a Giant Laser Pulse Focused on a Solid Target", Soviet Physics JETP, v.24, no. 4, pp 659-666, April 1967.

29. Godwin, R.P., and others, "Measured Polarization of X-rays from a Laser Produced Plasma", Bulletin of the APS, November 1972, pp 971, (paper presented at the Monterey meeting of the APS Division of Plasma Physics, November 13-16, 1972).

30. Shearer, J., and others, "Experimental Indications of Plasma Instabilities Induced by Laser Heating", Phy. Rev. A., v.6, no. 2, pp 764-769, August 1972.

31. Olsen, J.N., and others, "Parametric Correlations in Energetic Laser Plasmas", Bulletin of the APS, November 1972, pp 972 (paper presented at Monterey meeting of the APS Division of Plasma Physics, November 13-16, 1972.).

32. McLaughlin, T.A., Inductive Magnetic Probe Diagnostics in a Plasma, MS Thesis, Naval Postgraduate School, 1970.

33. Phillips, R.C., and Turner, E.B., "Construction and Calibration Techniques of High Frequency Magnetic Probes", Review of Scientific Instruments, v.36-12, pp 1822-1825, December 1965.

34. Ormsby, J.F.A., "Design of Numerical Filters with Applications to Missile Data", J. of Computing Machinery, pp 440-446, July 1961.

35. Malozzi, P.J., "X-ray Emission from Laser Generated Plasmas, Vol. II", Batelle Research Reports, January 1972, and presentation at Defense Nuclear Agency Laser Review Meeting, February 8-9, 1973.

36. Pendleton, W.K., "Laser Induced Tungsten Blow-Off", unpublished AFWL working paper, October 1970.

37. Boland, B.C., and others, "A Spectroscopic Study of the Plasma Generated by a Laser from Polyethylene", J. Phy. B. (Proceedings of Phys. Soc., ser. 2), v.1, pp 1180-1191, 1968.

38. Pendleton, W.K., "Determination of Spatial and Temporal Electron Density and Temporal Electron Temperature in Laser Produced Deuterium Plasmas", AFWL TR-71-71, September 1971.

39. Widner, M.M., Interpreting Self-Generated Magnetic Field Measurements in Laser Produced Plasmas, Sandia Laboratories Report SLA-73-0500, September 1973.

40. Koopman, D.W., "Langmuir Probe and Microwave Measurements of the Properties of Streaming Plasmas Generated by Focussed Laser Pulses, Physics of Fluids, v.14, no. 8, August 1971.

41. Hook, W.R., and others, "A TVR Laser Oscillator Using a Single Pockel's Cell for Q-switching and Synchronized Cavity Dumping", Applied Physics Letters, v.9, pp 125, 1966.

42. Hardway, G.A., and others, Annals of the New York Academy of Sciences, v.168, pp 440, 1970.

43. Patterson, S.R., and others, "Cold Cathode Electron Beam Sustained CO_2 Laser", Bulletin of the APS, April 1973, (paper presented at the Washington D.C. General Meeting of the APS, April 23-26, 1973.).

INITIAL DISTRIBUTION LIST

		No. Copies
1.	Defense Documentation Center Cameron Station Alexandria, Virginia 22314	2
2.	Library, Code 0212 Naval Postgraduate School Monterey, California 93940	2
3.	Professor Fred Schwirzke, Code 61Sw Department of Physics and Chemistry Naval Postgraduate School Monterey, California 93940	10
4.	Dr. Arthur H. Guenther Air Force Weapons Laboratory (DY) Kirtland AFB, New Mexico 87117	2
5.	Captain Roger S. Case, Jr. 2077b Mercury Drive Albuquerque, New Mexico 87118	10
6.	Mr. Kenneth Dick INRS - Energie 1800 Monte Ste. Julie Varemeo, Province of Quebec, Canada	1
7.	Dr. Erik Witalis Forsvarets Forskningsanstalt S-104 50 Stockholm 80, Sweden	1

SECURITY CLASSIFICATION OF THIS PAGE (When Data Entered)

REPORT DOCUMENTATION PAGE		READ INSTRUCTIONS BEFORE COMPLETING FORM
1. REPORT NUMBER	2. GOVT ACCESSION NO.	3. RECIPIENT'S CATALOG NUMBER
4. TITLE (and Subtitle) An Investigation of Self-Generated Magnetic Fields and Electron Emission in Laser-Produced Plasmas		5. TYPE OF REPORT & PERIOD COVERED Ph.D. Thesis; March 1974 6. PERFORMING ORG. REPORT NUMBER
7. AUTHOR(s) Captain Roger S. Case, Jr., USAF		8. CONTRACT OR GRANT NUMBER(s)
9. PERFORMING ORGANIZATION NAME AND ADDRESS Naval Postgraduate School Monterey, California 93940		10. PROGRAM ELEMENT, PROJECT, TASK AREA & WORK UNIT NUMBERS
11. CONTROLLING OFFICE NAME AND ADDRESS Naval Postgraduate School Monterey, California 93940		12. REPORT DATE March 1974 13. NUMBER OF PAGES
14. MONITORING AGENCY NAME & ADDRESS(if different from Controlling Office)		15. SECURITY CLASS. (of this report) UNCLASSIFIED 15a. DECLASSIFICATION/DOWNGRADING SCHEDULE

16. DISTRIBUTION STATEMENT (of this Report)

Approved for public release; distribution unlimited.

17. DISTRIBUTION STATEMENT (of the abstract entered in Block 20, if different from Report)

18. SUPPLEMENTARY NOTES

19. KEY WORDS (Continue on reverse side if necessary and identify by block number)

Laser plasma; self-generated magnetic fields; electron emission; magnetic probes.

20. ABSTRACT (Continue on reverse side if necessary and identify by block number)

An experimental study of magnetic signals from laser-produced plasmas has been performed. From 2 to 30 joules of laser energy impinged upon metallic and hydrocarbon targets in pulse lengths of from 4 to 80 nanoseconds, and at incident angles of 0° and 45°. Two magnetic signals were detected using inductive probes; one whose peak intensity is temporally coincident with, and whose rise time is a function of the in-

DD FORM 1 JAN 73 1473 (Page 1) EDITION OF 1 NOV 65 IS OBSOLETE S/N 0102-014-6601

SECURITY CLASSIFICATION OF THIS PAGE (When Data Entered)

Block 20 (Continued):

cident laser pulse length; the second longer-lasting and time-delayed from the arrival of the laser pulse on target. The first signal results from electrons emitted anisotropically from the laser-produced plasma. This emission current is limited by space charge effects, and is strongly dependent upon the ambient gas pressure over the range of 10^{-6} to 10^{+1} Torr. The second magnetic signal arises from misaligned temperature and density gradients within the laser plasma. The dependencies of these signals on residual gas pressure, laser pulse length and shape, and spatial location have been evaluated.

Thesis
C27465 Case
c.1 150325

An investigation of self-generated magnetic fields and electron emission in laser-produced plasmas.